January 2010

Exploring Tissue Microstructure in Healthy and Diseased Lung Tissue

Michelle Milne
Washington University in St. Louis

WASHINGTON UNIVERSITY

Department of Physics

Dissertation Examination Committee:
Mark Conradi, Chair
James Buckley
Sophia Hayes
Martin Israel
James Miller
Jason Woods
Dmitriy Yablonskiy

EXPLORING TISSUE MICROSTRUCTURE IN HEALTHY AND DISEASED LUNG
TISSUE

by

Michelle Lee Milne

A dissertation presented to the
Graduate School of Arts and Sciences
of Washington University in
partial fulfillment of the
requirements for the degree
of Doctor of Philosophy

August 2010

Saint Louis, Missouri

Abstract

This thesis is divided into two parts. The first part examines diffusion in a number of human lung samples, while the second deals with diffusion in the more simplified environment of a single capillary tube.

In the lung study we examine various types of lung samples (healthy and diseased) at a variety of diffusion lengths. Diffusion Magnetic Resonance Imaging (MRI) has been a very useful tool in the study of lungs and lung disease, particularly diffusion MRI using hyperpolarized gases, such as helium or xenon. However, since the polarized gas is difficult to prepare and, once prepared, suffers decay of the nonrenewable polarization (limiting both the number and strength of rf pulses that may be applied to the sample), most studies only measure diffusion at a handful of diffusion times, at most. Thus no extensive study has been performed to discover at what diffusion time (and hence diffusion length scale) the healthy and diseased lung differ most. By using fixed samples from lungs and gas at Boltzmann polarization, this study seeks to remedy that gap in knowledge. The immobile samples and continually renewed thermal polarization of the gas allowed signal averaging to make up for some of the signal lost by not using polarized gas, although the small signal-to-noise ratio did not allow for diffusion *images*. Instead, spectroscopic diffusion measurements were made, effectively treating the whole lung sample (approximately a 2 inch long by 1.34 inch diameter cylinder) as a single voxel. Because this study seeks to explore many different diffusion lengths, two gases were used, one with a large free diffusion coefficient, used to explore long length scales, and one with a smaller free diffusion coefficient, used to explore shorter length scales. In order to combine the measurements from both types of gas, the

restricted diffusion (D/D_0: measured diffusivity divided by the free diffusion of the gas used) is reported. T_1 in each sample was used to calculate the free gas diffusion coefficient; the bulk gas measurements used to establish this T_1 – diffusion relationship are reported as well.

In the capillary study, we examine the signal decay due to diffusion in a single cylinder, for short diffusion times (lightly restricted diffusion). The signals are well-modeled by a sum of two exponentials, despite the single compartment housing the spins. The results agree with a previous theoretical examination of the problem. The implication for biological systems is that multiple decay signal components *may not* correspond to multiple physical compartments, despite the fact that multi-exponential decays in diffusion experiments are often taken as evidence for spins in multiple distinct compartments.

Acknowledgements

Many people helped me during my time at Washington University and without their assistance my progress would have been very slow indeed. My first thanks go to Mark Conradi for his unfailing guidance and excellent mentoring. He has invested a great deal of time, effort, and funds training me as a scientist. I could not have asked for a better advisor. Jason Woods helped my research through every stage and provided much appreciated funding. Dmitriy Yablonskiy, David Gierada, and Jim Quirk all were very generous with their time and advice, guiding my research over difficult spots. Bill Spees and Alpay Özcan taught me how to keep the magnet running smoothly. Carla Hall, of Richard Pierce's lab, generously prepared histology slides for me. My thanks also goes to my fellow students: Yulin Chang, Lasitha Senadheera, Tim Ivancic, David Shane, Adam Hajari, Wei Wang, Jeff Anderson, and Jennifer Griffith, all of whom helped me immeasurably with their assistance overcoming the trials and tribulations of daily life in the lab. And finally, I would like to thank the anonymous people who donated the lungs used in this study. This study is dedicated to them.

Contents

List of Figures

List of Tables

Chapter 1 - Background

We begin with some background in nuclear magnetic resonance which will be useful for understanding both studies in this thesis.

1.1 Conventional Magnetic Resonance

Magnetic Resonance (MR) is a highly useful non-invasive tool which has made great contributions to a number of fields, one of those fields being medicine. MR uses external magnetic fields to interact with non-zero nuclear spins of select nuclei (such as ^{1}H, ^{3}He, ^{19}F, etc.) to gather information about the number of such spins as well as their local environment. However, because MR depends on the Boltzmann polarization of the nuclear spins in the sample, it is an extremely insensitive tool, acquiring signal from only on the order of one in 10^6 of the nuclear spins. Fortunately, many samples of interest have enough such nuclear spins to make MR an useful tool.

The basis of all MR is that nuclei which have non-zero spin react to external magnetic fields. In such a field, nuclei will partially align either parallel or anti-parallel to the direction of the external field (for spin = ½). Their alignment is governed by Boltzmann statistics and in normal conditions, the nuclear magnetic moments aligned with the field slightly outnumber those antiparallel by about one per 10^6, creating a small net magnetic moment of the sample in the direction of the magnetic field. This collection of nuclei can be perturbed out of alignment by a second oscillating field (called an rf field, because it oscillates in the radio frequencies), after which the nuclei will precess about the external field until returning to equilibrium (see Fig. 1.1 a and b) This precession occurs at the Larmor frequency, ω:

[1.1]
$$\omega = \gamma B$$
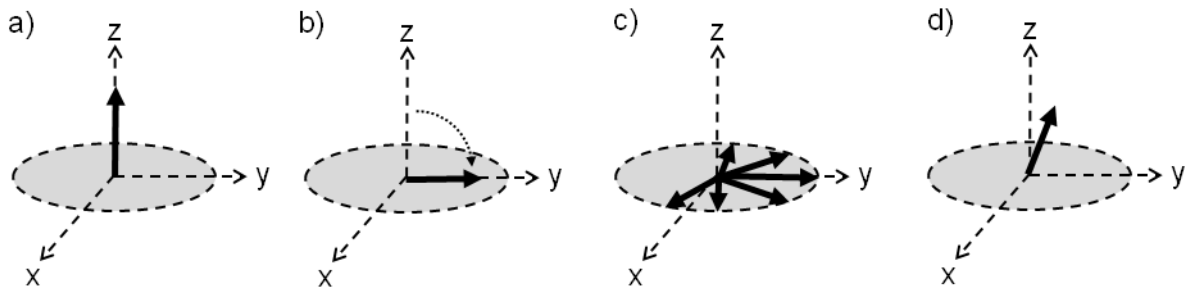
Figure 1.1. Sets of isochromatic spins (spins with the same precession frequency) as seen in the rotating frame. The static external magnetic field is along the z-axis. a) Isochromats in equilibrium, parallel with the static field. b) Isochromats after a 90° rf pulse is applied along the x-axis, rotating the isochromats onto the y-axis. c) A collection of spins sometime after a 90° rf pulse is applied, dephasing by T_2 processes in the form of fluctuations in the local field of each spin. d) Isochromats sometime after a 90° rf pulse is applied, relaxing back into equilibrium by T_1 processes.

where B is the strength of the local magnetic field at the nuclear spin and γ is the magnetogyric ratio of the nuclei. An rf pulse which tips the nuclei from alignment to perpendicular to the static external magnetic field is called a 90° pulse. A pulse which tips the nuclei from parallel to antiparallel is called a 180° pulse.

Relaxation of the longitudinal magnetization back to equilibrium with the static external field occurs at the spin-lattice relaxation rate, T_1^{-1},

[1.2] $$M = M_0(1 - Ae^{-t/T_1})$$

where M_0 is the longitudinal magnetization when the collection of nuclei is in equilibrium alignment with the field and the value of A depends on the initial state of the spins. There is also a second relaxation time, T_2. This relaxation time of the transverse magnetization has to do with the precession of nuclei in a collection becoming irreversibly dephased, due to the slightly different fluctuating local magnetic field at each nucleus, causing each nucleus to have a slightly different instantaneous Larmor frequency (see Fig. 1.1 c and d). T_2 is necessarily equal to or shorter than T_1.

In MR the signal itself comes from the nuclei precessing in the plane transverse to the static external field after being perturbed by an rf pulse. The signal is generally collected as a free induction decay (fid) in the time domain ("free" because the rf field is off during collection) and then can be Fourier transformed into the frequency domain. Over time, the signal is attenuated by the relaxation processes (primarily T_2). Once the nuclei have relaxed back into equilibrium (i.e. after a time of order T_1) a new rf pulse can be applied and the process can be repeated for signal averaging purposes.

Imaging in MR is achieved by exploiting the Larmor frequency dependence on the local magnetic field. A field gradient is used to vary the magnetic field with respect

to position, so the Larmor frequency will also vary with respect to position and the signal from the nuclei can be sorted by Fourier transformation into their respective positions, constructing an image. This is how conventional MRI in a medical setting works. The nucleus that is often used is ^{1}H which, given that the body is comprised primarily of water molecules, is in high concentration (about 100 moles per liter). Therefore there is sufficient signal to get high resolution images despite the inherent insensitivity of MR.

Signal intensity (related to the number of MR nuclei) is not the only parameter of interest in MR. Measurements can also be weighted with respect to the relaxation times, T_1 and T_2, which are properties of the nuclei and their local environments. The signal can also be weighted by diffusion, or Brownian motion, which is a property of the molecules that contain the MR nuclei. Diffusion-weighted imaging is used for a variety of medical applications, one prominent example being in the area of neural imaging. In general, T_1, T_2, and diffusion coefficients in the body are different in different organs, regions, and states of health and can be useful in diagnoses.

A short introduction to free diffusion MR follows. Diffusion measurements can be made with two diffusion sensitizing gradients, of the same strength and duration but in opposite directions (see Fig. 1.2). The gradients cause signal attenuation in the presence of diffusion. A quick and simple derivation of this attenuation in the classical description gives the basic idea behind diffusion MR:

As stated before, the precession frequency (ω) of a spin with a magnetogyric ratio (γ) in a magnetic field (B) is

$$\omega = \gamma \, B$$
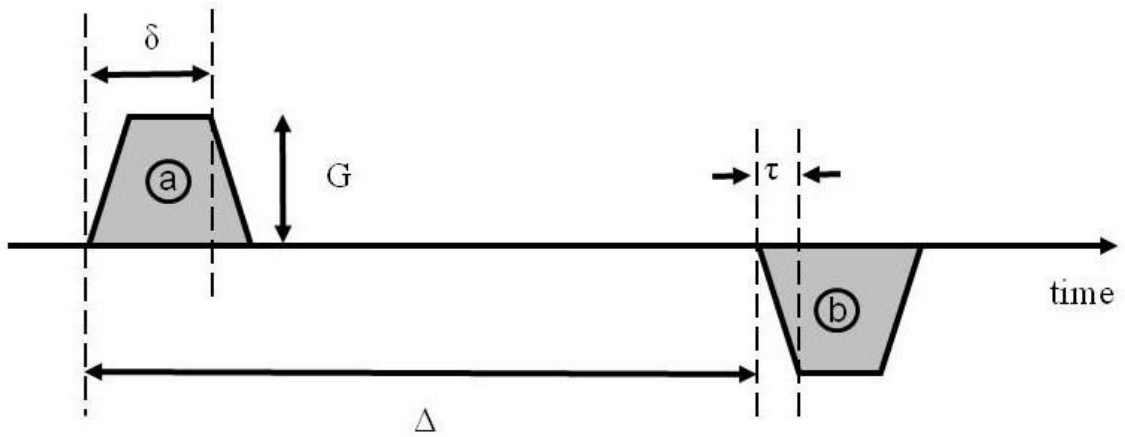
Figure 1.2. Bipolar pair of diffusion magnetic field gradients, *a* and *b*. The gradients

have duration δ, rise time τ, gradient strength G and separation Δ. The diffusion time, t_{diff},

is Δ - $\delta/3$ for this case.

If the spin is at position x_1 in a magnetic field that consists of a position-dependent field ($B = G\, x_1$, lobe a in Fig. 1.2) in addition to a background field (B_0) then the magnetic field strength at location of the spin is

[1.3]
$$B = B_0 + G\, x_1,$$

and its frequency is

[1.4]
$$\omega = \gamma\ (B_0 + G\, x_1).$$

If we consider the spin in a reference frame that is rotating at frequency

[1.5]
$$\omega_0 = \gamma\, B_0$$

then the spin will rotate at a frequency (relative to the reference frame) of

[1.6]
$$\omega_r = \gamma\, G\, x_1$$

Ignoring T_1 and T_2 processes, a time δ after the gradient is turned on the spin will have accumulated a phase of

[1.7]
$$\theta = \gamma\, G\, x_1\, \delta$$

(we assume the initial phase is 0, with no loss of generality). In a similar fashion, if the spin moves to a second position x_2 by the time the second magnetic field gradient pulse (lobe b in Fig. 1.2) is applied, the phase change due to the second gradient is

[1.8]
$$\theta = -\, \gamma\, G\, x_2\, \delta,$$

(recall that the second gradient is in the opposite direction from the first and consequently the second phase change will have the opposite sign from the first, while the magnitude, G, and duration, δ, of the second gradient is the same as that of the first). Thus the total phase change for a single spin from the two field gradient pulses will be

[1.9]
$$\theta_{net} = \gamma\, G\, (x_1 - x_2)\, \delta$$

Given that MR measures the signal of a collection of spins and that $<\theta_{net}>$ is zero (on average, just as many spins move from smaller x to larger x), a more appropriate quantity to consider is a measure of the mean squared phase change,

[1.10] $$<\theta_{net}^2> = \gamma^2 \, G^2 \, \delta^2 <(x_1 - x_2)^2>.$$

Recall the definition of the free diffusion coefficient (i.e. no restriction on the objects which are diffusing) for a given diffusion time (t_{diff})

[1.11] $$D \equiv <(x_1 - x_2)^2> / (2 \, t_{diff})$$

then

[1.12] $$<\theta_{net}^2> = 2 \, \gamma^2 \, G^2 \, \delta^2 \, D \, t_{diff}$$

Now the MR signal, which depends on the average phase coherence (which has a gaussian distribution of phases), is

[1.13] $$M = M_0 \, exp(-<\theta_{net}^2>/2)$$

or

[1.14] $$M = M_0 \, e^{-bD}$$

where

$$b = \gamma^2 \, G^2 \, \delta^2 \, t_{diff}$$

and M_0 is the unattenuated MR signal. This is the Stejskal-Tanner equation for narrow pulse diffusion $(\delta \ll \Delta)$[1]. Note that this result depends on Eq. 1.11, which only describes free diffusion.

A more rigorous derivation can be found in any number of MR textbooks or in Torrey's original paper[2]. The main equations in such a derivation are as follows: The Bloch-Torrey equation governing the MR signal, which adds a diffusion term to the standard precession and relaxation terms of Bloch's equations, is

[1.15]
$$\frac{\partial M_+}{\partial t} = -i\gamma \vec{r} \cdot \vec{G} M_+ - \frac{M_+}{T_2} + D\nabla^2 M_+$$

where $M_+ = M_x + iM_y$ is the signal perpendicular to the direction of the external field (along the z direction by convention) and T_2 is the relaxation time for the signal due to spin-spin interactions as stated above.

When the zeroth moment of the gradient pulses is zero, the solution to Eq. 1.15 is

[1.16]
$$M_+(\vec{r},t) = M_0 e^{-t/T_2} e^{-i\vec{r}\cdot\vec{k}(t)} e^{-bD}$$

where

[1.17]
$$\vec{k}(t) = \gamma \int_0^t \vec{G}(t')dt'$$

and

[1.18]
$$b(t) = \gamma^2 \int_0^t dt' \left(\int_0^{t'} dt'' \vec{G}(t'') \right)^2.$$

The first two exponential terms of Eq. 1.16 deal with the signal decay due to T_2 processes and the precession of the signal in the transverse plane (which does not affect the signal magnitude), respectively. The third is the diffusion attenuation term, previously seen in the quick derivation above. For a pair of field gradients with duration δ, rise time τ, gradient strength G and separation Δ (see Fig. 1.2)[3]

[1.19]
$$b = \gamma^2 G^2 \delta^2 [(\Delta - \delta/3) - \delta\tau^2/6 + \tau^3/30].$$

In general, the correction due to the rise time of the gradient (the last two terms in the brackets) is quite small. In this study it never amounted to more than 0.2% of the final b-value, and thus the correction is neglected. We consider Δ to denote the time from the start of the first gradient pulse's leading edge to the start of the second gradient

pulse's leading edge, and δ from the start of the gradient pulse rise to the start of the gradient pulse's fall (see Fig. 1.2).

1.2 Magnetic Resonance in the Lungs

The previous discussion has been primarily from the viewpoint of conventional ^{1}H MR, although all the equations and principles are valid for all MR nuclei. However, there are some cases where conventional MR, in particular MR used for imaging, is not capable of delivering the necessary level of sensitivity. Lung tissue, for example, has a low density of ^{1}H nuclei which is exacerbated by the high susceptibility gradients of the numerous tissue/air surface interfaces. Although with enough signal averaging the signal to noise ratio can be increased enough to make MR images, at realizable imaging resolutions an ^{1}H image contains little useful information, since the length scales of interest are very small (5-100 microns) in lung tissue. This problem has been overcome, somewhat counterintuitively, by imaging the gas inside the lung tissue rather than the tissue itself. Despite the loss in signal (by a factor of about 2500) due to the decreased density of gas, gas imaging provides the researcher with a variety of means to increase the signal in other ways (see below). Gas MR provides important advantages over simply imaging the lung tissue with a microscope. Foremost among these is the ability to examine the tissue *in vivo*, an approach that has been used in several studies[4,5]. In the present study, the tissue is excised and fixed, although one hopes the findings herein will inform clinical use in the future. Another advantage of gas MR over examination of microscope slides is the ability to study the tissue in three dimensions rather than in 2D slices or projections, which may distort the appearance of the tissue.

In addition, gas imaging can also be *functional* imaging of the lung rather than an image solely of the lung tissue structure. A simple spin density measurement of inhaled gas is, in effect, a ventilation image of the lung because signal only appears in areas where the gas has been inhaled. Unventilated areas of the lung, which may be cut off due to airway damage or a similar misfortune, contain no imaging gas and thus appear as dark spots on the ventilation image. Ventilation images have successfully been used to identify areas of the lung which suffer from gas trapping in emphysema[6], asthma[7], and cystic fibrosis[8].

Diffusion MR is also useful in gas MR in lungs. The lung tissue in airways and alveolar walls restricts the motion of gas molecules inside the lung. Where there is less tissue, the gas diffusion will be less restricted and consequently diffusion MR can serve as a measure of tissue destruction. In addition, because the gas diffusion is sensitive to changes in tissue at length scales which are smaller than that which can be imaged directly, diffusion MR provides a way to gain information about small length scales in vivo which are otherwise inaccessible.

It is important to note that gas diffusion inside lung tissue will not be free diffusion but restricted diffusion. Unlike free diffusion, restricted diffusion, even in very simple physical geometries, does not have a simple analytical solution to the Bloch-Torrey equation (Eq. 1.15)[9]. A great deal of research effort has been spent trying to decipher the signal attenuation in restricted diffusion. In certain situations in human lungs, a two exponent decay theory proposed by Yablonskiy and Sukstanskii[10] offers an excellent approximation of the signal decay as a function of *b*. Here the two diffusion coefficients correspond to lightly restricted diffusion down the airways of the lung and

heavily restricted diffusion across the airways. These two diffusion coefficients can be then traced back to physical parameters, such as the airway diameter. However, since there are many free parameters to fit to in the bi-exponential approach, the signal-to-noise ratio of the experimental measurements must be quite good to obtain unique fits to the data. Another approach is to fit the signal of restricted diffusion measurements using diffusional kurtosis, which contains exponential terms containing b and b^2. The kurtosis fit does not provide a physical interpretation of the terms in the same way as the bi-exponential fit, but it has fewer free parameters and thus requires a more modest signal-to-noise ratio than the bi-exponential approach. The diffusion coefficient measured by the kurtosis method is skewed to fit the small b-values, so it tends to be higher than a diffusion measurement taken which uses a mono-exponential fit.

In porous media, the behavior of restricted diffusion has been explored by Mitra and Sen in a couple of limiting cases. The signal attenuation behavior for restricted diffusion in the limit of short diffusion time and distance was calculated by Mitra and Sen[11]. They found that the restricted diffusion in a porous media is closely related to the surface to volume ratio (SVR) of that media in the short diffusion limit. Mitra and Sen have suggested that at diffusion lengths which are only a fraction of the characteristic length scale of the porous medium, the reduced diffusion coefficient (D/D_0, measured diffusion divided by the free diffusion of the gas used) should have a linear relationship with the diffusion length ($\sqrt{D_0}\, t_{diff}$, the square root of the free diffusion multiplied by the diffusion time). The initial slope of the decay will be directly related to the surface to volume ratio of the medium.

[1.20]
$$\frac{D}{D_0} = 1 - \frac{4}{9\sqrt{\pi}} \frac{S}{V} \sqrt{D_0 t_{diff}}$$

Their theory has been verified by many experiments in porous media (such as rocks).[12,13] This short diffusion length limit holds for diffusion times where $S/V \sqrt{(D_0 t_{diff})} \le 1$.[14]

Unfortunately in lungs it is difficult to access the length scales discussed in Mitra and Sen's work for an indirect measurement of SVR. To explore very short diffusion lengths small diffusion times must be used, which means that very large and very fast gradient pulses are required to obtain adequate signal attenuation. To access the surface to volume limit in lung tissue, the required of magnitude and slew rate (rise time) of the gradients are beyond the capabilities of our magnet. However, even at short diffusion length scales which are too long for SVR measurements the tissue destruction characteristic of emphysema results in an elevated diffusion coefficient. Many studies have confirmed that measurements at short diffusion lengths are a useful measure of the emphysema's severity in lung tissue.[1-3]

On the other end of the diffusion length scale, at the limit of longer length scales, the tissue destruction also means that the overall structure of the lung has changed in terms of the connections between various areas of the lung. The progression of the disease causes the tortuosity of the lung (a measure of how difficult it is to move from one area to another, i.e. the tortuousness of the path) to decrease as barriers of tissue are destroyed. Mitra and Sen's work suggest that at long diffusion lengths (lengths longer than the largest feature in the media) the reduced diffusion coefficient should go to a constant number; the inverse of the tortuosity (τ) [15]

[1.21]
$$\frac{D}{D_0} = \frac{1}{\tau}$$

This finding has been born out in experiments on rocks. Whether this limit can be reached in lung is an open question, since healthy lungs do not have a characteristic length scale beyond which they are self-similar. Thus D/D_0 may not reach a limiting value, even at very long diffusion times.

Another effect which is occasionally seen in diffusion studies is the edge-enhancement effect. The edge-enhancement effect occurs because spins which are close to an impermeable barrier, such as a sample container wall, will be reflected by the barrier and have diffusion which is more restricted than the rest of the gas in the sample (this will result in signal which is less attenuated, hence edge-*enhancement* effect). In this study the ends of the sample cylinder are out of the rf range of the coil, while the sides of the cylinder are perpendicular to the direction in which diffusion is being measured. Therefore we do not expect to see any edge-enhancement effects in this study.

Despite the fact that the ability to increase the MR signal is exploited to great effect in studies that use hyperpolarized gas, such as helium and xenon, hyperpolarized gas is not used in this study. One of the unique difficulties with hyperpolarized gas experiments is that T_1 becomes a relaxation back to Boltzmann polarization, thus limiting the overall duration of the entire experiment and requiring administration of additional prepolarized gas if further experiments are desired. Due to the difficultly in preparing hyperpolarized gas, as well as to the cost of the gas itself (particularly with regards to helium), this short effective lifetime of the signal limits the researcher to a small number of measurements in each study. Some research groups have begun to overcome these limitations by using continuous flow hyperpolarization of xenon[16], although this study takes a different approach. Due to the practical difficulties of replenishing

hyperpolarized gas in fixed tissue, thermally polarized gas was used. Signal averaging was used to obtain acceptable signal to noise ratios; the longer experimental times required by signal averaging presented no difficulty with fixed tissue.

Previous studies by this group[17] have shown that measuring the restricted diffusion coefficient by diffusion MR imaging is an excellent way to distinguish between healthy and emphysematous lung tissue, while also suggesting that there may be an optimal diffusion time (or, more correctly, an optimal diffusion length) at which to take such measurements. In particular, a study on dogs[18] in which each animal had one healthy lung and one emphysematous lung demonstrated this. In this study, long length scale diffusion (with a diffusion time on the order of seconds) was found to have a greater increase in the average diffusion coefficient of emphysematous over healthy tissue ($<D_{EMPH}> = 2.7 <D_{NORMAL}>$) than short length scale diffusion with a diffusion time of 2 ms ($<D_{EMPH}> = 1.8 <D_{NORMAL}>$). Due in part to the aforementioned difficulties of making measurements at multiple diffusion times (and hence diffusion lengths), a thorough study of restricted diffusion at a variety of length scales in lungs has been neglected before now.

Another obstacle to a diffusion study at a wide range of length scales is the relatively limited range of diffusion lengths available with any signal gas. Helium, with a fast diffusion coefficient, can probe longer diffusion lengths in the lung but shorter lengths are inaccessible. Earlier work studying packed bead systems[19,20] overcame this limited range difficulty by using water for the short diffusion lengths and gas for the longer diffusion lengths. The diffusion measurements for water and gas were normalized with the respective free diffusion coefficient (i.e. D/D_0, where D_0 is the free diffusion)

14

and plotted against the free diffusion length (i.e. $\sqrt{(D_0\, t_{diff})}$ where t_{diff} is the diffusion time). In this way, diffusion measurements from both water and gas could be combined to show the diffusion behavior over a large range of diffusion lengths, larger than could be measured with either water or gas alone. This study uses a similar strategy, combining short diffusion length measurements from a slowly diffusing gas (octafluoropropane, C_3F_8) with long diffusion length measurements from a quickly diffusing gas (helium).

1.3 Lung Physiology[21,22,2324]

To understand this study it is necessary to have a basic idea of the lung's structure and the diseases affecting the lung tissue used in this study. A short description of normal tissue and each disease follows.

1.3.1 Normal Lung

The purpose of the lung is to provide an efficient means of exchanging gases between the air and blood. This exchange is achieved by bringing the blood and inhaled air in close proximity, separated only by a thin barrier of tissue with a high surface area that the gases can travel through (confusingly, lung physiologists refer to this motion of gas through tissue as "diffusion". Here we use the term "diffusion" strictly to refer to Brownian motion of gas in the air space). Capillaries, which are only wide enough to accept a single red blood cell, transport the blood through this tissue for oxygenation. The greater the surface area of this thin barrier, the more efficient the gas exchange can be. The challenge therefore is to fit a very large gas exchange surface (approximately the size of a tennis court in healthy adult humans) into the chest in such a fashion that both blood and gas can easily reach the surface interface. This is accomplished by millions of tiny roughly spherical alveoli and blood capillaries that line a compact set of airways. It

is important that the lung be able to quickly move gas in and out of the lung, which the lung accomplishes by means of a series of airways. These airways are arranged in a binary branching structure in humans, meaning that the main airway (the trachea) splits into two smaller airways, which then themselves divide, and so forth until the terminal airways are reached. There are about twenty-three levels of branching airways in the human lung. The first sixteen levels are conducting airways, which serve to move gas quickly into and out of the lung but do not provide gas exchange. Gas here is moved primarily by conduction (hydrodynamic flow), which is controlled by contracting the diaphragm (which expands the volume of the lung, dropping the pressure in the lung compared to the pressure outside and causing gas to be pulled in: inhalation) and relaxing the diaphragm (decreasing the volume of the lung and expelling gas: normal exhalation). The lower seven levels of branching airways are acinar airways in the respiratory zone, where the majority of gas in the lung by volume resides and where the gas exchange between blood and air actually takes place. Alveoli cover the acinar airways like a bubbly sleeve, providing the interface between blood and air.

The branching structure means that areas of the lung that are physically close to each other (i.e. as measured by a straight line) may be quite distant in terms of their position on the lung tree (as gas would have to travel all the way up the airways on the tree to the common branch and then all the way down again through new airways to the destination). However, there are collateral pathways between airway branches in human lung tissue which can connect areas that are physically close but distant on the lung tree. These pathways include the pores of Kohn, canals of Lambert, and channels of Martin. The role of these pathways is not completely understood, but research done by this group

16

suggests that they are more important in the function of human lungs that previously thought[25]. In the lungs of some animals (such as pigs) the various branches are well separated and there are very few or no collateral paths between distinct branches of the airway tree.

The lungs have significant reserves, and injury to the lung must be quite severe before it has a significant effect on (non-athletic) lung function and quality of life. All the diseased samples in this study fall under this severely injured category, which lead their former owners to seek treatment and lung transplant.

1.3.2 Emphysema

A focus of this study is to contrast emphysematous tissue with healthy tissue. In general terms emphysema is a lung disease which tends to be suffered by smokers (although not everyone who smokes gets emphysema and some people who do not smoke do develop emphysema). The main result of emphysema is the destruction of lung tissue, in particular the alveolar walls. Because this destruction reduces the surface available for gas exchange, it results in lower oxygenation in the blood, which is one symptom clinicians look for when diagnosing emphysema. In addition, areas that have suffered tissue destruction tend to expand, encroaching on nearby tissue which may or may not be healthy and potentially sealing off airways to other parts of the lung. This air trapping increases the residual volume of the lung, forcing patients' lungs to remain in a high volume state while they take shallow breaths in an attempt to oxygenate their body. This overextension effectively hinders the proper working of the diaphragm, which is flattened due to the increased volume of the lung and forces the patient to breathe using their auxiliary respiratory muscles, vastly increasing the effort needed to breathe. For the

purposes of this study emphysema is expected to drastically reduce the surface to volume ratio of the tissue due to destruction and the lung structure should have a reduced tortuosity for the same reason.

1.3.3 Sarcoidosis

This is a disease of unknown cause where various organs suffer inflammation and scarring. Small inflamed tissue granulomatous nodules develop in the lungs and other organs. These nodules can block the lung airways and cause scarring or fibrosis (stiffening of the tissue) both of which can interfere with the proper inflation of the lung and the ease of inflation. Generally sarcoidosis is mild, but sometimes it causes difficulty breathing and chest pains (presumably due to stress on the pleura surrounding the lung, as there are no nerve endings in the lung itself). However, in sarcoid lungs which have been removed for a lung transplant, the disease and accompanying symptoms were severe enough that the patient's quality of life had been reduced (thus prompting them to seek a lung transplant). In these extreme cases, the patient's lungs are often severely scarred and consequently incapable of much inflation. However, note well that any area of the lung which was more severely afflicted and least capable of inflating was also least likely to be selected for this study (due to the extreme difficulty of cutting through frozen, uninflated and consequently dense fixed tissue without destroying the sample). Thus the sarcoid samples included in this study were from the healthiest regions of the lung and therefore might be expected to have characteristics similar to those of healthy tissue when studied by diffusion NMR.

1.3.4 Interstitial Pulmonary Fibrosis

Interstitial Pulmonary Fibrosis (IPF) lung disease is also characterized by fibrosis, as the name suggests. There is interstitial scarring of the lung tissue just as in sarcoid lungs, but the major cause of tissue stiffening is a drastic increase in the tissue thickness. This thickening of the tissue barrier hinders the body's efforts to effectively oxygenate the blood but is not expected to affect the diffusion properties of gas in the lung. For similar sample selection reasons as with the sarcoid lung, the practical considerations of IPF lung samples and sarcoid lung samples for this study are the same: The lung samples are expected to appear similar to healthy tissue in diffusion MR studies.

1.3.5 Healthy Pig

A non-human lung sample was also used in this study. Pig lungs are similar to human lungs in many respects. The main difference is that pig lungs have fully septated lobules and thus very few collateral pathways, drastically reducing gas diffusion between areas of the lung which are close in physical proximity but distant on the lung airway tree. This lack of collateral pathways is expected to decrease the long-range restricted diffusion coefficient and increase the overall tortuosity of the lung tissue. The healthy pig alveoli are also smaller than the healthy human's (pig alveolus volume 1.22×10^6 μm^3 vs. human alveolus volume 4.2×10^6 μm^3) so the surface to volume ratio would be larger for a pig and thus the slope of the reduced diffusion when graphed over short diffusion lengths would be expected to be somewhat steeper.

1.4 Gas characteristics

Because the reduced diffusion (D/D_0) is being analyzed, a variety of gases with different free diffusion coefficients can be used. This allows for an exploration of a

greater range of diffusion length scales. The two gases used in this study are helium

(mixed with oxygen in a controlled fashion) and octafluoropropane (C_3F_8), a Freon gas.

Helium has been successfully used in may diffusion MR studies. Here its high

diffusion coefficient makes it ideal for exploring long length scales in the lung. A near

50/50 mix of helium and oxygen at 1 atm total pressure was used in all cores, a mixture

which has a free diffusion of approximately 1 cm^2/s (the free diffusion of helium and

oxygen mixtures is between 0.80 and 1.86 cm^2/s depending on He/O_2 concentration; see

appendix A for a more detailed explanation). With the diffusion times accessible on our

system this meant that helium was used to explore diffusion lengths, $\sqrt{(D_0\, t_{diff})}$ of less

than 0.04 cm to just over 1 cm. Given the helium mixture's relatively long T_1 (about 5 s

in this study), longer lengths could have been explored, but it was not felt to be useful

considering the size of the lung cores and the fact that, for nearly all cores, the value of

the reduced diffusion was only slightly dependent on diffusion length after about 0.5 cm.

Because the gas was at Boltzmann polarization, the signal was relatively low due to the

low density and small magnetogyric ratio. Much signal averaging had to be done to

increase the signal to noise ratio (SNR) to acceptable levels. Incidentally, the fast

diffusion, small size, and inert gas characteristics of helium make it an accomplished

"escape artist" and consequently a great deal of care had to be used in designing sample

containers that could successfully contain the gas for a reasonable period of time (see

appendix B). We saw no evidence that helium absorbed into the fixed lung tissue.

For shorter length scales, a gas with a lower free diffusion was needed.

Octafluoropropane (C_3F_8), with a diffusion coefficient of 0.0208 cm^2/s at 1 atm pressure,

was suitable. It was used for diffusion lengths just under 0.007 cm to around 0.05 cm. In

order to obtain diffusion measurements for the longer lengths it was necessary to use

diffusion times about five times T_1 (the longest diffusion time = 100ms, T_1 = 20 ms) and

signal averaging was used to obtain acceptable SNR. There are six equivalent fluorine

spins per molecule (the remaining two fluorine spins, of the CF_2 group, have a chemical

shift of 48 ppm, about 9 kHz in our magnet, and were easily excluded from the

measurements). As with helium, there was no evidence that the C_3F_8 gas was absorbed

into the lung tissue.

[1] E.O. Stejskal, J.E. Tanner, Spin diffusion measurements: spin echoes in the presence of time-dependent field gradient, J Chem Phys 42 (1965) 288–292.

[2] H.C. Torrey, Bloch Equations with Diffusion Terms, Physical Review, 104 (1956) 563-565.

[3] P.Basser, J. Mattiello, D. LeBihan, Estimation of the Effective Self-Diffusion Tensor from the NRM Spin Echo, J Magn. Res. Ser. B, 103 (1994) 247-254.

[4] R. E. Jacob, K. R. Minard, G. Laicher, C. Timchalk, 3D ^{3}He diffusion MRI as a local in vivo morphometric tool to evaluate emphysematous rat lungs, J Appl Physiol. 105. (2008) 1291-1300.

[5] C. Wang, T.A. Altes, J.P. Mugler, G.W. Miller, K. Ruppert, J.F. Mata, G.D. Cates, L. Borish, E.E. de Lange, Assessment of the lung microstructure in patients with asthma using hyperpolarized ^{3}He diffusion MRI at two time scales: Comparison with healthy subjects and patients with COPD, J of Magn. Reson. Imaging 28 (2008) 80-88.

[6] D.S. Gierada, B. Saam, D. Yablonskiy, J.D. Cooper, S.S. Lefrak, M.S. Conradi, Dynamic echo planar MR imaging of lung ventilation with hyperpolarized 3He in normal subjects and patients with severe emphysema, NMR Biomed. 13 (2000) 176–181.

[7] E.E. de Lange, T.A. Altes, J.T. Patrie, J.D. Gaare, J.J. Knake, J.P. Mugler, T.A. Platts-Mills, Evaluation of asthma with hyperpolarized helium-3 MRI: correlation with clinical severity and spirometry, Chest. 130 (2006) 1055-1062.

[8] C.J. McMahon, J.D. Dodd, C. Hill, N. Woodhouse, J.M. Wild, S. Fichele, C.G. Gallagher, S. J. Skehan, E.J. R. van Beek, J.B. Masterson, Hyperpolarized ^{3}helium magnetic resonance ventilation imaging of the lung in cystic fibrosis: comparison with high resolution CT and spirometry, Eur. Radiol. 16 (2006) 2483-2490.

[9] A.L. Sukstanskii, D.A. Yablonskiy, Effects of Restricted Diffusion on MR Signal Formation, J Magn. Res. 157 (2002) 92–105.

[10] D.A. Yablonskiy, A.L. Sukstanskii, J.C. Woods, D.S. Gierada, J.D. Quirk, J.C. Hogg, J.D. Cooper, M.S. Conradi, Quantification of lung microstructure with hyperpolarized ^{3}He diffusion MRI, J Appl Physil 107 (2009) 1258-1265

[11] P.P. Mitra, P.N. Sen, L.M. Schwartz, Short-time behavior of the diffusion coefficient as a geometrical probe of porous media, Phys. Rev. B, 47 (1993) 8565-8574.

[12] L.L. Latour, P.P. Mitra, R.L. Kleinberg, C.H. Sotak, Time-dependent diffusion coefficient of fluids in porous media as a probe of surface-to-volume ratio, J Magn. Reson. A 101 (1993) 342–346.

[13] M.D. Hurlimann, K.G. Helmer, L.L. Latour, C.H. Sotak, Restricted diffusion in sedimentary rocks: determination of surface-area-to-volume ratio and surface relaxivity, J Magn. Reson. A 111 (1994) 169–178.

[14] R.E. Jacob, Y.V. Chang, C.K. Choong, A. Bierhals, D.Z. Hu, J. Zheng, D.A. Yablonskiy, J.C. Woods, D.S. Gierada, M.S. Conradi, 19F MR Imaging of Ventilation and Diffusion in Excised Lungs, MRM 54 (2005) 577-585.

[15] P.N. Sen, L.M. Schwartz, P.P. Mitra, B.I. Halperin, Surface relaxation and the long-time diffusion coefficient in porous media: Periodic geometries, Phys. Rev. B., 49 (1994) 215-225.

[16] B. Driehuys, J. Pollaro, G. P. Cofer, In Vivo MRI Using Real-Time Production of Hyperpolarized ^{129}Xe, Magn. Reson. Med. 60 (2008) 14–20.

[17] M.S. Conradi, D.A. Yablonskiy, J.C. Woods, D.S. Gierada, R.E. Jacob, Y.V. Chang, C.K. Choong, A.L. Sukstanskii, T. Tanoli, S.S. Lefrak, J.D. Cooper, 3He diffusion MRI of the lung. Academic Radiology, 12 (2005) 1406-1413.

[18] J.C. Woods, D.A. Yablonskiy, K. Chino, T.S.K. Tanoli, J.D. Cooper, M.S. Conradi, Magnetization Tagging Decay to Measure Long-Range ^{3}He Diffusion in Healthy and Emphysematous Canine Lungs, Magn. Reson. Med. 51 (2004) 1002–1008.

[19] RW Mair, GP Wong, D. Hoffmann. M.D. Hürlimann, S. Patz, L.M. Schwart, R.L. Walsworth, Probing Porous Media with Gas Diffusion NMR, Phys Rev Let. 83 (1999) 3324-3327.

[20] R.W. Mair, P.N. Sen, M.D. Hürlimann, S. Patz, D.G. Cory, R.L. Walsworth, The Narrow Pulse Approximation and Long Length Scale Determinaton, in Xenon Gas Diffusion NMR Studies of Model Porous Media, JMR 156 (200) 202-212.

[21] E.R. Weibel What makes a good lung?, Swiss. Med. Wkly. 139 (2009) 375-386.

[22] Respiratory Physiology, J.B.West, 5th ed. Williams & Wilkins 1995. Baltimore

[23] Pulmonary Pathophysiology, J.B. West, 4th ed. Williams & Wilkins 1992 Baltimore

[24] H. Lum, W. Mitzer, A species comparison of alveolar size and surface forces, J. Appl. Physiol. 62 (1987) 1865-1871.

[25] S-E.T. Bartel, S.E. Haywood, J.C. Woods, Y.V. Chang, C.Menard, D.A. Yablonskiy, D.S. Gierada, M.S. Conradi, Role of collateral paths in long-range diffusion in lungs, J Appl Physiol 104 (2008) 1495-1503.

Chapter 2 - Lung Study Preliminaries

Sample cylinders were designed and rf coils were built specifically for this experiment. The performance of the magnetic field gradients on the MR system were checked and preliminary testing with water and bulk gas was done on the stimulated echo sequence, both to make sure the sequence was measuring the known diffusion coefficient for free gases and to establish the T_1 and free diffusion relationship for various concentrations of the gases. This relationship would be used later to determine free diffusion of the MR gases in the lung samples.

2.1 Sample Cylinders

Small, inert, and quickly diffusing, helium is very difficult to contain successfully in a closed container for any length of time. Therefore, great care was taken in designing containers for the lung samples that were as helium-tight as possible. The body of the container was a cylinder cut from an acrylic tube with an inner diameter of 1.35 inches and an outer diameter of 1.75 inches. A matched cap was created to fit and was glued on to the body to seal the lung sample in. The ends of the cylinder were fitted to copper tubing with valves on the ends to allow for gas filling (see appendix B for details). This set-up was tested for helium containment both with a helium based leak detector and a pressure gauge. Later, during the study, the amount of helium in the cylinder was also monitored in each individual sample by noting the free induction decay (FID) height (signal height) of a 90 rf pulse before diffusion measurements. The measurement of the FID height indicated that helium loss in the chambers was negligible over a two week long period, although there was noticeable helium loss over a month long period.

Consequently, all helium measurements were taken within two weeks of being filled with helium. No signal loss was noticed for the octafluoropropane (C_3F_8) gas.

2.2 Magnet and rf Coils

The lung cores were measured in the same 4.7 T (198.35 MHz frequency for ^1H), 16 cm bore, Oxford magnet as was used in the capillary study. In this magnet ^3He has a frequency of 151.05 MHz and ^{19}F has a frequency of 186.65 MHz. The hardware was a Varian system and the software was VnmrJ 2.3A.

Two rf coils were used in this study. Both are homemade single-turn solenoids inductively coupled to the MR electronics. They are 1.75" in diameter, close fitting to the outside surface of the lung sample cylinder.

The rf coil for helium frequencies is 2.5 cm in length and tuned to 151.1 MHz. It is a copper strap with an equivalent 11pf capacitor (two 22 pf capacitors in series) connected in parallel with a 2-15 pf variable capacitor. The helium coil has a quality factor of 275.

The rf coil for fluorine is 3.2 cm in length and tuned to 186.65 MHz. It is also a copper strap with a 10 pf capacitor in parallel with a 2-10 pf variable capacitor. The fluorine coil has a quality factor of 115.

2.3 Magnetic Field Gradients

Due to the central importance of the magnetic field gradients to diffusion measurements, great care was taken to ensure that the gradients were responding accurately. An inductive pick-up coil set with an integrating amplifier made by Yulin Chang was used to measure the gradients inside the bore while the generating current from the gradient amplifiers was monitored with an oscilloscope. The results from the

two methods agreed well for all three directions. The slope of the gradient rise was constant, so the rise time of the gradients depended on the final gradient strength, with a maximum rise time of 250 μs for a gradient strength of 45 G/cm. The x gradient was the focus of the preliminary test because it was the direction used for the diffusion measurements (the z-axis is down the bore of the magnet from the back of the magnet towards the front or west to east as the magnet is currently positioned, and the y-axis is vertical from bottom to top. The x-axis is horizontal, perpendicular to the bore of the magnet, from south to north). Details can be found in appendix B.

2.4 MR Sequences

T_1 was measured for all samples using an inversion-recovery sequence (the Varian sequence t1puls.c, see Fig. 3.1). This sequence used a 180° rf pulse to invert the magnetization, allowed the magnetization to recover for a time t then measured the recovered longitudinal magnetization. The sequence was repeated for an array of recovery times and the resulting data were fitted to Eq. 1.2 from chapter one (with $A = 2$ since the spins are inverted at $t = 0$):

[2.1] $$M = M_0 (1 - 2e^{-t/T_1})$$

A diffusion stimulated echo sequence was used for diffusion measurements (Fig. 2.2, the same diffusion sequence used in the capillary study). This sequence applied a 90° rf pulse to the net magnetization of the sample in order to rotate it into the x-y plane and then dephased the magnetization for diffusion with the first magnetic field gradient pulse, coding the spins for initial location. The dephased magnetization was then stored along the external magnetic axis (the z-axis) with a second 90° rf pulse during the diffusion time. A third 90° rf pulse removed the magnetization from storage so that the

26
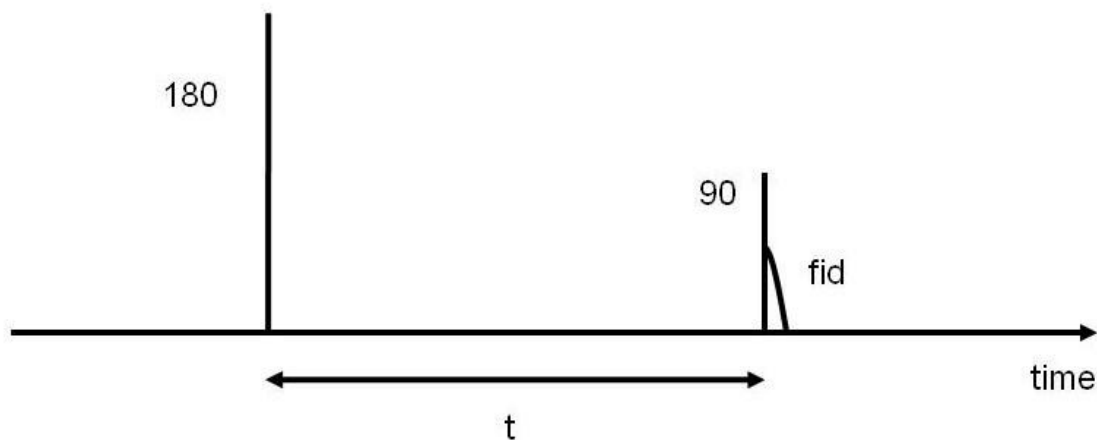
Figure 2.1. T_1 inversion recovery sequence. The 180° rf pulse inverts the spins so they are anti-parallel to the static magnetic field. After waiting the recovery time, t, the FID following a 90° rf pulse measures the amount of longitudinal magnetization that has recovered back to equilibrium via T_1 processes. The sequence is repeated with various recovery times to measure T_1, and the results are fitted to $M = M_0 (1 - 2e^{-t/T1})$.
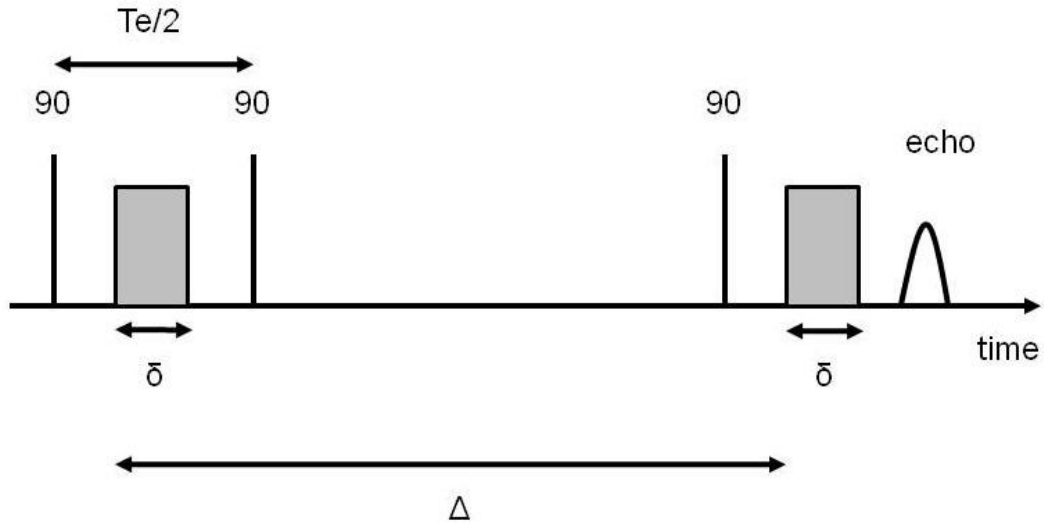
Figure 2.2. A diagram for the stimulated echo sequence. The first 90° rf pulse places the spins in the transverse plane, where they are encoded for position by the first magnetic field gradient pulse. After they are encoded, the second 90° rf pulse stores half of the spins (either those along the x- or y-axis) parallel to the static external field (z-axis) where the spins are subject to minimal relaxation during the diffusion time (Δ). The third 90° rf pulse takes the spins out of storage so they can be encoded the second time for position and finally the second half of the stimulated echo from the three 90° rf pulses is collected.

second diffusion gradient could tag for position at the end of the diffusion time. The great advantage of this sequence is that the only relaxation parameter that attenuates the signal during the potentially long waiting period between the second and third 90° pulses is T_1, which is the longest possible relaxation time the magnetization can experience.

The sequence was a slight modification of a commercially available sequence by Varian (stepuls.c, see appendix C). The main modification was to the phase cycling, i.e. the series of directions in which the 90° rf pulses were applied in subsequent iterations of the MR sequence. In general, phase cycling is used to ensure that any spurious signals are canceled out as the signal is collected while the desired signal is reinforced. The phase cycling in the commercially available version of the stimulated echo sequence handled this function of the phase cycling perfectly. However, it only stored spins that were along one of the two transverse directions prior to the 2nd rf pulse. Because some of the diffusion measurements in this study were taken at small b-values, the dephasing of the spins due to the diffusion tagging was occasionally very small, often spread less than 180°. It therefore made a great deal of difference whether the x or y axis was chosen for longitudinal storage. Storing the magnetization from only one of the two transverse directions means that the attenuated signal will be either incorrectly large or incorrectly small, depending on whether the dephasing cluster is around the axis that was stored or not. To negate this effect, an 8-step phase cycle was used that stored magnetization from the x axis for 4 steps and magnetization from the y axis for 4 steps. The modified phase cycle was tested with a water sample to ensure that the echoes and fids had the correct relative phases in each individual step and that all echoes and fids, which the exception of

the stimulated echo, canceled out when all eight steps were added together at the end of the cycle. A more through discussion of this topic can be found in appendix C.

A second minor modification made to the sequence was a correction to the calculation of the b-values. The sequence, as written, used the magnetogyric ratio (γ) for ^{1}H, regardless of the nucleus used in the experiment. This was easily corrected by multiplying the results by the square of the correct ratio of gammas (γ_{3He}/γ_{1H}, for example).   Six b-values were used for each diffusion measurement.

2.5 Sequence Testing

2.5.1 Water

The stimulated echo diffusion was first tested on a water phantom (doped with copper sulfate to reduce T_1) using parameters (especially b-values) similar to those to be used on the lung tissue samples. It was determined that an echo time of 4 ms was necessary to allow sufficient rise and especially fall times for the gradient pulse strengths used in this study. With the pulse widths used in this study (0.4 ms for the diffusion gradient pulses and 100 µs for the rf pulses), this left about 1 ms between the end of the first gradient pulse and the start of the 2nd rf pulse and 1 ms between the end of the second gradient pulse and the peak of the stimulated echo (Fig. 2.2). No reduction in signal due to diffusion was observed, in accordance with expectation for the slow diffusivity of water and the small b-values used (chosen to be suitable for use with the more rapidly diffusing gases in the lung sample). This negative result confirmed that the two diffusion gradient pulses were not causing extraneous attenuation. Any attenuation in signal due to the diffusion gradients in the sequence should be due to diffusion in the sample, rather than an inequality of the two diffusion gradient pulses, for example.

2.5.2 Bulk Gas Samples

Next the diffusion sequence was tested with bulk gas samples. This test served a dual purpose: The literature has known values for both T_1 and free diffusion for C_3F_8 and helium/oxygen mixtures, so this preliminary experiment served to test our experimental set-up with known samples and known results. The second function of the bulk gas experiment was to establish the relationship between gas concentration, T_1, and free diffusion for later use with the lung samples. This relationship is discussed in detail in Appendix A. A brief discussion is presented here.

Because it was vital to know what the free diffusion of the gas in the sample was in order to calculate both the reduced diffusion (D/D_0, were D_0 is the free diffusion) and the diffusion length ($\sqrt{D_0\,t_{diff}}$) and because it was impossible to measure the free diffusion once the gas was in the lung core, an alternative method was used. Ideally, one might hope that by filling the sample cylinder to a known pressure with a gas with a known free diffusion would suffice, but there were concerns about the possible effects of formalin vapor or out-gassing from the lung tissue on the free diffusion. Consequently, a second test was used. Since T_1 of the MR gases is not expected to be affected by the presence of the lung tissue, it was possible to measure T_1 in each lung sample and use the T_1 measurements made in bulk gas to calculated the gas's concentration in the sample cylinder. The free diffusion of the bulk gas was also measured with respect to the gas's concentration, resulting in the following relationships. For C_3F_8:

[2.2]
$$D_0 = \frac{1}{2570(1/_{cm^2})T_1 - 5.41(s/_{cm^2})}$$

31

For helium:

[2.3]
$$D_0 = \frac{1}{1.78(s^2/cm^2)\frac{1}{T_1} - 0.528(s/cm^2)}$$

Since the relationship between concentration of the MR gas in the mixture and free diffusion was known from the measurements with bulk gas, it should be possible to determine the free diffusion of the gas in the lung sample, despite the fact that there was no unrestricted gas in the sample available for a direct measurement.

During diffusion measurements on the samples, an experiment was performed to test the validity of the above theory. A second, empty, cylinder was placed in series with one of the lung samples (Fig. 2.3). The second cylinder did not contain any lung tissue and thus could serve as a way to measure both T_1 and free diffusion of the bulk gas. The two cylinders were filled in series, by flowing gas through both cylinders simultaneously. The cylinders were attached in such a way that the gas flowed first through the cylinder containing lung tissue and then through the bulk gas cylinder. This flow pattern helped ensure that if there was any effect on T_1 or D_0 from the MR gas being in contact with the lung tissue (from out-gassing from the lung or formalin vapor, for example) the effect would appear in both cylinders. Once sufficient gas had flowed through the container to fill the space with the expected gas mixture, the outside valves on the containers were shut, while the valve connecting the two cylinders was left open, so that the two cylinders remained in communication with each other. Then T_1 was measured in both cylinders and free diffusion measurements were made in the bulk gas cylinder. The T_1 measured in both cylinders was used to calculate the expected free
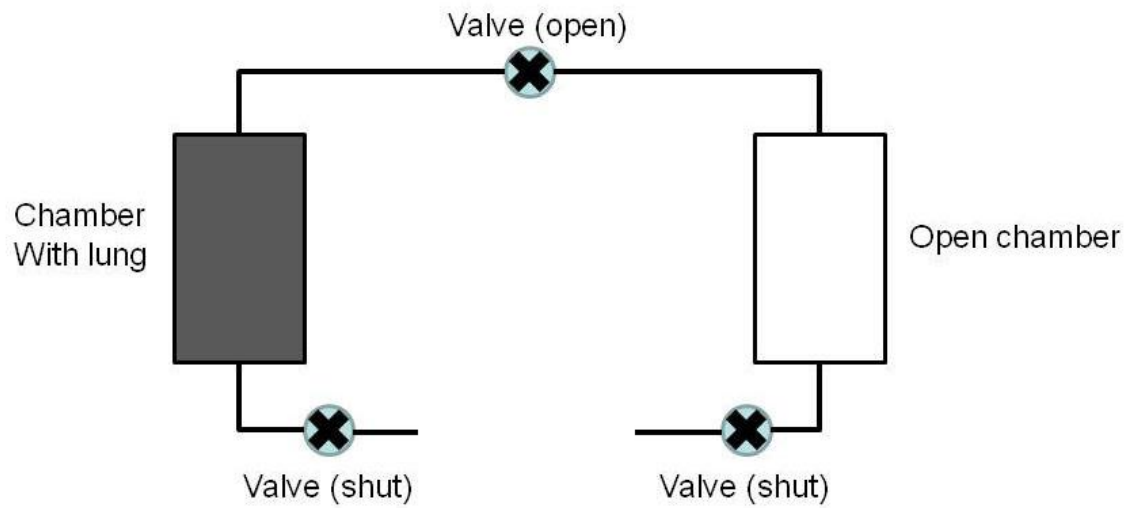
Figure 2.3. Diagram of a cylinder with a lung sample in series with an open cylinder used to test the T_1 and D_0 relationships for the gases used in the study. The two cylinders were in constant communication with each other through the open valve connecting them and were filled by flowing the same gas though both cylinders, and thus they were filled with the same gas mixture.

diffusion from Eqs. 2.2 and 2.3, which was then compared with the measured free diffusion. The measured T_1s from both types of gas agreed with each other within 2%. The free diffusion coefficient measured in the bulk gas and the free diffusion calculated from T_1 in the lung sample (for both types of MR gases) agreed within 6.5%. Consequently, T_1 was considered to be a reliable way to find the free diffusion of the gas in the lung cylinders, and the extra bulk gas cylinder was not routinely used with the remaining lung samples in order to ration gas (in particular, the precious helium-3 gas) and simplify the experiment.

It should be noted that in a helium/oxygen mixture, the T_1 of helium depends only on the partial pressure of oxygen. Therefore measuring T_1 in the lung sample gas mixture will not provide warning of a loss in the partial pressure of helium such as by permeation of the helium through the cylinder walls. This concern about helium loss was why the initial height of the fid from a single 90° rf pulse was measured at the start of each set of diffusion experiments. Given that the volume inside the rf coil remained consistent with each lung sample, the fid height ought to remain consistent as well, assuming the amount of helium in the sample has not changed. So long as the diffusion measurements in the sample were made within two weeks of filling the sample cylinder with helium, the fid height was found to be constant.

Chapter 3 - Sample Preparation

3.1 Lung Samples

The human lung samples for this study were obtained through the Washington University medical school lung transplant program. Generally, only a right or left lung was received, rather than a complete set. The majority of lung samples used in the study were diseased lungs removed from transplant patients. One healthy donor lung was deemed unsuitable for transplant and was given to this study.

Each lung was prepared within 48 hours of surgery. Before fixation the lung was fitted with a barb fitting attachment. First tubing of an appropriate matched size was sewn onto the bronchus of the excised lung. The tissue-tubing seam was sealed with Vetbond glue (3M, St. Paul, MN, USA) and a barbed fitting was placed in the free end of the tubing and secured with cable ties, allowing the lung to be attached to a breathing bellows and later to the fixation box apparatus. The seams of the tubing and barbed fitting were covered by a thin latex tube (a cut finger from a latex glove), which was then secured with Vetbond glue (Fig. 3.1). This arrangement helped prevent gas leaks and consequent deflation while the lung was being fixed. After the glue had dried the lung was attached to a bellows and inflated. Because of the nature of the diseased lungs, the lung often had to be "massaged" by (gloved) hand to encourage uniform distribution of air throughout the lung. Gently rubbing the tissue while it was being inflated by the bellows helped move gas through airways that had partially or fully collapsed as the lung deflated after removal from the body. While inflated the lung was also tested for leaks, often arising from small cuts suffered during surgery or the transportation process. Leaks in the lung were repaired by gluing small pieces of latex over the punctures as they were identified.

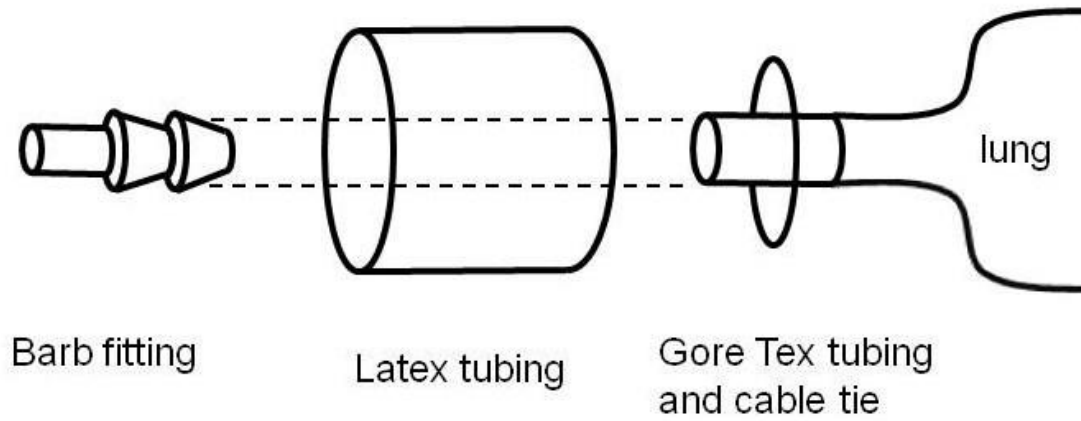Barb fitting Latex tubing Gore Tex tubing and cable tie lung

Figure 3.1. Preparation of the lung's main airway for attachment to external breathing devices. Gore Tex tubing is sewn directly onto the lung and then fitted onto a barb fitting and secured with a cable tie. The connection is covered with latex tubing and all seams are sealed with Vetbond glue.

3.1.1 Fixation

Once the lung was able to hold a minimum pressure of 10 inches of water (0.024 atm) it was transferred to the fixation box, designed by Rick Jacob and Jason Woods. The fixation box is a large, clear plastic box about three feet by two feet by two feet, with a barbed fitting attachment on the ceiling of the box for the lung bronchus/tubing arrangement, a shelf to rest the weight of the lung, and reservoir for a solution of 50% formaldehyde with a heating coil submerged in it (see Fig. 3.2 for a simplified diagram and appendix B for a more complete description). The barbed fitting attachment on the ceiling is attached to an apparatus that imitates a human breathing cycle. Since the lung was to be fixed at nearly normal lung capacity, the lung was placed under a pressure differential of no more than 10 inches of water, as measured by a water column integrated into the breathing apparatus. The inhale/exhale cycle was approximately 10 seconds long with a 1 second exhale. Breathing the lung during fixation (rather than simply inflating it) prevented the formalin vapor from pooling in the lung. While the lung was fixing, the temperature in the box was kept at 47° C to ensure there was plenty of formalin vapor available. A small window wiper on the door of the fixation box allowed formalin condensation to be wiped away so the fixation progress could be monitored. The change in volume between exhalation and full inhalation of the lung became less pronounced as fixation progressed, but even when the lung was completely fixed a slight change in volume was observed between the inhale and exhale portion of the breathing cycle. Each lung was breathed in the heated fixation box between 10 and 14 hours, more than enough time to thoroughly fix all the tissue in the lung. At the end of fixation the heater was turned off to allow the remaining formalin vapor to condense into the reservoir and the
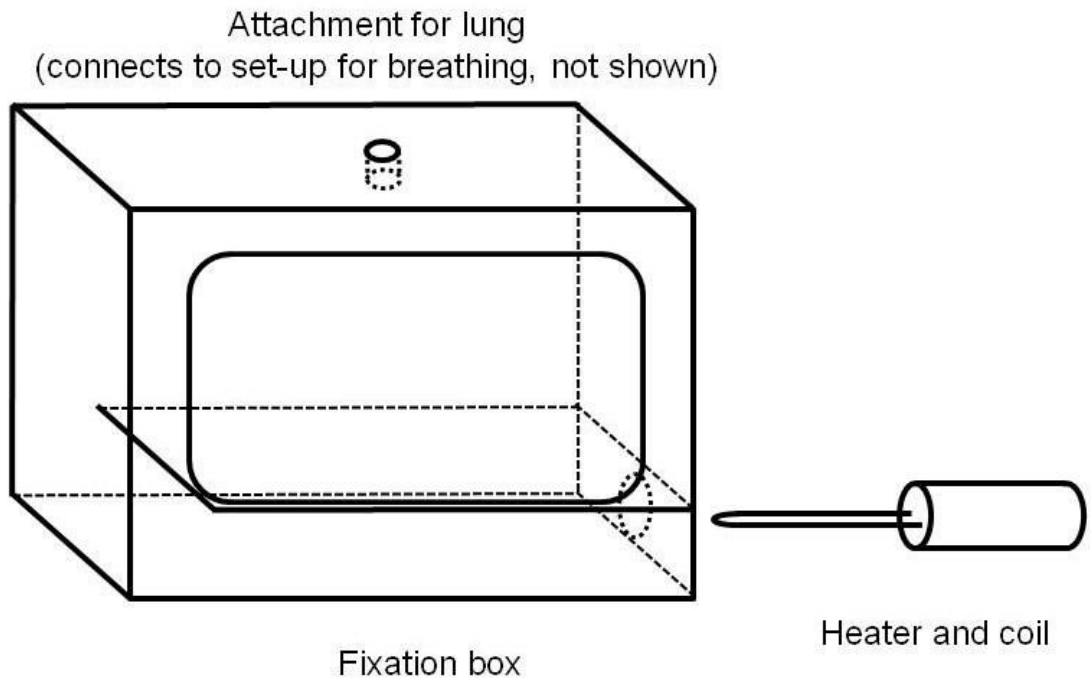
37

Figure 3.2. Apparatus for formalin fixation of lungs while breathing them. The box has a door on the front, attached by screws and sealed by an o-ring. The lung's large airway is attached to the fitting on the top of the box while the bulk of the lung rests on the interior shelf. The bottom of the box is filled with formalin and a heating coil (here shown outside the box) heats the formalin into vapor.

fixed lung tissue to cool. The lung was breathed during the cooling process, which took a
few hours.

3.1.2 Freezing and Cutting

Because the lung tissue is very hard to cut accurately when it is pliable, the lungs
were frozen overnight or longer (in the case of the healthy and emphysematous lungs, the
storage happened to be for much longer, on the order of years). After being frozen solid
the lungs were cut into two inch-thick slabs using a band saw that was dedicated to tissue
preparation. The slabs were then refrozen. Then sample cores were cut from the slabs
using a cylindrical meat cutter made of hardened steel, of 1 3/8 inch diameter (see
appendix B for details). All the coring paraphernalia (meat cutter, a plastic cutting board,
and plastic cylinder to assist in removing the sample core from the meat cutter) were pre-
frozen beforehand to help keep the lung tissue from thawing during cutting and to keep
the meat cutter from shattering during cutting (the thin cutting edge was found to be
vulnerable to cracking when subjected to the stress of cutting while simultaneously
undergoing an extreme change in temperature from room temperature to near 4° C).
During cutting the lung and all coring paraphernalia were kept in a Styrofoam ice chest
with dry ice to keep them cool.

3.1.3 Gas Filling

After cutting, the cores were placed in specially prepared cylinders (see Fig. 3.3 for a
photograph of the lung cylinder set-up). A few drops of 10% formalin solution were
added to the samples to keep them from drying out and the sample cylinders were glued
shut with 5-minute epoxy (Devcon) and, once the glue was dry, the sample cylinders
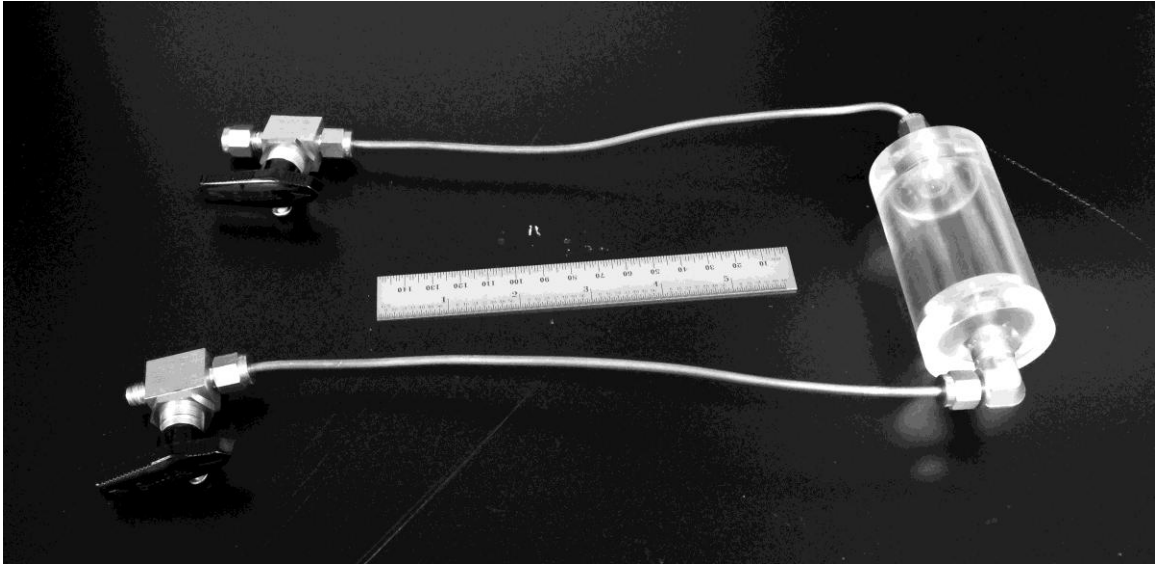were filled with the MR gas.

Figure 3.3. Photograph of the lung sample container. The lung sample is placed inside the plastic cylinder and the lid (show in place on the cylinder) is glued on. The cylinder has copper tubing leading to valves that can be opened to flow gas into the sample. A six inch ruler is placed in the image for scale.

The gas filling procedure was slightly different for octafluoropropane (C_3F_8) and helium. For C_3F_8 the gas was simply flowed neat through a regulator into the sample. In the case of the helium/oxygen mixture, the gas was first prepared by filling a 150 cc mixing chamber on a gas apparatus to a given pressure with helium (generally 7.7 psig), shutting the mixing chamber and evacuating the rest of the gas apparatus and then filling the apparatus with oxygen to pressure above that of the mixing chamber (so that oxygen would flow into the mixing chamber when it was opened, rather than helium flowing out). The mixing chamber was opened and filled with oxygen to the desired total pressure (generally 30 psig) for a 50/50 mixture of gases. Then the mixing chamber was immediately shut again, removed from the gas apparatus and shaken (small metal balls in the mixing chamber helped fully mix the two gases; concentration gradients are very slow to equilibrate by diffusion alone).

Each time before a sample was filled with gas a few extra drops of 10% formalin were added in an effort to keep the lung tissue from drying out. After the gas and sample were prepared, the gas or gas mixture was flowed slowly through the sample at a rate of about 10 ml/hr. This filling method was used to avoid subjecting the lung tissue to extreme changes in pressure (such as would be experienced under vacuum). Such pressure stresses can easily damage the delicate tissue and destroy the lung geometry this experiment is endeavoring to study. The gas was flowed through the tissue and out into a water bath, which prevented backflow of air and ensured that the total pressure of the imaging gas in the tissue was 1 atm (Fig. 3.4).

Large volumes of gas were not flowed through the samples for fear of drying out the tissue, which would cause it to shrink. Enough gas was flowed through the sample to
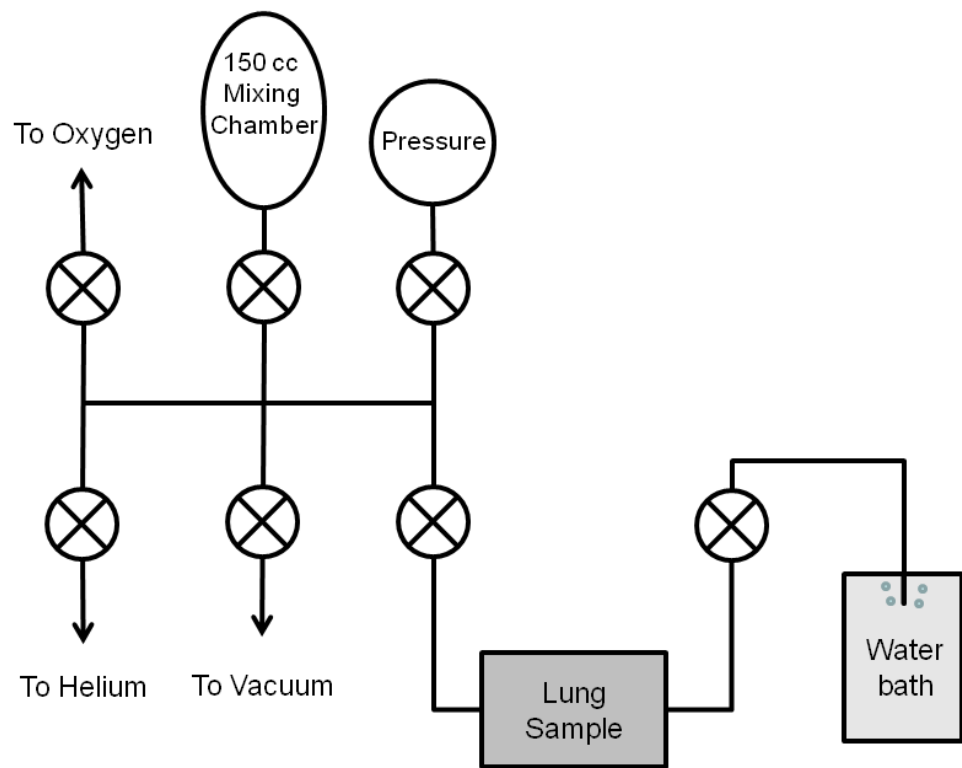
41

Figure 3.4. Gas apparatus for filling the lung sample with helium. While the pressure is monitored with the pressure gauge, the mixing chamber is filled with helium and oxygen and then the gas mixture is flowed through the lung sample with excess gas flowing out through the water bath.

fill the volume of the sample cylinder and the various tubing used approximately three times (at pressures and temperatures near STP, which was the constant condition of the samples). The volume was estimated by noting the gas flow rate and timing the length of the fill. This method of filling was found to ensure that the sample was well filled with the desired gas without damaging the tissue. Just before the sample cylinder was closed off, the exhaust tube was raised to less than 1 cm below the water surface, insuring that the total pressure was no more than 0.001 atm greater than atmosphere.

3.2 Histology Slides

For all lung cores, slides were made of the tissue so that the mean linear intercept could be measured for each sample. The mean linear intercept of lung tissue is used by the medical field as a way to quantify tissue damage in emphysema[1,2,3]. In most cases, after all diffusion measurements were made the sample containers were cut open and the tissue was retrieved to make slides. In one case (the IPF sample), tissue immediately adjoining the cut lung cores was used to create the tissue slides instead. Because the IPF sample was expected to be uniform with regards to mean linear intercept and diffusion MR properties, using different tissue from a nearby area of the lung for the diffusion measurements and the histology measurements should be acceptable (in this study, the IPF sample is expected to have the properties of a healthy lung). The tissue was sent off to be processed into slides by Dr. Richard Pierce's lab.

[1] A.A. Robbesom, E.M. Versteeg, J.H. Veerkamp, J.H. van Krieken, H.J. Bulten, H.T. Smits, L.N. Willems, C.L. van Herwaarden, P.N. Dekhuijzen, T.H. van Kuppevelt, Morphological Quantification of Emphysema in Small Human Lung Specimens: Comparison of Methods and Relation with Clinical Data, Mod Pathol, 16 (2003) 1-7.

[2] E.R. Weible, Principles and methods for the morphometric study of the lung and other organs, Lab Invest, 12 (1963) 131-155.

[3] M.S. Dunnil, Quantitative methods in the study of pulmonary pathology, Thorax 17 (1962) 320–328.

Chapter 4 - Methods and Analysis

4.1 Lung Samples

A total of nine lung cores were studied, from five different lungs. Two cores were from one emphysematous lung, four were from one healthy lung, one was from an Interstitial Pulmonary Fibrosis (IPF) lung, one was from a sarcoid lung, and one was from a healthy pig. IRB and ASC approval was obtained for the collection of all samples.

As stated in chapter 3, two homebuilt single turn solenoid rf coils were used. The coils were at least 3 cm smaller in length than each of the lung samples and the coils were placed so that the signal did not include contributions from the ends of the sample cylinders where a very small amount of free gas generally remained. Occasionally, part of the lung core was slightly damaged during sample preparation. Often this damage was confined to one end of the lung core, usually resulting from difficultly cutting through the last bit of the frozen tissue with the meat cutter. When the damage only affected a small area of the core the sample was not rejected. Instead the rf coils were selectively placed away from the damaged area and over the intact area of the lung sample. Measurements were taken at a range of diffusion times, between 3 ms and 100 ms for C_3F_8 (100 ms being approximately five times T_1 for this gas) and between 3 ms and 1300 ms for the helium/oxygen mixture. For spectroscopy (non-imaging) diffusion measurements 6 b-values were used, with the maximum b-value being the best approximation for a signal attenuation of 1/e. All spectra had a signal to noise (SNR) ratio of at least 18[1]. Signal averaging was exploited to achieve these SNR. The collection of b-values was interleaved so as to remove any time-based bias that might affect the measurements. An

echo time (*TE*) of 4 ms was used, as was determined by prior diffusion measurement with water. The maximum gradient pulse amplitude was 20 G/cm. The width of the gradient pulses was 0.4 ms (Fig. 4.1).

4.2 Analysis of Diffusion Measurements

The diffusion analysis was performed with Matlab software. The half echoes collected during the pulse sequence were acquired (the positive halves of the echoes, at and after the echo peaks, were collected), the phase was corrected and the sum of points 2 through 5 of the second half of the echo was calculated. The first point was neglected as it was tainted by spurious signal from the receiver which was turned on shortly before the first acquisition.

Restricted diffusion does not result in mono-exponential decay of signal as a factor of *b*, although at many small b-values, such as were used in this study, the deviation from a monoexponential decay is small. However, even at such small signal attenuation (1/e), non-monoexponential decay was still quite pronounced in some cases (ex. Fig. 4.2). Consequently the 6 diffusion data points from the 6 b-values were not fitted to the simple mono-exponential curve ln(*S/So*) = -*bD* but instead were fitted to a kurtosis curve:

[4.1]
$$\ln(S/S_0) = -bD + \frac{1}{6}KD^2b^2$$

Occasionally the signal for the sixth b-value was dropped if the signal attenuation was much greater than 1/e and only 5 b-values were used. This peculiar method of selecting maximum b-values was used because of the wide range of apparent diffusion coefficients measured. Because the signal decay is not mono-exponential for restricted diffusion, the
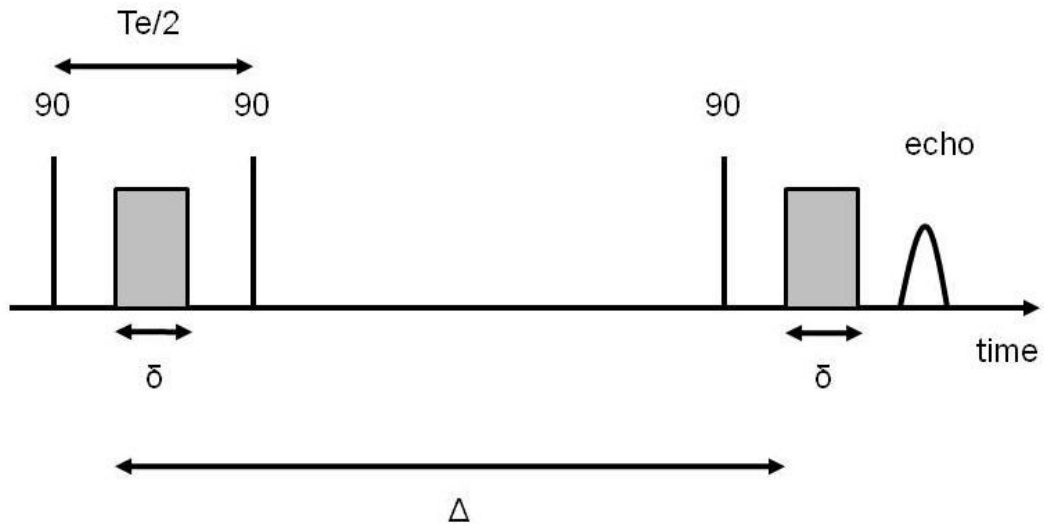
Figure 4.1. A diagram for the stimulated echo sequence. For this study $\delta = 0.4$ ms, $TE =$ 4 ms, Δ ranges from 3-100 ms for C_3F_8 and 3-1000 ms for the helium/oxygen mix, and the maximum gradient pulse amplitude used was 20 G/cm. The two diffusion gradient pulses occurred just after the 1st and 3rd 90° rf pulses (which are 100 μs long), leaving about 1 ms between the end of the first gradient pulse and the start of the 2nd 90° rf pulse and the end of the second gradient pulse and the echo peak.
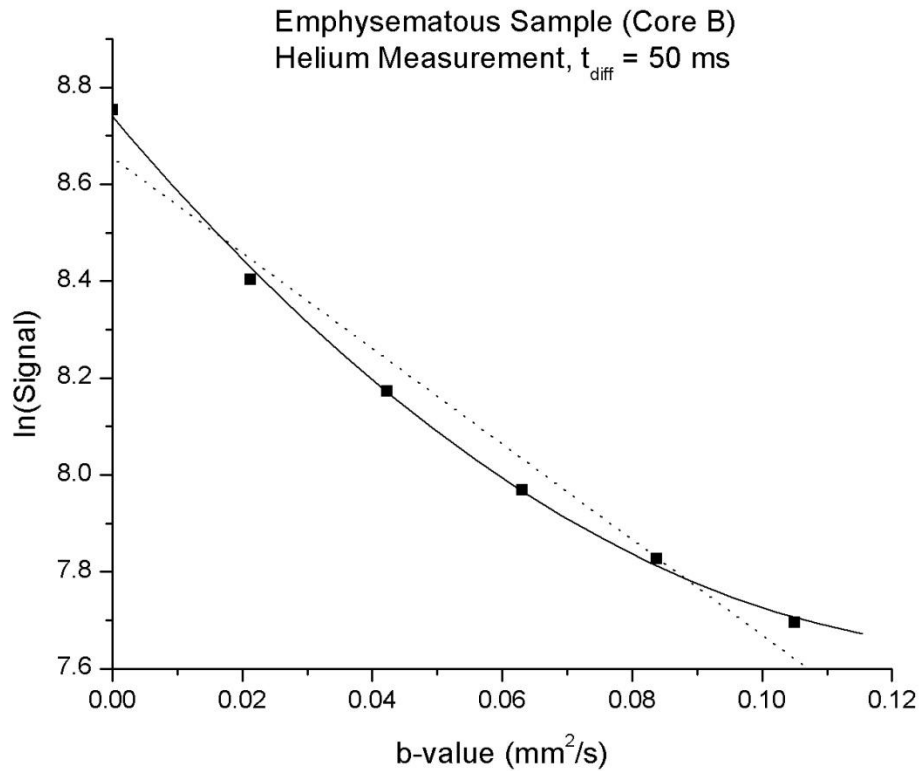
Figure 4.2. A sample of diffusion signal attenuation. The signal attenuation is clearly not monoexponential (note that the vertical axis plots the log of the signal). The dash line is a fit to a monoexponential equation, $ln(S) = (8.66 \pm 0.06) + (-9.9 \pm 0.9)(s/mm^2)b$. The solid line is a fit to equation 4.1, a kurtosis fit, where the exponent has terms in b and b^2, $ln(S) = (8.74 \pm 0.02) + (-15.9 \pm 0.8)(s/mm^2)b + (58 \pm 7)(s^2/mm^4)b^2$.

measured diffusion coefficient depends on which b-values are used to measure it. The wide range of diffusion coefficients in this study made it impossible to select one b-value or even just a few b-values for each type of gas measurement. Although selecting an appropriate range of b-values for each diffusion measurement involved guessing at the diffusion coefficient (the object of the measurement), it did provide a consistent method to measure diffusion across a vast array of apparent diffusion coefficients. As the precise calculation of the maximum b-value for each measurement requires knowing the diffusion coefficient being measured, this maximum b-value was a best guess. If the guessed maximum b-value proved to be only slightly too large, the 6th point was dropped and only 5 points were used. If the guess was quite incorrect the measurement had to be redone. Quick preliminary "scout" diffusion measurements were done for each lung at a few diffusion times to ensure that very few measurements had to be repeated. All accepted spectra measurements had a signal to noise ratio of at least 18, above the SNR threshold for accurate restricted diffusion measurements[1].

4.3 Histology Slides

Two slides were made from each of the samples. In most cases, the tissue for the slides was taken directly from the core itself after all diffusion measurements were made, but in one case (the IPF lung sample) the tissue for the slide was taken from lung tissue immediately adjoining the sample tissue. The tissue was processed into slides by Dr. Rich Pierce's lab and then a series of images were taken under the microscope at 5x objective lens. These images were stitched together in Photoshop to create approximately a 5 mm x 5 mm image. Two sections were taken from each of the two slides for each core, making four sections in total for each lung sample. A collection of

seven vertical lines, spaced evenly 0.43 mm apart from each other, was placed over each

quadrant of a slide section in turn and the number of tissue interceptions with each line

was recorded. Quadrants that happened to contain blood vessels were discarded. The

same measurements were taken for a similar collection of horizontal lines. For each

collection of lines, the number of tissue interceptions was averaged and then the total

length of each line (2.57 mm) was divided by this average to give the mean linear

intercept, which was then divided by 0.8 to account for tissue shrinkage due to formalin

fixation and slide preparation[2,3]. The corrected average and standard deviation of mean

linear intercepts of each selection are reported later for each sample.

[1] R.L. O'Halloran, J.H. Holmes, T.A. Altes, M. Salerno, S.B. Fain, The effects of SNR on ADC measurements in diffusion-weighted hyperpolarized He-3 MRI, JRM 185 (2007) 42-49.

[2] A.A. Robbesom, E.M. Versteeg, J.H. Veerkamp, H.J. van Krieken, H.J. Bulten, H.T. Smits, L.N. Willems, C.L. van Herwaarden, P.N. Dekhuijzen, T.H. van Kuppevelt, Morphological Quantification of Emphysema in Small Human Lung Specimens: Comparison of Methods and Relation with Clinical Data, Mod Pathol, 16 (2003) 1–7.

[3] L.N. Willems, J.A. Kramps, T. Stijnen, P.J. Sterk, J.J. Weening, J.H. Dijkman, Relation between small airways disease and parenchymal destruction in surgical lung specimens, Thorax, 45 (1990) 89-94.

Chapter 5 - Results and Conclusions

The diffusion and histology results for each lung core are presented. The diffusion results for each sample are given in two plots: one which shows D/D_0 for all diffusion lengths measured in this study and one which displays the details of the short diffusion length measurements.

5.1 Healthy Lung Samples

The healthy samples (cores 2, 3, 6 and 7) were taken from different areas of the same lung, removed from the donor and fixed in early 2007. They were stored at $4°$ C until cut in mid 2009 (cores 2 and 3) and early 2010 (cores 6 and 7). Healthy lungs are a precious resource for transplantation into patients, given to research only when they are deemed unsuitable for transplant. Each core is considered individually here.

5.1.1 Healthy Lung Core 2

The histology slides (a typical slide is shown in Fig. 5.1) for core 2 show healthy human lung tissue, with alveoli intact and no sign of tissue damage. The corrected mean linear intercept measured for core 2 is 0.27±0.03 mm, which is within the range for fixed healthy human tissue reported in the literature (0.311±0.066 mm)[1,2]. We note that slides at this magnification give us no information about collateral paths in the sample (the pores of Kohn are approximately 2 μm in diameter while the slides are approximately 6.4 by 6.4 mm). The diffusion results for core 2 are shown in Fig. 5.2. The diffusion measurements make a smooth, continuous curve through all measured diffusion lengths, even at the boundary where the MR gas switches from C_3F_8 to helium. This continuity across MR gas types reaffirms the correctness of our choice to combine measurements

from the two gases by normalizing by their respective free diffusion coefficients and graphing against the diffusion length ($\sqrt{D_0 \, t_{diff}}$).

Two sets of helium measurements are shown, taken nearly two months apart, to demonstrate the reproducibility of the measurements. Because there is an appreciable loss of helium in the sample cylinders after a month, the sample had to be refilled with a helium/oxygen mixture before the second measurement. Although this is the only repeated set of measurements presented here, other samples demonstrated a similar reproducibly in both helium and C_3F_8 diffusion measurements.

The mean linear intercept is related to the surface to volume ratio by $S/V = 4/L_m$. As stated above, the literature reports $L_m = 0.311$ mm for healthy tissue so we expect S/V to be 129 cm^{-1}. Since the short diffusion length regime is limited by $\sqrt{(D_0 \, t_{diff})} \, S/V < 1$, the short diffusion length range for a surface-to-volume ratio calculation in healthy human tissue as suggested by Mitra et al. would be lengths less than 0.008 cm, clearly not possible here[3] as the smallest measured diffusion length is 0.014 cm.

The tortuosity limit (where diffusivity is independent of diffusion time) depends on many factors, including, perhaps most importantly in human lungs, collateral paths between the various airway branches. While we cannot say with confidence that a true limit is reached at long diffusion lengths, our measurements suggest that the diffusion length dependence becomes very weak after 0.4 cm.

5.1.2 Healthy Lung Core 3

As with core 2, the histology slides for core 3 (ex. Fig 5.3) show healthy tissue. The mean linear intercept for this sample is 0.25±0.02 mm, in agreement with the literature reported values. The diffusion curve for core 3 (Fig. 5.4) is similar to that of

core 2, both healthy samples from the same lung. Again, the curve appears to be continuous even across the boundary between the two MR gases. For long diffusion lengths, D/D_0 for core 3 has a weak dependence on diffusion length even for the longest diffusion lengths measured in this study.

5.1.3 Healthy Lung Core 6

As with the other two healthy cores, the histology slides for core 6 (ex. Fig 5.5) show healthy lung tissue. The mean linear intercept is 0.32 ± 0.02 mm, consistent with measurements for healthy tissue. The diffusion curve for core 6 (Fig. 5.6) displays little discontinuity across the gas boundaries and the intercept of the reduced diffusion appears to be close to 1. The diffusion length dependence becomes much weaker by 0.6 cm.

5.1.4 Healthy Lung Core 7

As with the other healthy samples, core 7's histology slides (ex. Fig. 5.3) are those of healthy tissue. The mean linear intercept (0.29 ± 0.04 mm) agrees with values in the literature. The diffusion measurements are shown in Fig 5.4. As with the other healthy cores, the SVR diffusion length range is not accessible for core 7. After a diffusion length of 0.8 cm, the reduced diffusion's dependence on diffusion length is very weak.
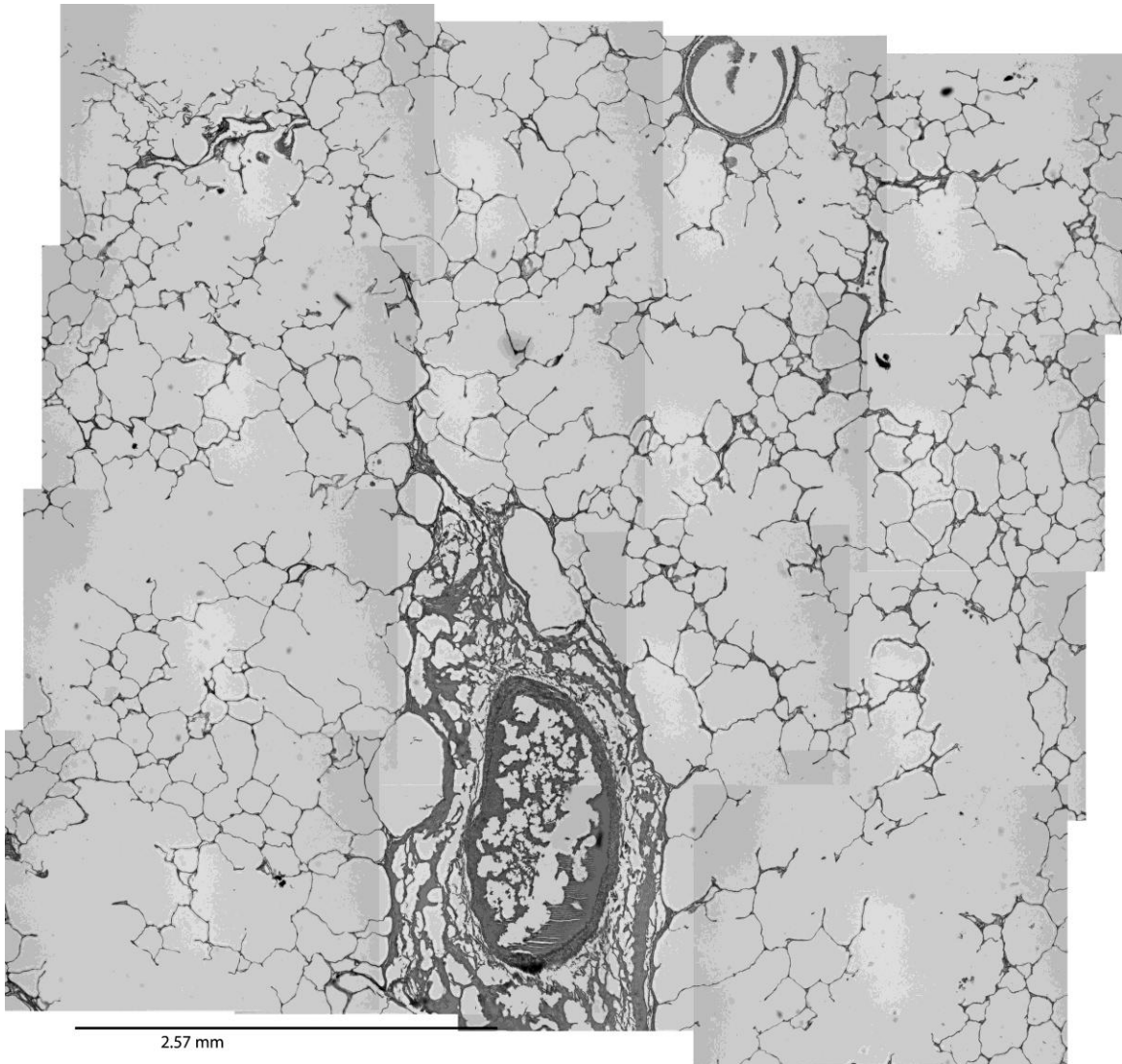
Figure 5.1. Healthy core 2 histology slide. A good cross section of alveoli and airways, with blood vessels. The vessel in the lower half of the side is filled with blood, with more blood around the edges.
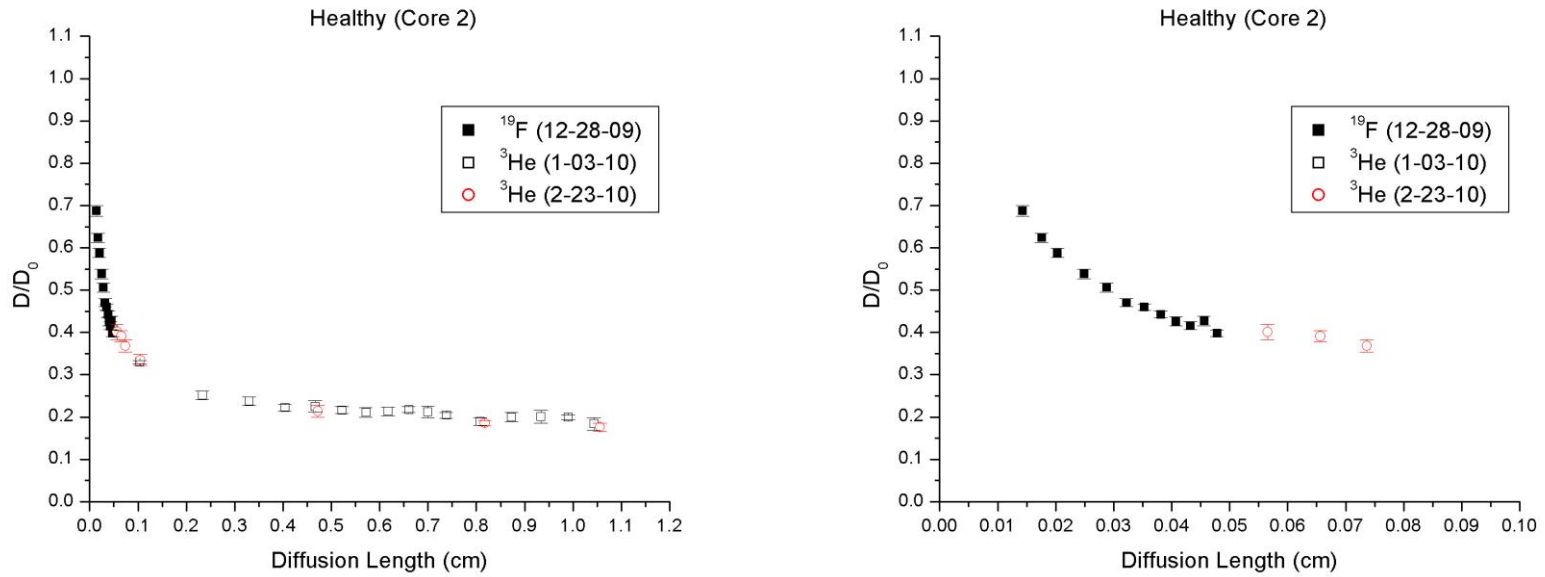
Figure 5.2. Diffusion results for healthy lung core 2. The results for each sample are presented in two forms: a full plot and an

expanded plot to show the details of the short diffusion length measurements. Although there is no overlap between the measurements

from the two MR gases the diffusion measurements appear to be continuous. In addition, the two sets of helium measurements (the

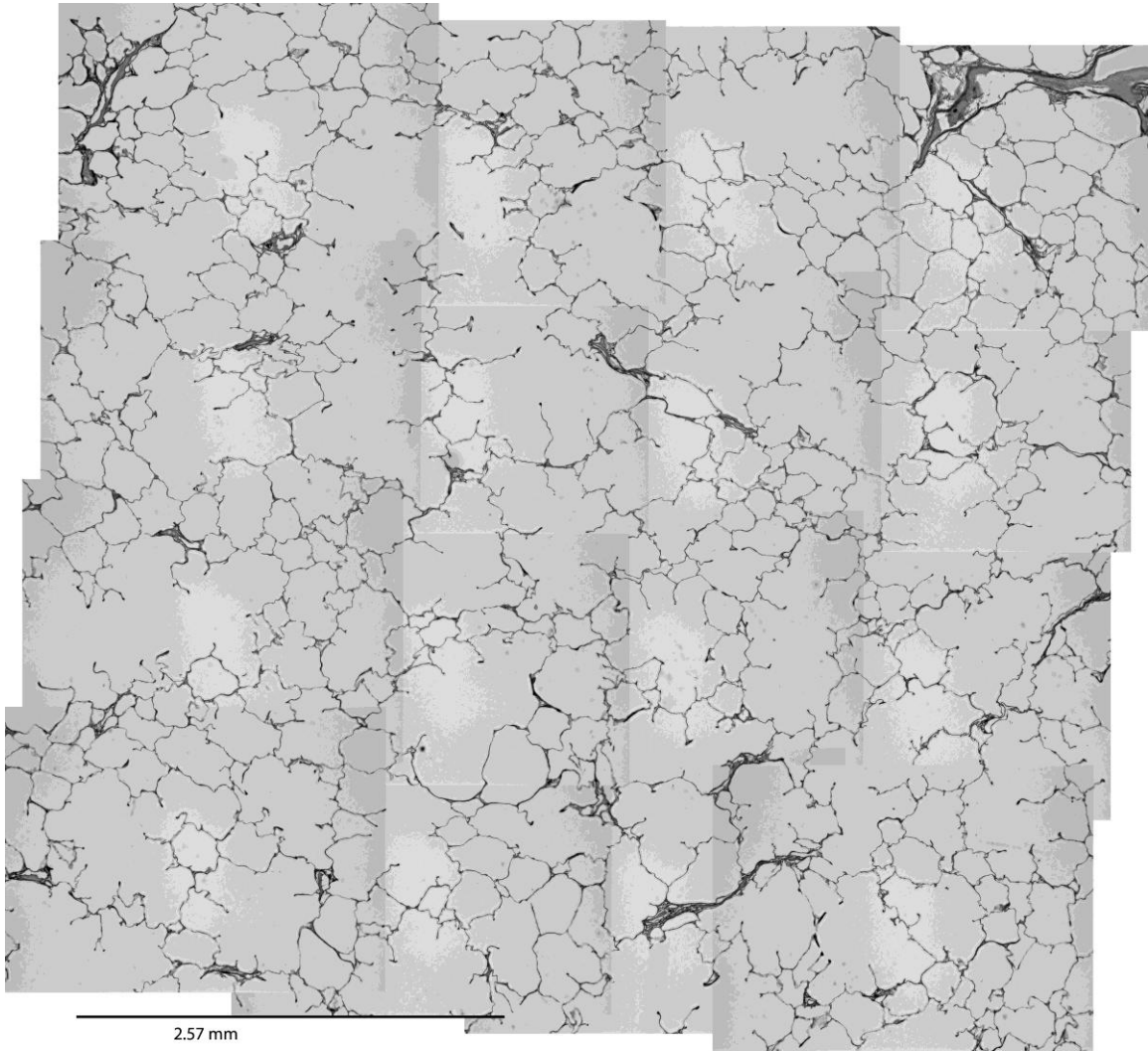open circles and squares), taken nearly two months apart, agree quite well.

2.57 mm

Figure 5.3. Healthy core 3 histology slide. There are no vessels in this slide, but in the

upper right corner there is a branching airway (the two branches are pointing towards the
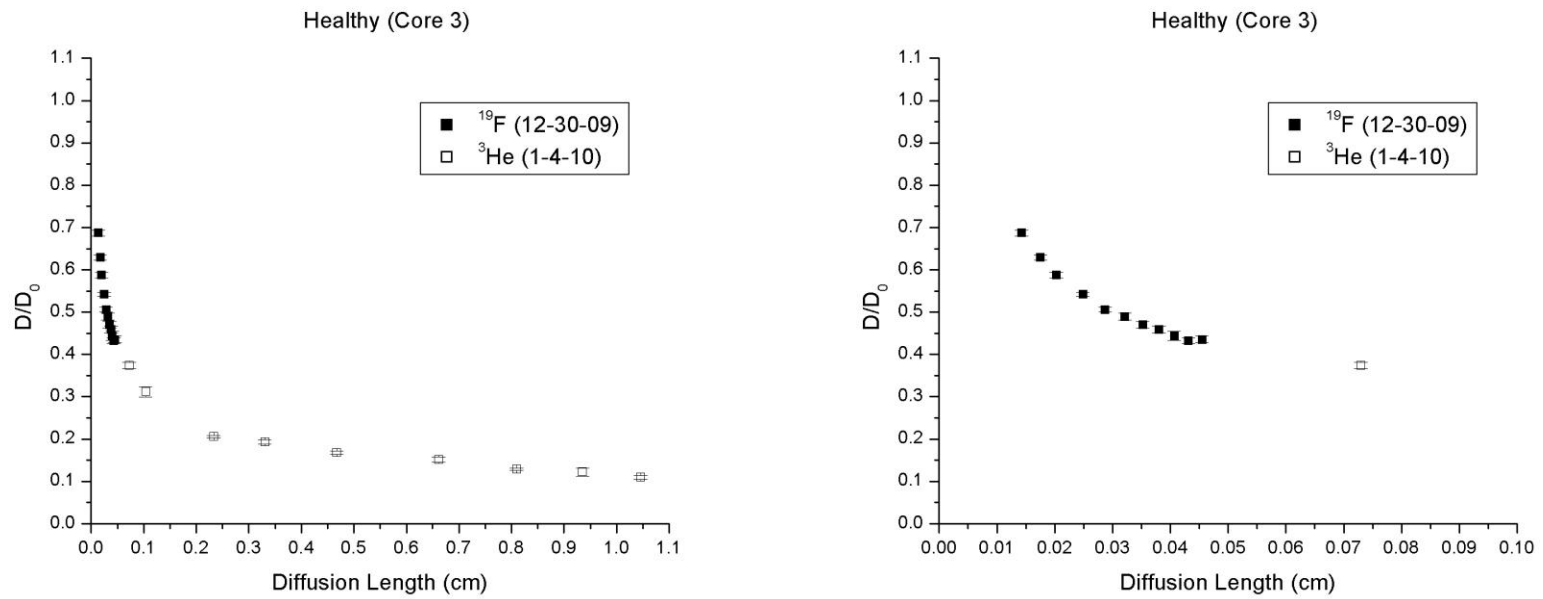
bottom of the image).

Figure 5.4. Diffusion results for healthy lung core 3. As with core 2, from the same healthy lung, there is no overlap between the measurements from the two MR gases, but the diffusion measurements appear to be continuous.
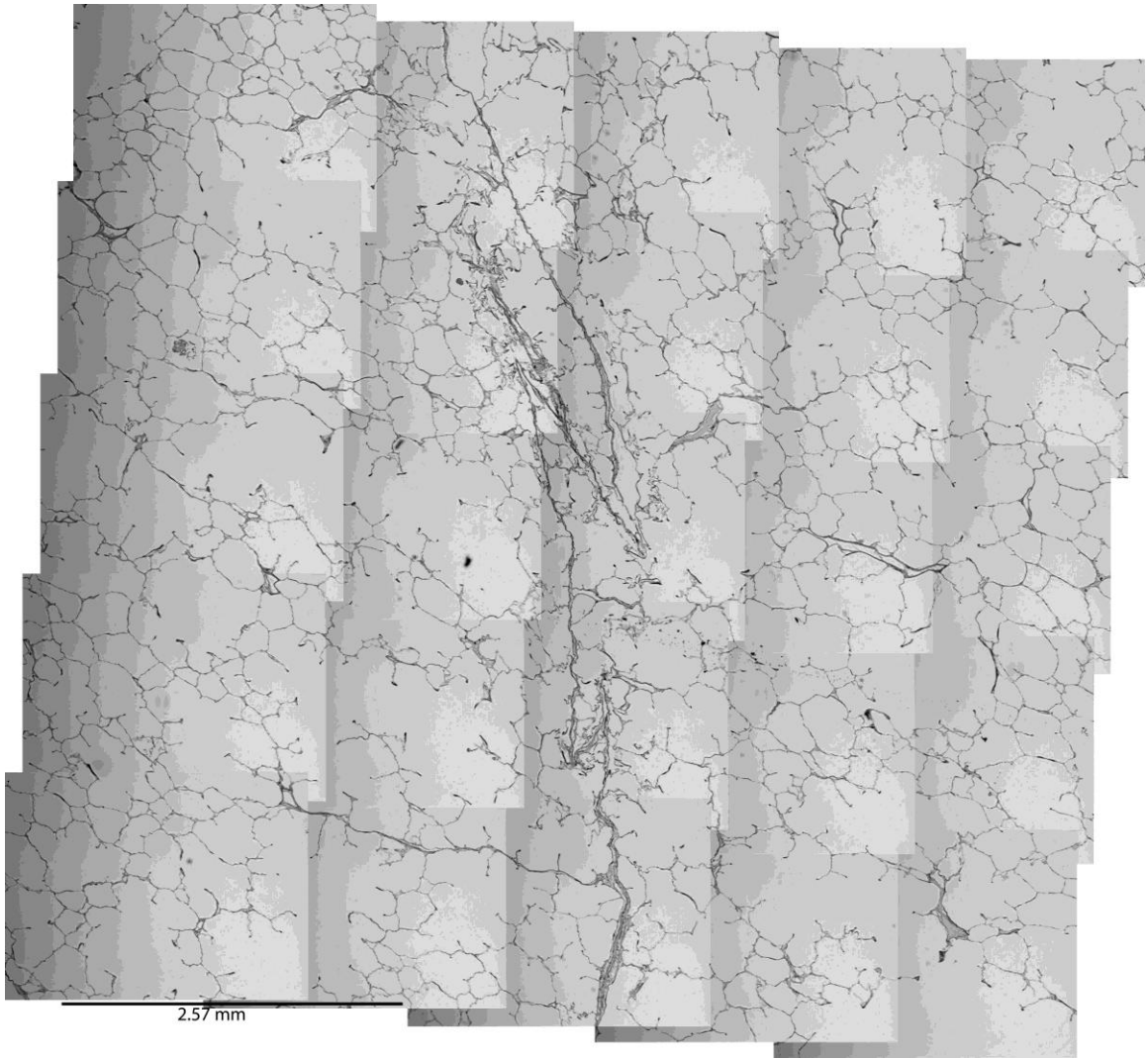
Figure 5.5. Healthy core 6 histology slide. Some airways and alveoli shown, with septa in the middle of the slide.
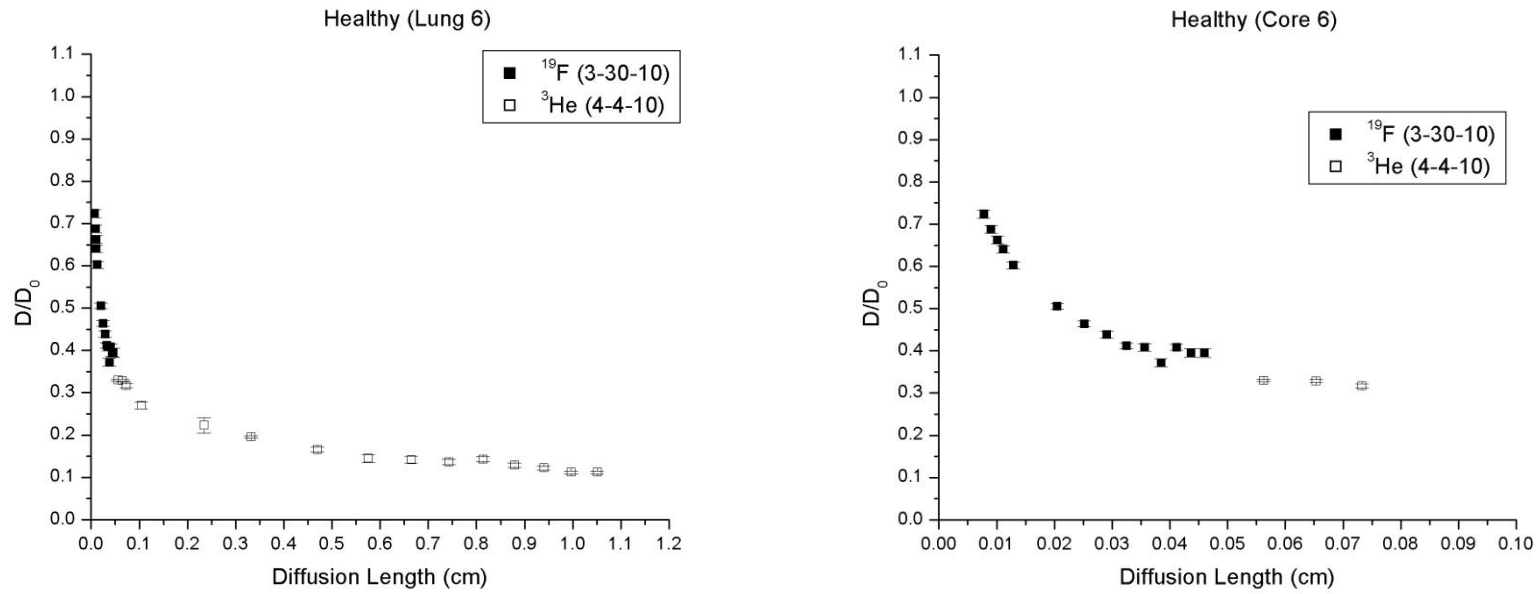
Figure 5.6. Diffusion results for healthy lung core 6. Again the measurements appear to be continuous. The short time diffusion measurements are consistent with the expected intercept of $D_0/D = 1$ when the diffusion length is 0.
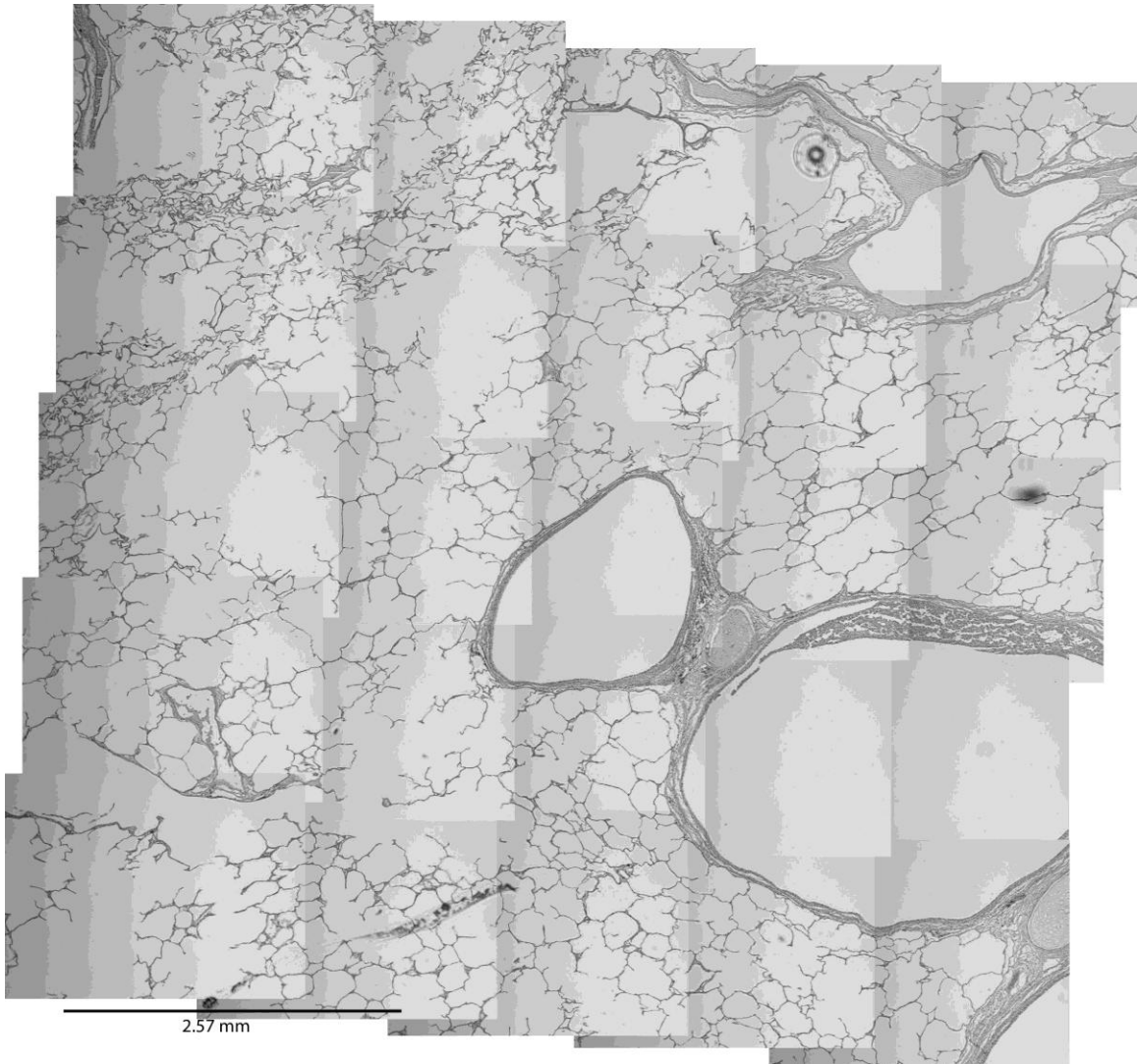
2.57 mm

Figure 5.7. Healthy core 7 histology slide. This slide has normal tissue with a number of

large vessels (to the right) and airways (to the left). There are also some flaws on the

slide, unrelated to the tissue (circle in the upper right and a smudge on the right)
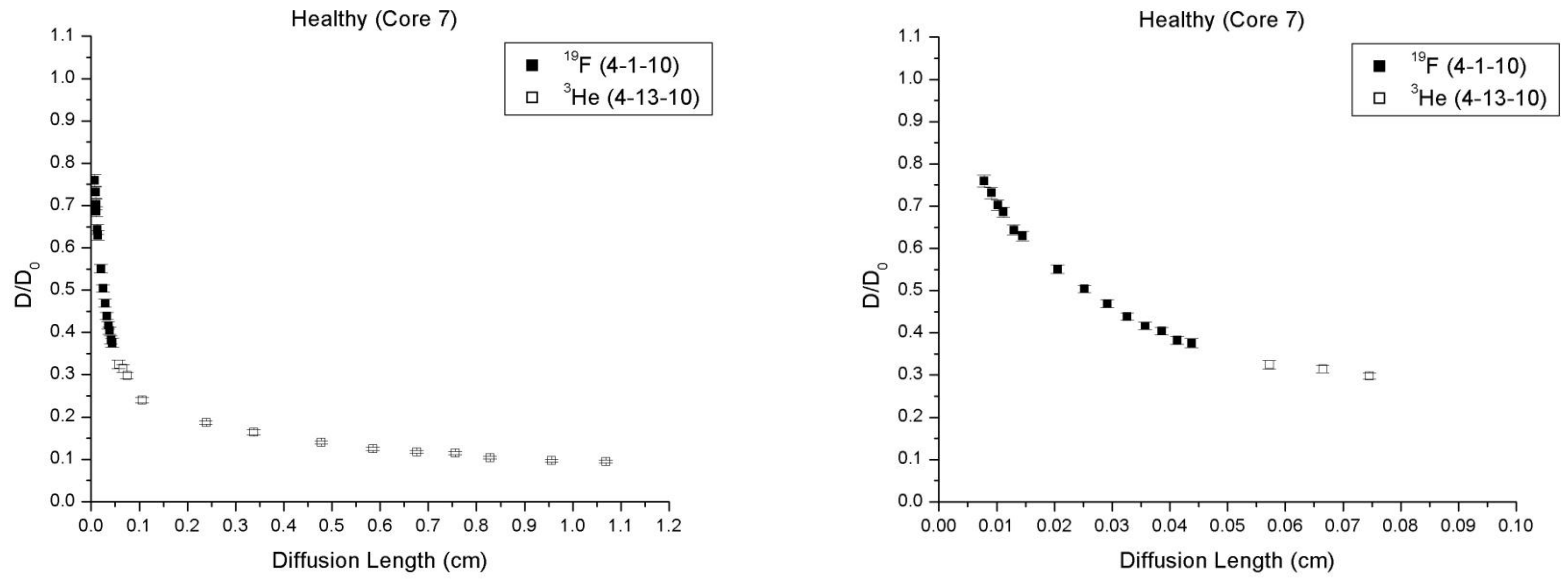
Figure 5.8. Diffusion results for healthy lung core 7. As with the other healthy samples, the measurements seem to be continuous.

5.1.5 All Healthy Lung Cores

Mitra and Sen's equation from chapter 1

[1.20]
$$\frac{D}{D_0} = 1 - \frac{4}{9\sqrt{\pi}} \frac{S}{V} \sqrt{D_0 t_{diff}}$$

predicts that D/D_0 should go to 1 as t_{diff} goes to 0. This intercept reflects the fact that at

shorter and shorter diffusion times, fewer and fewer gas molecules have a chance to

collide with the tissue surface and have their diffusion restricted. Thus at a diffusion time

of 0 s, all the gas should have unrestricted diffusion, and the ratio D/D_0 should be 1. In

Fig. 5.9, the short diffusion length values of D/D_0 are consistent with an intercept of 1 for

the healthy cores.

At short length, there is some spread in the diffusion measurements for the

different healthy cores and at long diffusion lengths core 2 has elevated diffusion

compared to the other cores. Some systematic variation in measured diffusion over the

volume of the lung in healthy[4] and sub-clinical diseased lungs[5] has been noted before,

with the measured diffusion tending to increase toward the top of the lung. However this

trend does not explain the differences found in this study. Core 6, cut from the apex of

the lung, has a lower reduced diffusion at all lengths compared to core 2, taken from

lower in the lung. We feel the difference is more likely due to varying amounts of tissue

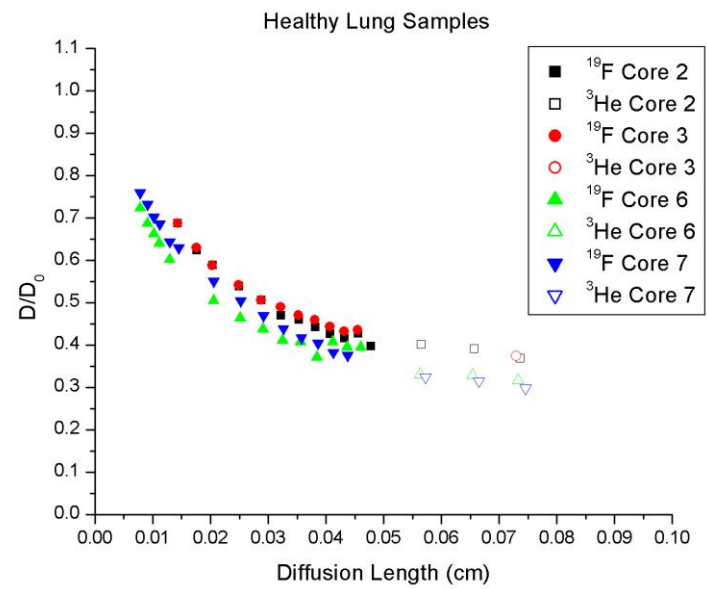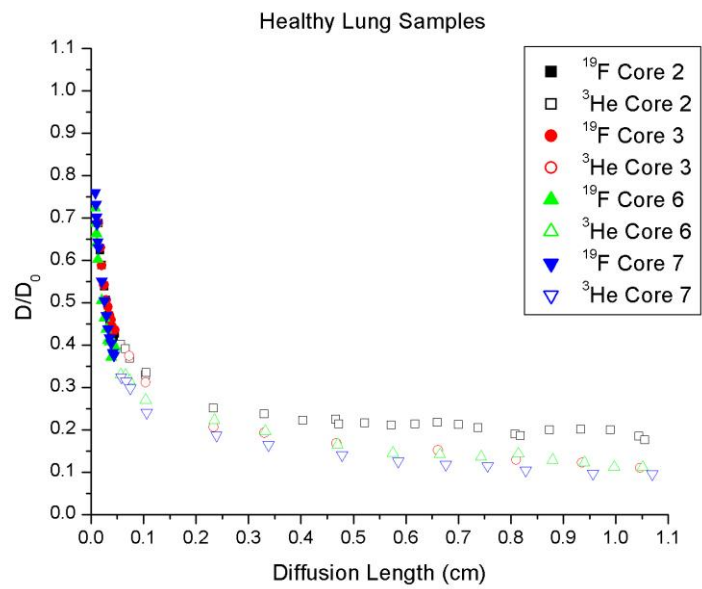damage in suffered in the samples (discussed below).

Figure 5.9. Diffusion measurements for all healthy samples.

5.2 Emphysematous Lung Samples

The two emphysematous sample cores were taken from the same lung, removed from the transplant recipient and fixed in late 2006. They were stored at 4° C until they were cut in mid 2009.

5.2.1 Emphysematous Lung Core B

As seen in Fig. 5.10, core B has some tissue destruction, resulting in enlarged airspaces compared to the healthy samples. Its mean linear intercept is 0.46±0.07 mm, increased from the values seem for the healthy samples and larger than the values in the literature for emphysematous samples (0.329±0.059 mm[1] , 0.343±0.045 mm[2]. Note that severity of disease is not taken into account for the reported values). Thus we expect that its short diffusion length measurements should be greater than those of the healthy lungs, as is in fact the case (Fig 5.11). For this core, the diffusion length dependence has weakened by 0.8 cm.

5.2.2 Emphysematous Lung Core C

Core C has severe tissue destruction, seen in Fig. 5.12. Its mean linear intercept is 1.18±0.34 mm, much higher than those found in the literature. Because emphysema measurements are often reported without specifying the level of emphysema, the elevated mean linear intercept of this core is not regarded as contradicting the values found in other studies, but rather as indicative of the severity of disease in this particular sample. The great loss of tissue experienced by this core means that gas diffusion will hardly be restricted at all at short diffusion lengths, as seen in Fig 5.13. Because the SVR has been immensely reduced by tissue destruction in this core, it is possible that Mitra and Sen's SVR regime is accessible for this sample. In severe emphysema, SVR has previously

been measured[6] to be as low as 43 cm^{-1} (although the severity of disease in "severe" emphysema is poorly defined and for this sample SVR might be lower) meaning that the short length limit might extend as far as 0.02 cm. The slope of a line fitted to the reduced diffusion at lengths less than 0.02 cm is -4±1 cm^{-1}, yielding a SVR of 17±4 cm^{-1} which is very low but is in accord with the extreme tissue damage in this sample. The SVR fit can be seen in Fig 5.13, where it should also be noted that the reduced intercept is 1.00±0.02, as predicted by Mitra and Sen's equation.
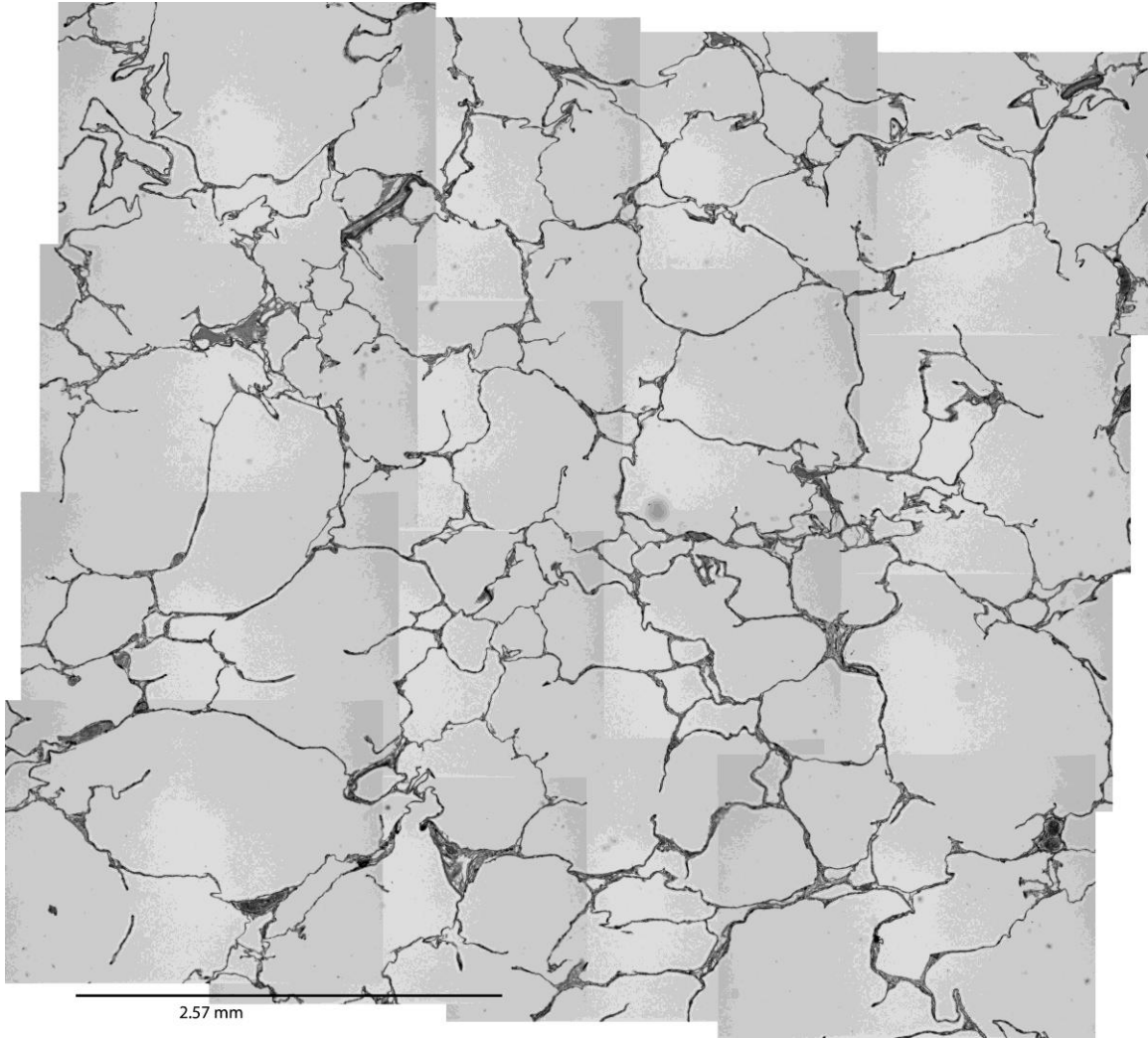
2.57 mm

Figure 5.10. Emphysematous core B histology slide. As is typical for emphysema, the alveoli have suffered some tissue destruction, resulting in enlarged airspaces which are expected to increase the measured diffusion at short diffusion lengths.
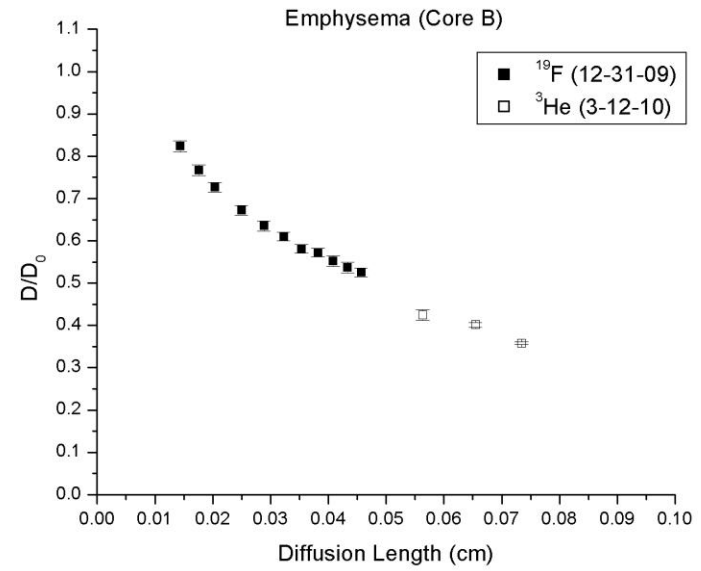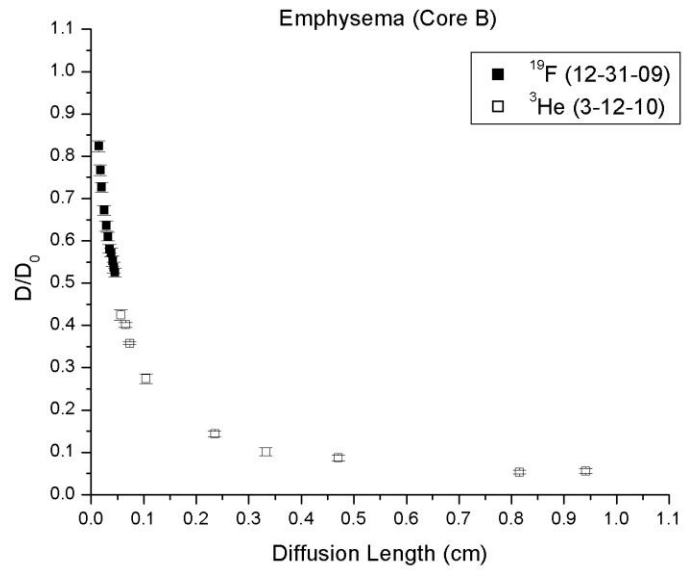
Figure 5.11. Diffusion results for emphysematous lung B. This core had mild emphysema.
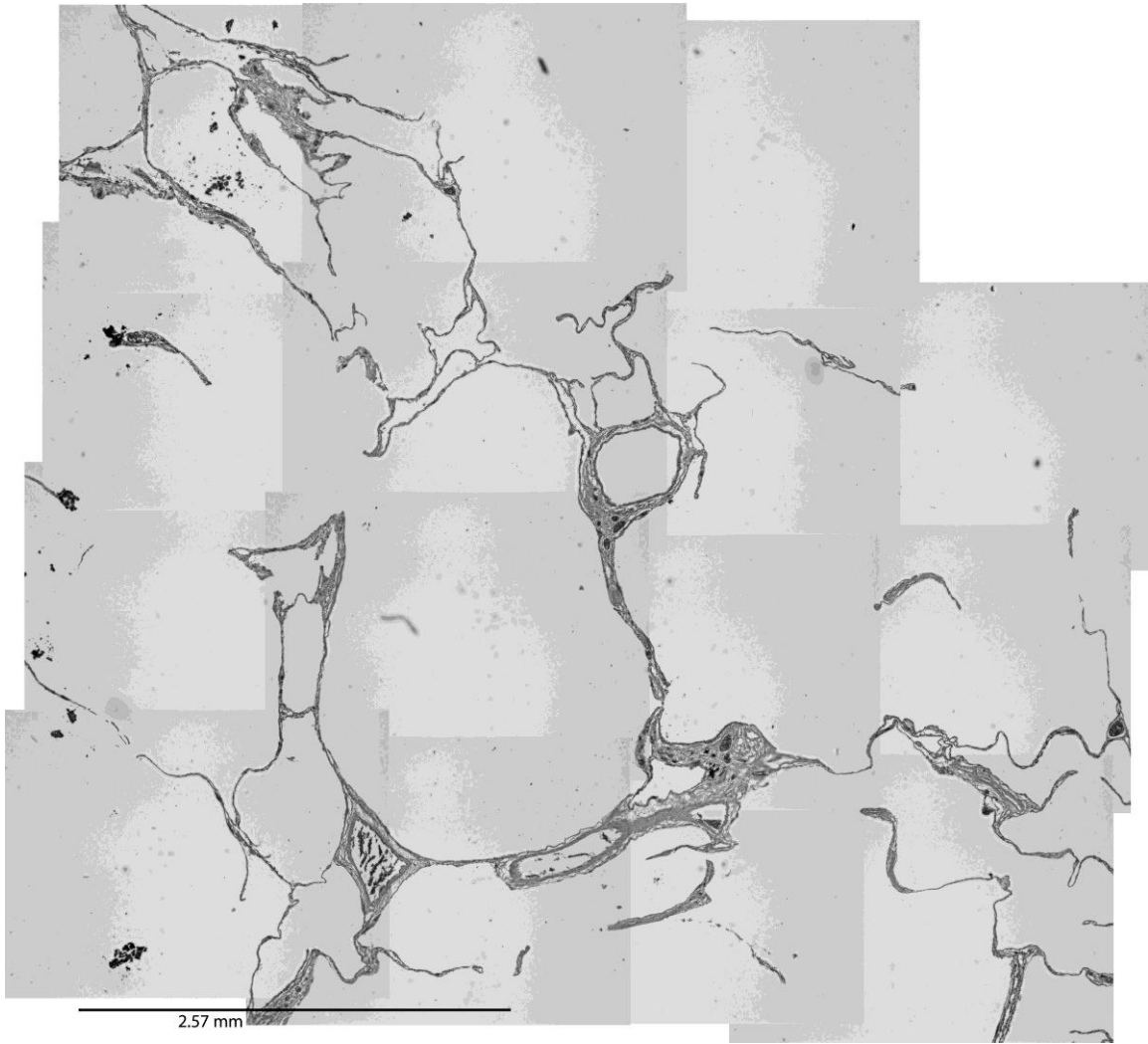
Figure 5.12. Emphysematous core C histology slide. The tissue destruction is very severe

for this core, in keeping with the diffusion results. Note there was no tissue in the upper

right corner, so Photoshop was unable to match that section to the rest of the slide.
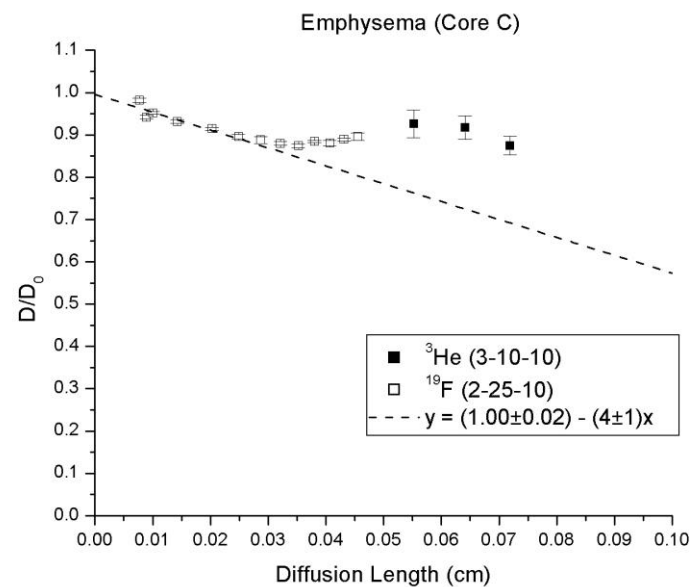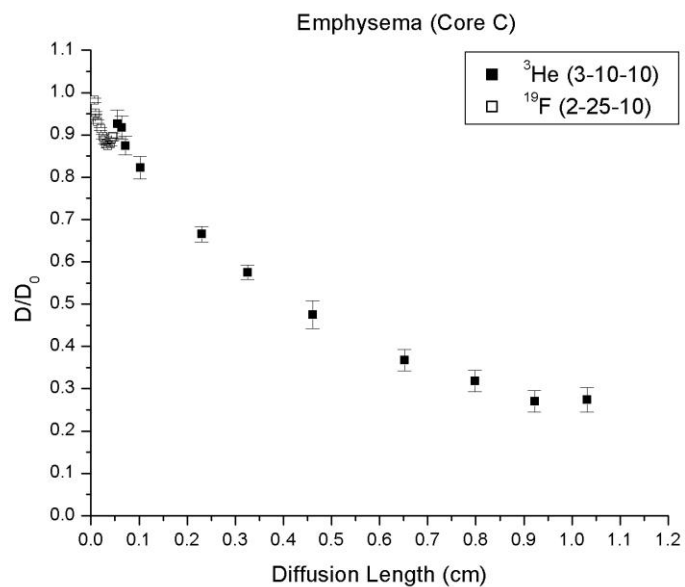
Figure 5.13 The diffusion measurements for emphysematous core C.   This is the only sample where the initial slope of the reduced diffusion could be fit for a SVR calculation (dashed line).

5.2.3 All Emphysematous Lung Cores

It is not surprising that the two cores have very different reduced diffusions, as seen in Fig. 5.14, since emphysema can have varying severities even within the same lung. Indeed, the tissue damage seen in the histology slides for the two cores predicted they will have very different diffusion values. The shortest diffusion lengths are consistent with the predicted intercept of 1 for both cores. Both emphysematous cores have a reduced dependence on diffusion length longer lengths compared to the healthy cores.
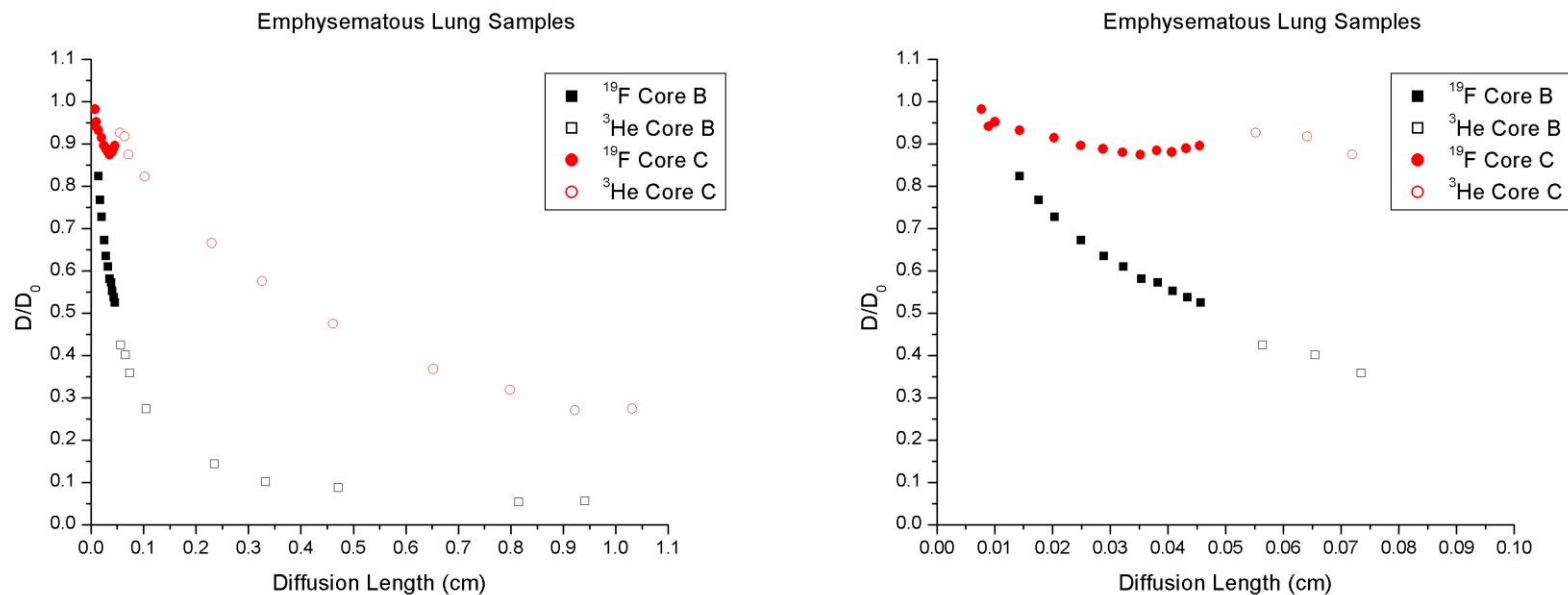
Figure 5.14. Diffusion measurements for both emphysematous samples. Despite the fact that these samples are from the same lung, it is not necessarily unexpected that they should have such different reduced diffusion curves, as emphysema severity can vary across the lung. This difference in the results for the two cores is consistent with the difference their results from the histology slides.

5.3 Sarcoid Lung Sample

     The sarcoid histology slides (ex. Fig. 5.15) have much thicker tissue walls than seen in either the healthy samples or in the emphysematous samples. This is in keeping with the characteristic fibrosis and tissue scaring associated with sarcoidosis. The mean linear intercept for this sample is 0.33 ± 0.04 mm, only slightly higher than those of the healthy cores. At shorter diffusion lengths, the sarcoid core has diffusion values close to those of healthy, but a long times the diffusion values are much lower (Fig 5.16).
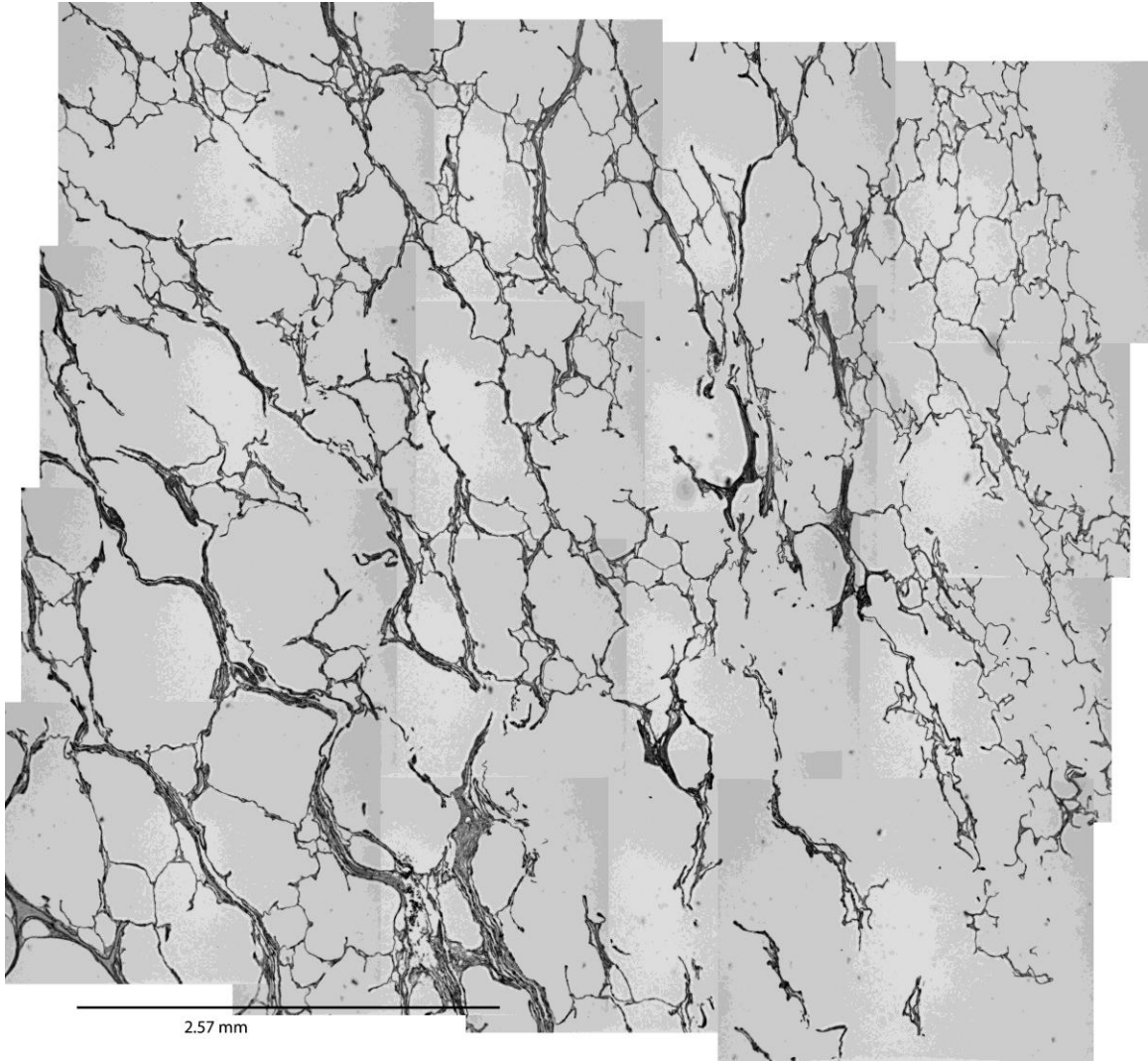
Figure 5.15. Sarcoidosis core histology slide. Fibrosis of the lung tissue is clearly visible

as thicken alveolar walls in this slide.
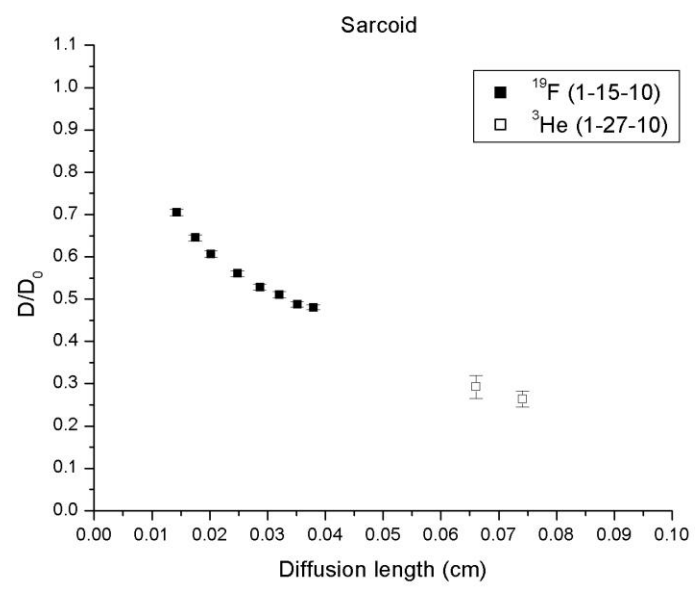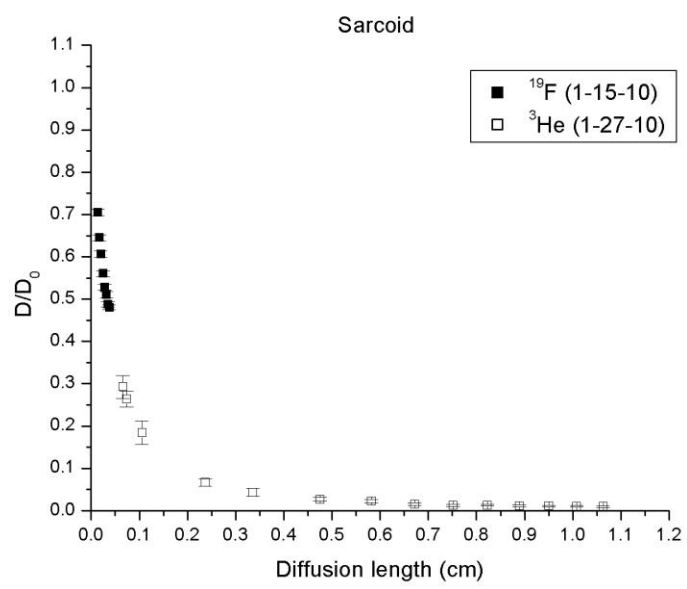
Figure 5.16. Diffusion measurements for the sarcoid lung sample.

5.4 Interstitial Pulmonary Fibrosis Sample

The histology slides for the IPF sample (ex. Fig 5.17) shows some thickening of the tissue, as well as some enlarged airspaces. The tissue thickening is characteristic of the tissue fibrosis in this disease. The enlarged airspaces seen in the slide and the mean linear intercept of 0.43±0.14 mm, between that of the healthy samples and the emphysematous samples, agrees with the diffusion measurements show in Fig. 5.18, where the diffusion measurements at short lengths are slightly higher than those of the healthy cores and lower than those of the emphysematous cores.

2.57 mm
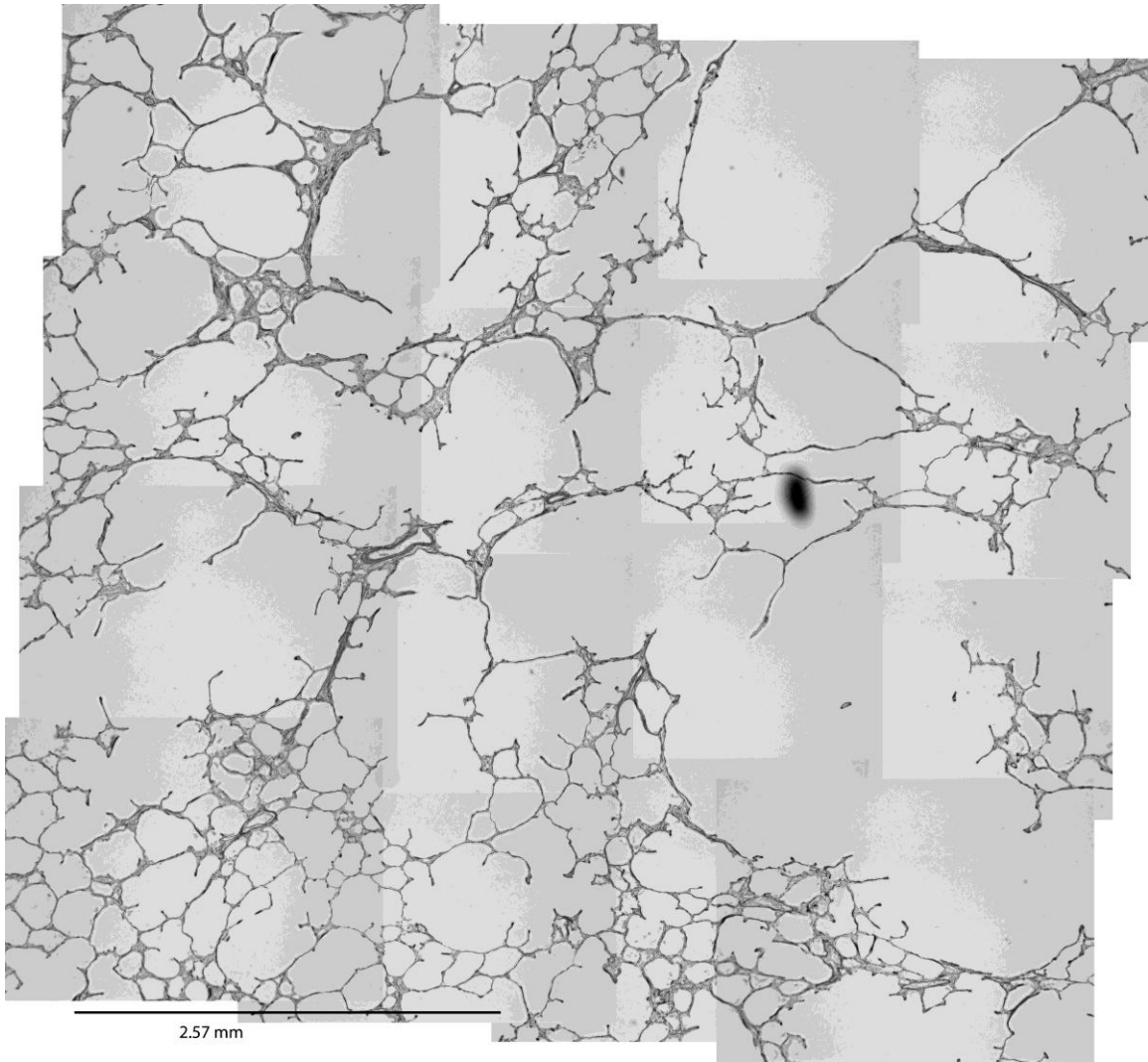
Figure 5.17. IPF core histology slide. Some thickening of the tissue is visible (as well as some dust on the slide on the right).   There is some enlargement of the airways, which is more typical of emphysema.
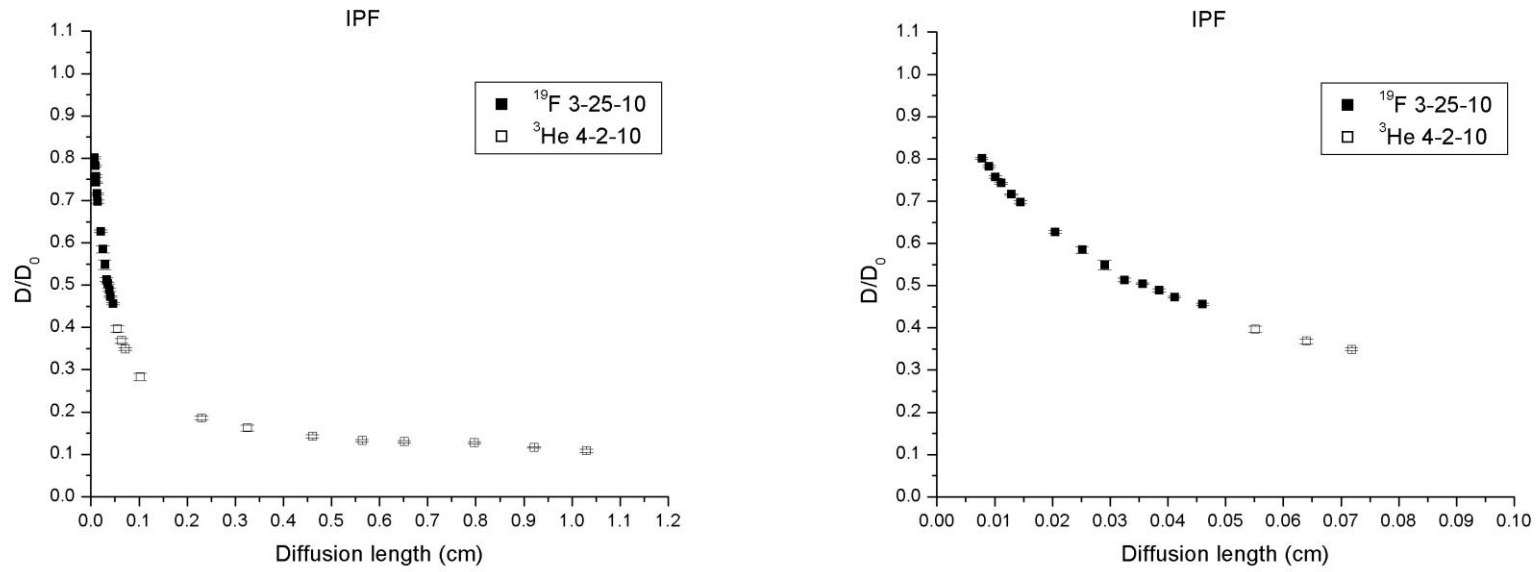
Figure 5.18. Diffusion measurments for the interstitial pulmonary fibrosis sample. This sample has little-to-no discontinuity between its two sets of measurements.

5.5 Healthy Pig Sample

In Fig 5.19, as for the other histology slides for the pig, the alveoli are clearly smaller than the alveoli for the healthy human cores and the pig has the lowest mean linear intercept of any of the lung samples: 0.15 ± 0.01 mm. The diffusion curve in Fig 5.20 is consistent with the measurements from the histology slide, with the most restricted diffusion at short lengths of any of the samples. At longer lengths, the lack of collateral pathways in the pig lungs is consistent with the low measured diffusion. The dependence on diffusion length is very weak after 0.45 cm for the pig core.

2.57 mm
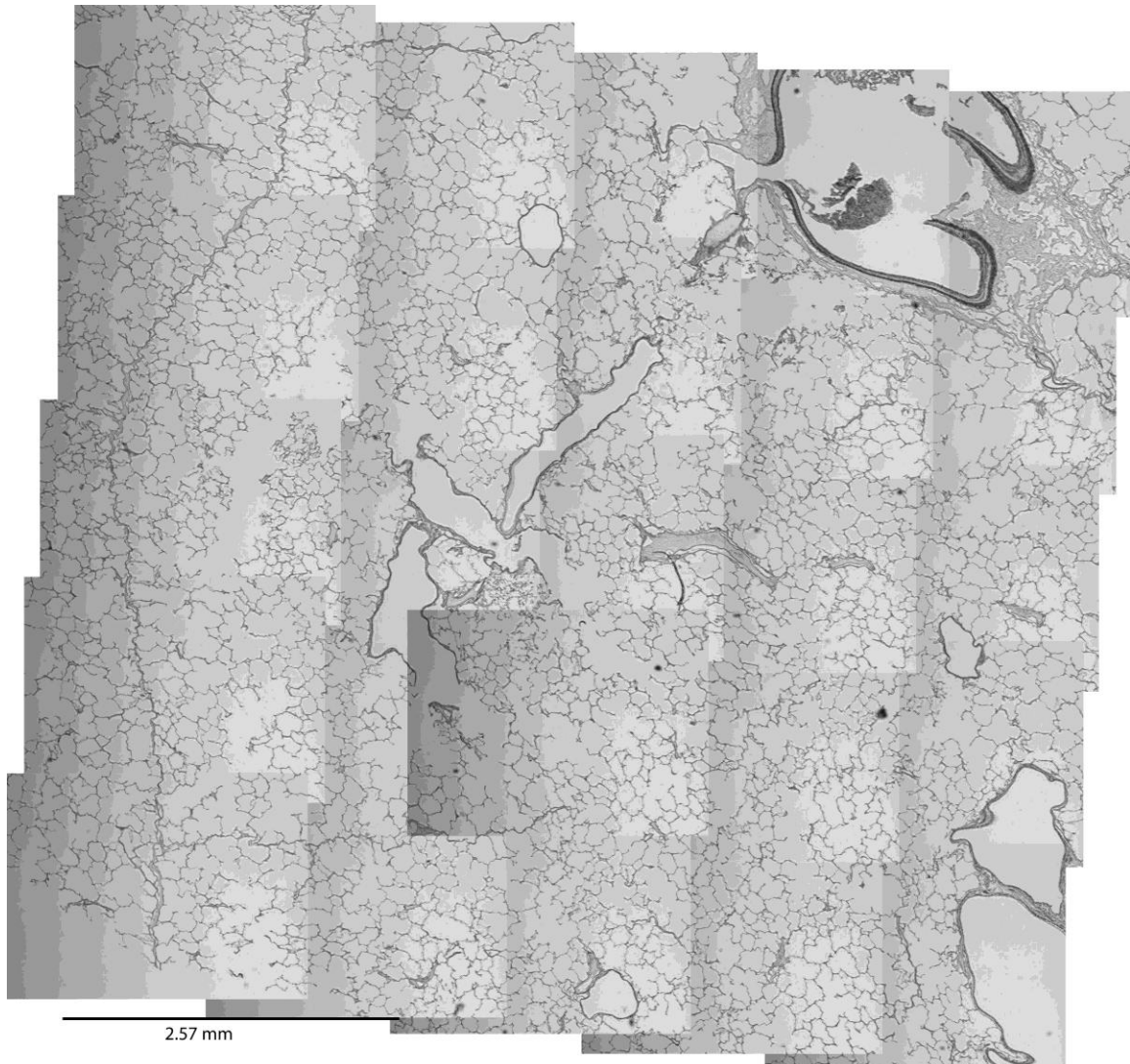
Figure 5.19. Pig core histology slide. The alveoli are much smaller for the pig than for the healthy human samples and septa dividing the lung tissue are clearly visible (see the roughly vertical curve on the left, for example). The large open airspaces are bronchioles, cut on the bias and branching in some cases (see the lower bronchiole in the cluster in the middle, which is branching below into two alveolar ducts).
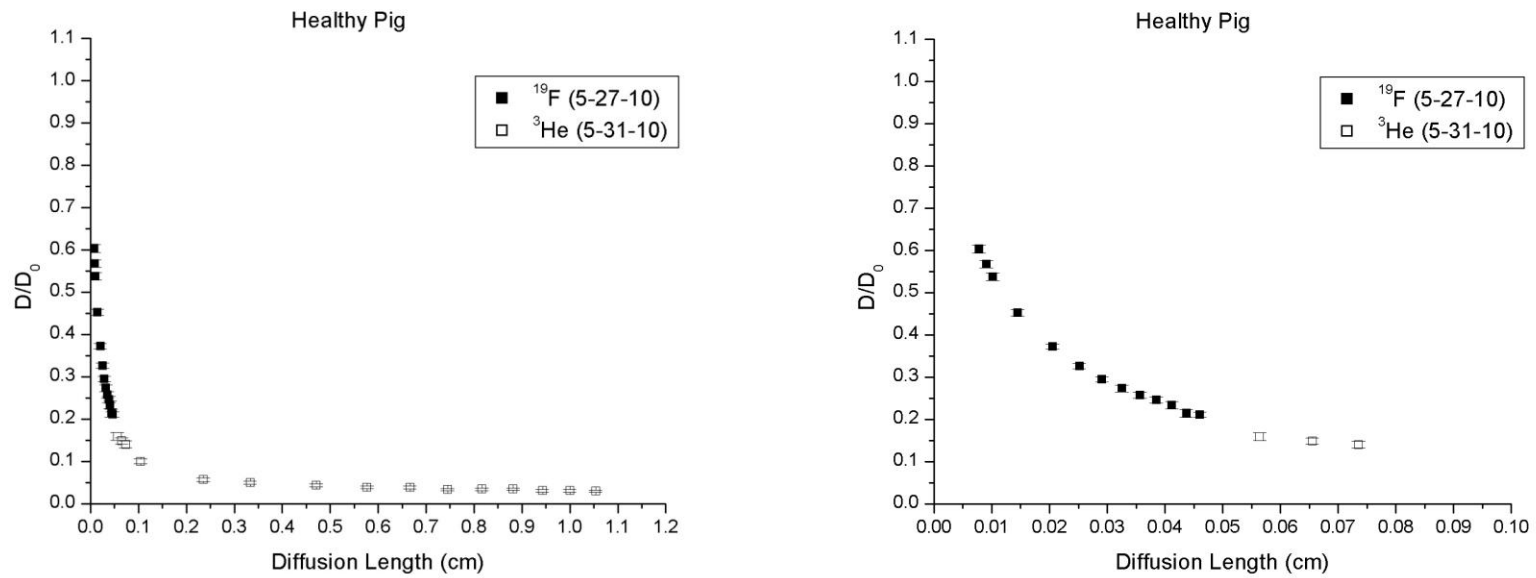
Figure 5.20. Diffusion measurements for the pig sample. In this sample, the diffusion is heavily restricted, in keeping with the small aveolar size and scarcity of collateral paths in pig lungs. There appears to be a very slight discontinuity between the two sets of diffusion measurements.

5.6 Short Diffusion Length

We will now compare the short length scale measurements for all lungs together. The diffusion measurements for all lungs for diffusion lengths less than 0.05 cm are displayed in Figure 5.21. Reduced diffusion measurements for the lung samples at various diffusion lengths are displayed in table 5.1. First, we note that all the lungs have the correct ordering of reduced diffusions relative to each other; that is, the lung samples suffering from emphysema have the highest, or least restricted, diffusion, then the samples taken from healthy lungs (or lungs with diseases that are expected to mimic healthy tissue in diffusion MR studies, i.e. the IPF and sarcoid samples) have more restricted diffusion, and finally the pig lung sample has the most restricted diffusion. For example, at 0.02 cm, the emphysematous samples have an average reduced diffusion of 0.82, while the average for the healthy tissue is 0.56 (sarcoidosis is 0.607 and IPF is 0.627) and the pig's reduced diffusion is 0.372. It is worthwhile to note that the difference between the emphysematous samples and the average of the healthy samples increases as the diffusion distance increases. For core B, the least damaged of the two, D/D_0 increases from 30% at 0.02 cm to 31% at 0.04 cm, when calculated as $(D/D_{0emphy} - D/D_{0ave\ healthy}) / (D/D_{0ave\ healthy})$. For core C the difference increases from 63% to 110% for the same lengths.

As stated in the discussion of the individual samples above, the necessary diffusion lengths for SVR calculations are out of reach for the gases and diffusion times of this study, with the exception of the very emphysematous sample C. However, even if the shortest diffusion lengths reached in this study are too long for the SVR regime for the majority of the lung samples, the general behavior of the diffusion measurements
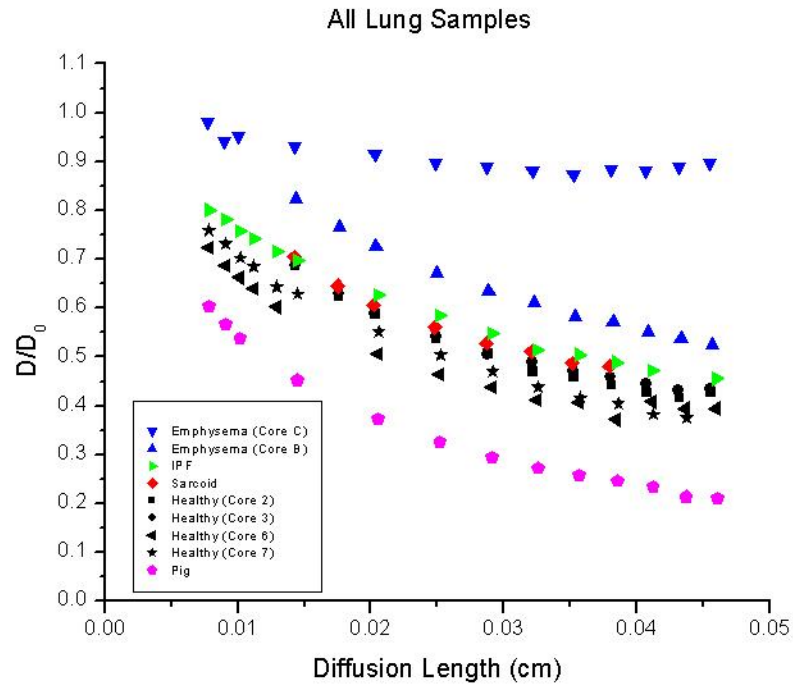
Figure 5.21. Reduced diffusion at short diffusion lengths. In this graph, all the healthy samples are shown in black and both the emphysematous samples are shown in blue. At short time, the relative values of the cores' diffusion measurements are in line with expectation; the tissue that has suffered destruction due to emphysema has lightly restricted diffusion, while the healthy, IPF and sarcoid cores have more heavily restricted diffusion, and the pig sample has the most heavily restricted diffusion.

Core and type	D/D_0 at 0.01 cm	D/D_0 at 0.02 cm	D/D_0 at 0.04 cm
Healthy (2)	No data	0.588±0.011	0.426±0.011
Healthy (3)	No data	0.588±0.006	0.444±0.011
Healthy (6)	0.663±0.009	0.506±0.007	0.408±0.007
Healthy (7)	0.702±0.013	0.551±0.010	0.382±0.009
Average Healthy	-	*0.56±0.04*	*0.42±0.03*
Emphysema (B)	No data	0.727±0.012	0.552±0.012
Emphysema (C)	0.952±0.003	0.914±0.003	0.880±0.006
Sarcoid	No data	0.607±0.008	No data
IPF	0.757±0.003	0.627±0.003	0.473±0.0020
Pig	0.538±0.008	0.372±0.007	0.24±0.01

Table 5.1. Restricted diffusion for all the samples at various short diffusion lengths. As

stated with the short time graph (Fig. 5.15), the relative order of the core's reduced

diffusion is expected: the emphysema cores have the highest D/D_0 at all diffusion lengths

shown here, followed by the other human samples, with the pig sample having the lowest

D/D_0, although at these short lengths the pig values are only slightly lower than the

average healthy values. Note that the fractional difference between the diffusion of the

emphysematous samples and the average diffusion of the healthy samples increases with

diffusion length: For core B, $(D/D_{0emphy} - D/D_{0ave\ healthy}) / (D/D_{0ave\ healthy})$ is 30% at 0.02

cm and 31% at 0.04 cm. For the more severely emphysematous core C, $((D/D_{0emphy} -$

$D/D_{0ave\ healthy}) / (D/D_{0ave\ healthy})$ is 27% at 0.01 cm, 63% at 0.02 cm and 110% at 0.04 cm.

should still be closely related to SVR. That is, healthy lung tissue that has not suffered

the destruction characteristic of emphysema (and which will consequently have a high

SVR) should highly restrict the diffusion of gas in its airspace, while emphysematous

lung tissue will have both a lowered SVR and a higher D/D_0 measurement for gas in its

airspace.

Since we can not calculate a SVR from these measurements, we look instead at

what length D/D_0 is reduced by a given amount. These results are presented in table 5.2.

When the measured diffusion is reduced by ½ (i.e. D/D_0=0.5), the pig is at the smallest

diffusion distance (0.012 cm), and the two emphysematous samples have D/D_0= 0.5 at

the longest diffusion length (0.050 cm and 0.43 cm).   The healthy samples have an

average half reduced diffusion at 0.027 cm while the sarcoid sample is at 0.034 cm and

the IPF sample is at 0.036 cm. The pig core has its measured diffusion reduced by ½ at

the smallest lengths. This is in accord with expectations because the pig tissue has the

smallest alveoli and thus the most restricted diffusion, so its reduced diffusion should

decrease the fastest at short diffusion lengths. The emphysematous samples will have

suffered tissue destruction, so they are expected to have less restricted diffusion, as is

found.

5.7 Long Diffusion Length

Diffusion measurements for all cores at long diffusion lengths are shown in Fig.

5.22 . Mitra and Sens's work with diffusion in porous medium suggests that at

sufficiently long diffusion lengths the reduced diffusion will tend to a constant, the

inverse of the medium's tortuosity. For the purpose of this study, a sufficiently long

diffusion length may be thought of as the length where the diffusing gas has traveled far

Core and Type	Diffusion length where $D/D_0=0.50$
Healthy (2)	0.029 ± 0.002
Healthy (3)	0.030 ± 0.002
Healthy (6)	0.021 ± 0.002
Healthy (7)	0.026 ± 0.002
Emphysema (B)	$0.050\pm0.004°$
Emphysema (C)	$0.43\pm0.07*$
Sarcoid (D)	0.034 ± 0.002
IPF (E)	0.036 ± 0.001
Pig	0.012 ± 0.002

Table 5.2. Diffusion length where D/D_0 is reduced by ½.   The order of these diffusion

lengths is expected. The pig reaches the specified value of reduced diffusion at the

shortest length, followed by the healthy, sarcoid and IPF samples, with the

emphysematous samples only reaching the reduced diffusion values at long lengths (in

the case of core C, only in the long length helium diffusion measurements)

°extrapolation from lower boundary of C_3F_8 data
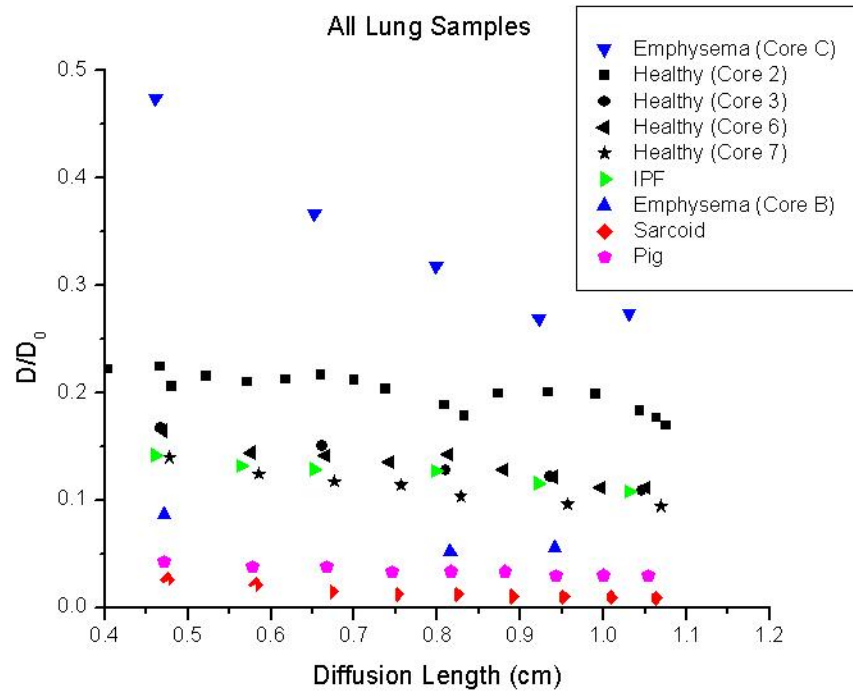
*From helium measurements

Figure 5.22. Diffusion at long diffusion lengths. At long lengths, two unexpected findings stand out: first that emphysematous core B has lower D/D_0 than most of the non-emphysematous human samples and that the human sarcoid lung has lower D/D_0 than even the pig lung.

enough to average out the effects of any large geometric features of the medium. In a whole lung it is an open question if this limit will ever be reached, mainly due to the many levels of bifurcating airways. Collateral pathways in the lung will tend to let the gas reach the tortuosity limit at shorter diffusion lengths, because they allow the gas to "short-circuit" the larger airways and sample different areas of the lung more quickly. In Fig. 5.22, all the diffusion curves of the samples eventually reach a point where the reduced diffusion has only a very weak dependence on diffusion length. Because the measurements in this study do not go to diffusion lengths much longer than 1 cm, it is unclear if these shallow ends of the diffusion curves are truly the tortuosity limits for the lung or if D/D_0 will continue to decrease slowly as diffusion length increases. Under the assumption that these plateaus do represent the tortuosity limit, the values of D/D_0 at long diffusion length can be found in table 5.3. These values are the averages D/D_0 for diffusion lengths greater than 0.85 cm, by which length D/D_0 for all cores had very weak dependence on diffusion length. The tortuosity, simply the inverse of this number for all cores, is also reported in table 5.3.

In some aspects, the relative values of the reduced diffusion at long time agree with expectations: The healthy core and the IPF core have similar reduced diffusion measurements; the IPF core is expected to have similar properties as a healthy core in an diffusion MR measurement (fibrosis inhibits the lung's expansion to full volume, but is unaccompanied by airway expansion or alveolar destruction). Emphysematous core C has much higher D/D_0; the severity of tissue destruction in this core is such that there are almost no tissue barriers left, dramatically decreasing the lungs tortuosity. The pig has very low D/D_0 at long lengths as would be expected with the low number of collateral

Core and Type	Long Diffusion Length value	Tortuosity	Corrected Mean Linear Intercept (mm)
Emphysematous Core C	0.262±0.003	3.82	1.18±0.35
Emphysematous Core B	0.05±NA	18.64	0.46±0.07
Healthy Core 2	0.189±0.008	5.30	0.27±0.03
Healthy Core 3	0.104±0.008	9.59	0.25±0.02
Healthy Core 6	0.12±0.01	8.38	0.32±0.02
Healthy Core 7	0.092±0.001	10.82	0.29±0.04
IPF	0.108±0.005	9.26	0.43±0.14
Sarcoid	0.0100±0.0007	100.5	0.33±0.04
Pig	0.031±0.002	31.98	0.15±0.01

Table 5.3 Long diffusion lengths, tortuosity, and mean linear intercept. The long diffusion length values are the average of D/D_0 for lengths greater than 0.85 cm, with the standard deviation as the error. Tortuosity is the inverse of the long length value. The corrected mean linear intercept given is the average from the slides from each sample.

paths in pig lung tissue, tending to increase the tortuosity and decrease the measured diffusion.

Two unexpected findings stand out at long lengths. First, emphysematous core B has lower D/D_0 than most of the non-emphysematous human samples. The destruction of tissue in emphysema is expected to cause more collateral pathways to open up in the tissue, leaving the long length diffusion less restricted than in healthy tissue. Second, the human sarcoid lung has the lowest D/D_0, lower than even the pig lung. Since pigs are known to have less collateral paths than humans, diffusion is expected to always be more restricted in healthy pig tissue than in human tissue, although it is possible that the fibrosis associated with sarcoidosis might have the effect of closing off some of the collateral paths in human tissue.

Figs. 5.23 and 5.24 show diffusion for the healthy and emphysematous cores compared to reduced diffusion measurements reported in the literature[4,5,7,8,9,10]. For emphysematous cores, in Fig 5.24, the wide range of reported values overlaps D/D_0 for both cores, disparate as their diffusion curves are. The wide range is a result of the varying severity of emphysema in the studies: lungs with very mild emphysema and consequently little tissue destruction would be expected to have D/D_0 only slightly elevated over that for healthy tissue with no tissue destruction. Lungs with very severe emphysema and extreme tissue destruction might barely restrict the diffusion of gas and have D/D_0 which are close to unity.

In Fig. 5.23, it is clear that D/D_0 for the healthy samples in this study is much higher that D/D_0 reported in the literature. This disagreement with measurements in other studies, combined with the unexpectedly low long length diffusion for emphysematous

Figure 5.23. The solid points are measurements taken in this study. The numbers are

measurements collected from the literature, with the error bars being the standard

deviation for each study when reported (all literature values were taken from in vivo

studies). The points are taken from:

1) Wang, JMRI 2008
2) Yablonskiy PNAS 2002
3) Mugler Acad Radiol 2008
4) Saam MRM 2000
5) Wang MRM 2006
6) Wang, JMRI 2008
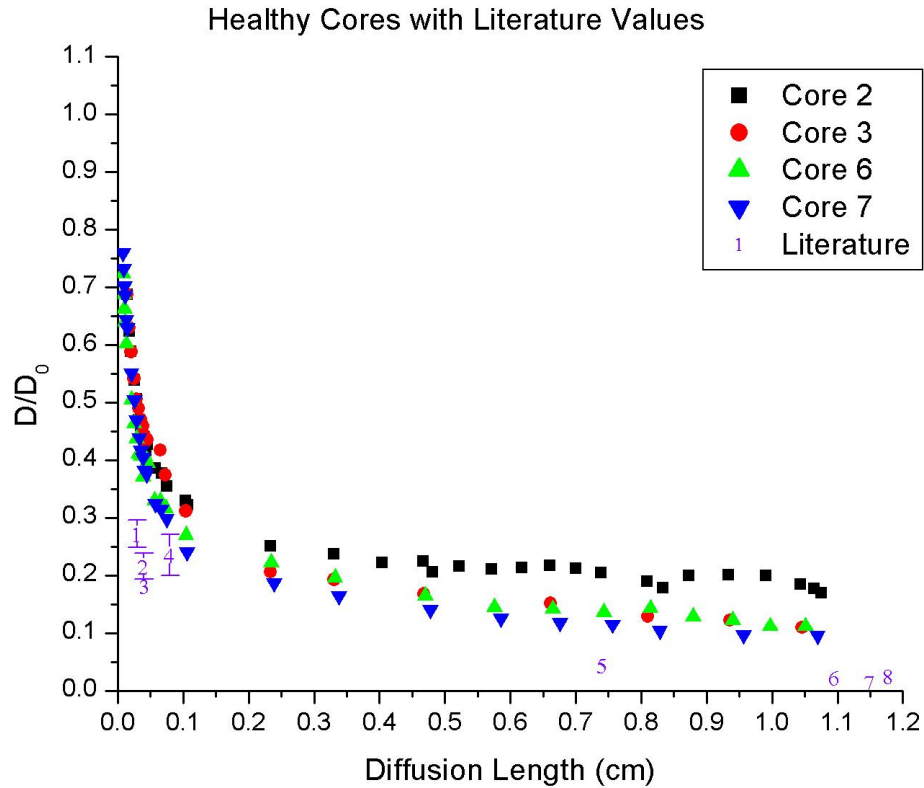7) Mugler Acad Radiol 2008
8) Wang MRM 2006

Figure 5.24. The solid points are measurements taken in this study. The numbers are measurements collected from the literature, with the error bars being the standard deviation for each study when reported. It should be noted that the literature points are given without regard to the severity of emphysema in the patients (all literature values, except #8 , were taken from in vivo studies). The points are taken from:

1) Wang, JMRI 2008
2) Yablonskiy PNAS 2002
3) Mugler Acad Radiol 2008
4) Saam MRM 2000
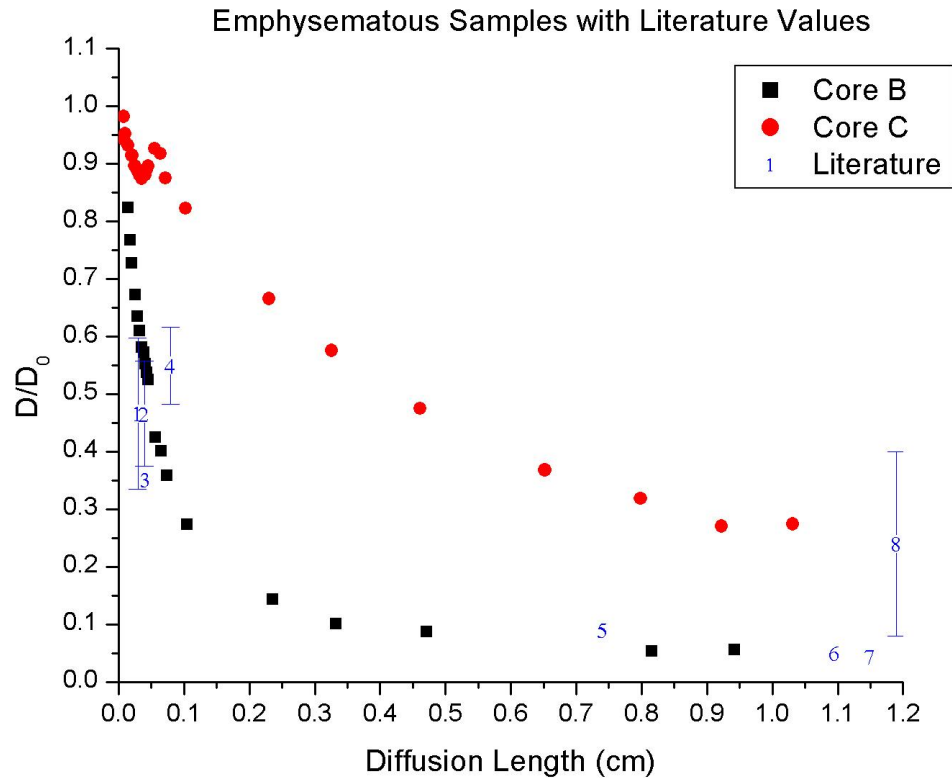5) Wang MRM 2006
6) Wang, JMRI 2008
7) Mugler Acad Radiol 2008
8) Woods J Appl Phys 2005 (measurement actually taken at a diffusion length of 3 cm, but shown at a shorter length to avoid distorting the graph)

core B and the sarcoid core, lead to the conclusion that the long length measurements in this study are unreliable as indicators of what is happening in lung tissue in vivo.

There are a few possible explanations for this unexpected long diffusion length behavior. It is worth noting that both the healthy and emphysematous lung were fixed and frozen for a few years before the cores were cut and the measurements were taken (the healthy lung was removed from the donor and frozen in early 2007, the measurements were taken early 2010; the emphysematous lung was frozen in 2006, the measurements were taken in late 2009 and early 2010). A previous study by Gierada[11] found that formalin fixation has minimal effect on the MR diffusion properties of lung tissue, but the long storage time for the healthy and emphysematous samples in this study may have affected the tissue properties, for example by opening additional collateral paths in the lung tissue by tears or other tissue damage. In addition, the samples may also have been damaged when the lungs were cut into slabs or when the cores were cut out of the slabs. An earlier study[12] has found that even a relatively small fractional concentration of collateral pathways can have a large effect on long-range diffusion. This study stimulated human lung tissue with no collateral paths and measured the long length diffusion in such a system. The result was a diffusion coefficient of 0.001 cm^2/s, which is much smaller than the diffusion coefficient actually found in experiments with lungs in vivo. Using, $D/D_0 = 2nrL$, where n is the number of paths per wall area, r is the radius of those holes and L is the airway diameter, they calculated that a relatively low density of paths $n = 3.3$ mm^{-2} and physically realistic values of $r = 5$ μm and $L = 0.6$ mm results in $D/D_0 = 0.02$, close to the measured diffusion in *in* vivo experiments and an order of magnitude increase over the simulation results (which lacked collateral pathways). A

number density of 3.3 mm^{-2} means that the paths occupy a very small fraction of the tissue wall, $f = n\pi r^2 = 2.6$ x 10^{-4}. For the long diffusion length values for healthy tissue in this study, $D/D_0 \approx 0.1$, which would require a number density of paths of 16.7 mm^{-2}, or a fractional area of $f = 1.3$ x 10^{-3}. A 1.3 x 10^{-3} fractional area of 5 μm holes in the tissue walls would not be visible in the histology slides at the magnification used in this study. We emphasize that this discussion is speculative, but the unusually large D/D_0 seen at long lengths and the near independence of D/D_0 upon $\sqrt{(D_0\ t_{diff})}$ at long diffusion lengths strongly suggest some kind of collateral paths are present in these samples.

5.8 Conclusions

The results for short diffusion length and histology for this study agree well with each other and with qualitative expectations. We regard these diffusion measurements as correct and reflective of in vivo measurements.

However, the measurements taken at long diffusion lengths appear to be unreliable indicators of lung tissue in vivo. Given the extensive preliminary tests on the sequence with water and bulk gas phantoms, it is unlikely that the faulty measurements result from difficulties with the MR sequence or analysis. Moreover, although only one set of repeat measurements for helium diffusion in healthy core 2 were shown, measurements in the other lung cores have also been found to be reproducible in this study, even over periods of months. Unfortunately, the scarcity of lungs available for this study limits our ability to try to adjust our preparation and storage practices and compare the results from the present lungs to measurements of other healthy and emphysematous lungs. Nonetheless, this study may serve as a starting point for future studies of lungs at different diffusion lengths than have been used before in diffusion MR studies.

[1] A.A. Robbesom, E.M. Versteeg, J.H. Veerkamp, H.J. van Krieken, H.J. Bulten, H.T. Smits, L.N. Willems, C.L. van Herwaarden, P.N. Dekhuijzen, T.H. van Kuppevelt, Morphological Quantification of Emphysema in Small Human Lung Specimens: Comparison of Methods and Relation with Clinical Data, Mod Pathol, 16 (2003) 1–7.

[2] L.N. Willems, J.A. Kramps, T. Stijnen, P.J. Sterk, J.J. Weening, J.H. Dijkman, Relation between small airways disease and parenchymal destruction in surgical lung specimens, Thorax, 45 (1990) 89-94.

[3] R.E. Jacob, Y.V. Chang, C.K. Choong, A. Bierhals, D.Z. Hu, J. Zheng, D.A. Yablonskiy, J.C. Woods, D.S. Gierada, M.S. Conradi, 19F MR Imaging of Ventilation and Diffusion in Excised Lungs, MRM 54 (2005) 577-585.

[4] B.T. Saam, D.A. Yablonskiy, V.D. Kodibagkar, J.C. Leawoods, D.S. Gierada, J.D. Cooper, S.S. Lefrak, M.S. Conradi, MR Imaging of Diffusion of 3He Gas in Healthy and Diseased Lungs, MRM 44 (2000) 174-179.

[5] J.P. Mugler, C. Wang, G.W. Miller, G.D. Cates, J.F. Mata, J.R. Brookeman, E.E. de Lange, T.A. Altes, Helium-3 Diffusion MR Imaging of the Human lung over Multiple Time Scales, Acad Radiol, 15 (2008) 693-701.

[6] H.O. Coxson, R.M. Rogers, K.P. Whittall, Y.D'Yachkova, P.D. Paré, F.C. Sciurba, J.C. Hogg, A Quantificationof the Lung Surface Area in Emphysema Using Computed Tomography, Am J Respir Crit Care Med 159 (1999) 851-856.

[7] C. Wang, T.A. Altes, J.P. Mugler, G.W. Miller, K. Ruppert, J.F. Mata, G.D. Cates, L. Borish, E.E. de Lange, Assessment of the lung microstructure in patients with asthma using hyperpolarized 3He diffusion MRI at two time scales: comparison with healthy subjects and patients with COPD. J Magn Reson Imaging. 28 (2008) 80-8.

[8] D.A. Yablonskiy A.L. Sukstanskii , J.C. Leawoods, D.S. Gierada, G.L.Bretthorst, S.S. Lefrak, J.D. Cooper, M.S. Conradi, Quantitative *in vivo* assessment of lung microstructure at the alveolar level with hyperpolarized ^{3}He diffusion MRI PNAS 99 (2002) 3111-3116

[9] C. Wang, G.W. Miller, T.A. Altes, E.E. de Lange, G.D. Cates, J.P. Mugler, Time dependence of 3He diffusion in the human lung: measurement in the long-time regime using stimulated echoes. Magn Reson Med. 56 (2006) 296-309.

[10] J.C. Woods, D.A. Yablonskiy, C.K. Choong, K. Chino, J.A. Pierce, J.C. Hogg, J.Bentley, J.D. Cooper, M,S. Conradi, and P.T. Macklem, Long-range diffusion of hyperpolarized ^{3}He in explanted normal and emphysematous human lungs via magnetization tagging, J Appl Phys 99 (2005) 1992-1997

[11] D.S. Gierada, J.C. Woods, R.E. Jacob, A.J. Bierhals, C.K. Choong, S.T. Bartel,Y.V. Chang, N.A. Das, C. Hong, B.A. Lutey, J.H. Ritter, T.K. Pilgram, J.D. Cooper, G.A.

Patterson, R.J. Battafarano, B.F. Meyers, D.A. Yablonskiy, M.S. Conradi, Emphysema Quantification in inflation-fixed lungs using low-dose CT and 3He MR imaging, J Comput Assist Tomogr, (2010) in press

[12] S.E.T. Bartel, S.E. Haywood, J.C. Woods, Y.V. Chang, C. Menard, D.A. Yablonskiy, D.S. Gierada, M.S. Conradi, Role of collateral paths in long-range diffusion in lungs, J Appl Physiol, 104 (2008) 1495-1503.

Chapter 6 - Capillary Diffusion

The second study in this thesis is an exploration of diffusion in a simple capillary tube.

6.1 Introduction

Measurement of restricted diffusion with magnetic resonance (MR) is a valuable and well-known tool for characterizing features too small to be imaged directly[1,2,3,4]. In particular, it has been used to make surface to volume measurements of small features[5,6,7,8,9]. There are many applications of restricted diffusion MR, particularly in the areas of biomedical systems and porous media. Diffusion data are generally obtained from the decay of a spin or gradient echo signal after the application of a pair of field gradient pulses with diffusion sensitizing strength, *b* (see Eqn 6.3 below). For freely diffusing spins the signal decays mono-exponentially as *exp(-b D_0)*, where D_0 is the free diffusion coefficient[10] (further explanation in chapter 2) . If the motion is restricted by physical barriers (such as airway or cell walls or the walls of the sample container) the measured diffusion will be reduced from the free value and the decay will generally no longer have strictly mono-exponential behavior.

In biological systems as well as porous media, one often finds that the signal decay as a function of *b* can be expressed as a sum of multiple exponentials. A common and seemingly natural interpretation is that the observed signal is a superposition from spins in distinct compartments of multiple types or sizes[11] or orientations[12,13] in the case of anisotropic systems. However, a report[14] (hereafter referred to as SAY) showed that even for certain simple, single-compartment geometries, the signal *S* decay is not mono-exponential but can be well modeled as bi-exponential:

[6.1]
$$S = \zeta e^{-bD_s} + \left(1 - \zeta\right) e^{-bD_F} .$$

Here ζ is the relative amplitude of the component with slow apparent diffusion D_S; the component with fast apparent diffusion is described by D_F. In this study, as in SAY, we examine the case of a single long cylinder of radius r, oriented perpendicular to the diffusion gradient (we emphasize that a distribution of sample orientations is *not* involved in this study). Now D_F describes spins far from the cylinder walls with virtually unrestricted motion, so D_F is approximately equal to the free diffusion coefficient. D_S describes spins which are near the cylinder wall and consequently have restricted diffusion, so D_S is a fraction of the free diffusion coefficient. The relative amplitude ζ is *approximately* the fraction of spins that can diffuse to the wall during the diffusion time, Δ. In SAY, the key condition for a good fit of the data with the bi-exponential model is that only a small fraction of the spins are close enough to sample the barriers (here, the cylinder walls) during the diffusion time. This condition is represented by $\alpha \ll 1$, where the parameter α is

[6.2]
$$\alpha \equiv \frac{\sqrt{D_o \Delta}}{r} .$$

The calculations from SAY show that the relative amplitude ζ and parameter α are nearly linearly related for small α, in accord with the above explanation.

The purpose of this first study in the thesis is to explore multi-exponential signal decay in a simple geometry. This study serves to verify the important message of SAY, which is to warn that multi-exponential diffusion decay may be misinterpreted in terms of spins in multiple compartments. We note that the present work is a different approach to

the seminal treatment of lightly restricted diffusion and surface-to-volume ratio by Mitra and Sen[15]. In detail, Mitra and Sen examine the mean diffusion as would be extracted from the initial slope of signal as a function of b; here the entire decay is examined. The present study is also related to studies of the edge enhancement effect[16,17,18,19]; the spins near the boundaries with a lower diffusion coefficient (here D_S) suffer less attenuation, thus enhancing the relative signal near the boundaries.

6.2 Methods

6.2.1 Samples

The sample vessels used in the experiment were single smooth silica tubes from Polymicro Technologies, intended for chromatography. Two different sizes were used, with inner radii 160±1 μm and 50.5±1 μm. The glass tubes were filled with water with a small amount of copper sulfate ($CuSO_4$) added in order to shorten T_1 to about 300 ms. This decreased T_1 allowed more rapid signal averaging to increase the signal to noise ratio (SNR) of the data. Every point had a SNR of at least 20 even after very substantial attenuation from the diffusion gradients. Each sample was long enough (at least 8 cm) that susceptibility effects were negligible[19]. Each coil was long enough (at least 1cm) that the effect of spins diffusing out of the rf field was also negligible.

6.2.2 Magnetic Resonance

The small volume samples dictated the use of rf coils with high filling factors. For each sample, an rf coil of small diameter wire was constructed, loosely fitting the sample tube. The active lengths of the rf coils were 1 and 2 cm for the large and small diameter samples, respectively. Hydrogen MR measurements were performed in a 4.7 T Oxford magnet with a Varian imaging spectrometer and VnmrJ software.
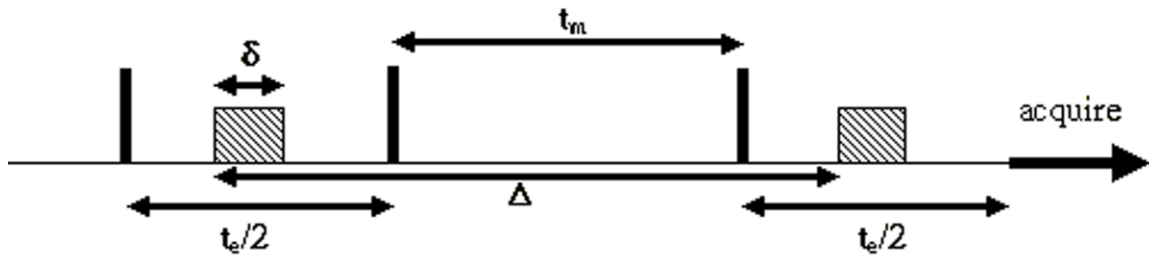
Figure 6.1. Stimulated echo sequence for the experiment. Solid rectangles represent $\pi/2$ rf pulses and shaded rectangles represent diffusion gradient pulses.

6.2.3 Sequence

Measurements were taken with a stimulated echo sequence (Fig. 6.1) to minimize signal losses from diffusion of spins through background field gradients[20]. The background gradients only act upon the spins during the two relatively short periods of duration $t_e/2$, for a total here of 30 ms. For signal to noise reasons, each measurement used at least 128 averages. The duration (δ) of the diffusion-gradient pulses was 3.0 ms (effective rectangular width), with the separation between gradients (Δ) being either 54 ms or 138 ms (for the smaller or larger cylinder, respectively). Thus the parameter α from Eq. 6.2 is 0.2 for the cylinder with 50.5 μm radius and 0.1 for the cylinder with $r = 160$ μm. Diffusion was measured in a direction perpendicular to the long axis of the sample; diffusion was also measured parallel to the long axis once in each sample to determine the free diffusivity D_0. Since δ is much smaller than both Δ and the diffusion time across the tube, the narrow pulse regime applies here[21]. The b-value is then the well-known Stejskal-Tanner result[22]

[6.3]
$$b = (\gamma G \delta)^2 \left(\Delta - \frac{\delta}{3} \right) \approx (\gamma G \delta)^2 \Delta \, .$$

We used a wide range of b-values, from 0.15 to 6000 mm^2/s, in order to capture signal from both the rapid and slow signal decay components in Eq. 6.1. Since the weighting parameter for the slow component is expected from SAY to be quite small (ζ is of order 5% in all cases), the slow component's contribution to the signal is dominant only once the signal has decayed to a few percent of the initial value.

6.2.4 Analysis

The fast Fourier transform of the spin echo time domain data for each set of b-values was phased and plotted in MatLab, and the real spectral peak area was determined. The peak areas were plotted as a function of b and fitted to the bi-exponential model of Eq. 6.1 using Origin software. Occasionally, mono-exponential fits were performed for comparison; they were always found to be vastly inferior (see Fig 6.2, for example). In order to ensure a good fit for both large and highly attenuated signals, the fitting routine was weighted appropriately.

6.3 Results and Discussion

6.3.1 Diffusion Perpendicular to Long Axis of Cylinder

At the larger b-values, the signal is reduced to less than 1% of the original signal. Fig. 6.2 demonstrates that the decay is not mono-exponential; the dashed line represents a mono-exponential fit to the small-b data. Note that for b-values less than 2500 s/mm^2, the signal follows a mono-exponential decay quite closely. It is only after more than 97% of the original signal is attenuated that the multi-exponential nature of the decay becomes apparent. The bi-exponential fit to the same data set is shown with the solid curve.

Each data set was fitted with the bi-exponential model, as shown in Fig. 6.2. The parameters obtained from the bi-exponential fits are given in Table 6.1. Also given in the table are parameter values calculated by the authors of SAY for a range of b-values similar to those used in this study. We note that the parameter values are sensitive to the b-range of the fitting, so the theory values in Table 6.1 differ from those in the publication[14]. This sensitivity demonstrates that the double exponential is not an exact fit to the analytically-derived signal decay. Since the calculated diffusion parameters are

	Trial	D_S (mm^2/s)	D_F (mm^2/s)	D_S/D_F	ζ
	1	0.00034	0.00171	0.20	0.01958
Larger sample	2	0.00029	0.00161	0.18	0.01700
$\alpha = 0.1$	3	0.00036	0.00168	0.21	0.02533
(r = 160 µm)	4	0.00041	0.00181	0.23	0.02796
	5	0.00037	0.00166	0.22	0.01474
	experiment average	0.00035	0.00169	0.21	0.02092
	theory*	0.00044	0.00163	0.27	0.02910
	1	0.00028	0.00143	0.20	0.03180
Smaller sample	2	0.00036	0.00159	0.23	0.04234
$\alpha = 0.2$	3	0.00027	0.00145	0.19	0.03025
(r = 50.5 µm)	4	0.00034	0.00159	0.21	0.03887
	5	0.00034	0.00156	0.22	0.03646
	experiment average	0.00032	0.00152	0.21	0.03590
	theory*	0.00040	0.00151	0.27	0.05037

Table 6.1. Data for bi-exponential fits to experiment and theory.

* Theory values obtained from authors of reference 14; dimensionless values of D_S and

D_F have been scaled here by the measured free diffusion coefficient $D_0 = 0.001735$
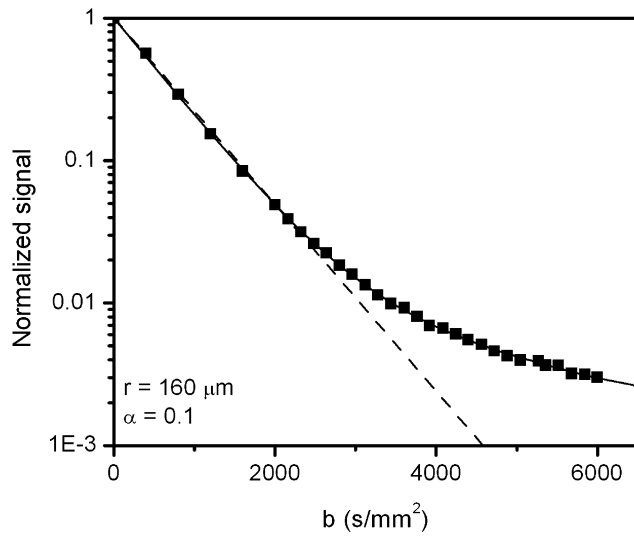
mm^2/s.

Figure 6.2. Data for the large cylinder ($r = 160$ µm, $\alpha = 0.1$) with diffusion gradient perpendicular to the long axis, fitted to a mono-exponential decay (dotted line) and to the bi-exponential model (solid curve). Note the logarithmic vertical axis.
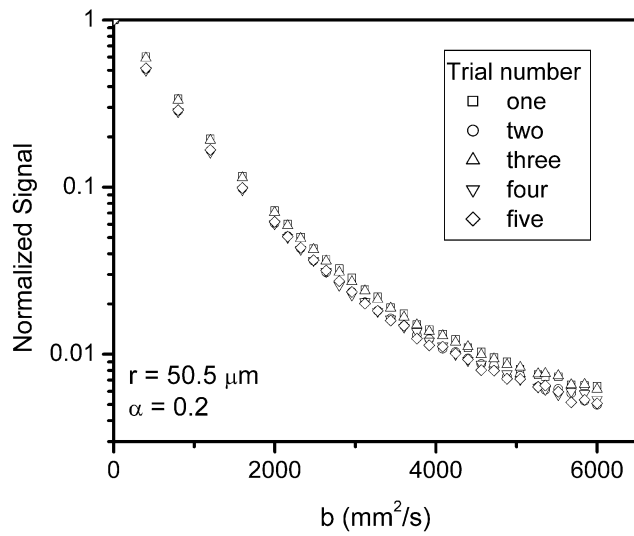

Figure 6.3. The data for multiple measurements of the smaller sample. The data from all trials are quite similar.

dimensionless (i.e., they assume a free diffusivity of unity), we multiplied them by the free diffusion measured for our samples (see below), 0.001735 mm^2/s. The experimental results generally agree with the theory, although some variation between trials is seen in Table 6.1. However, as is evident from Fig. 6.3, the data sets themselves agree closely. Thus, the variation in parameter values is due to the well known sensitivity of bi-exponential fits to small changes in the data[23].

6.3.2 Diffusion Parallel to Long Axis of Cylinder

Diffusion was also measured in one instance for each sample in the direction parallel to the long axis of the cylinder, to determine the free diffusivity D_0. The results were fitted to a mono-exponential decay (Fig. 6.4). Clearly, the decay is mono-exponential for as long as there is sufficient signal. Since the diffusion of the spins is unrestricted down the long axis of the cylinder, the signal attenuates completely into the noise at a much lower b-value than it does with the diffusion gradient perpendicular to the long axis. The free diffusion coefficient measured for the larger sample was 0.00173 mm^2/s and for the smaller sample was 0.00174 mm^2/s, giving an average value of 0.001735 mm^2/s. The work of Krynicki et. al. suggest that the expected free diffusion coefficient for water at 17°C (the temperature inside the bore of the magnet) is 0.00185 mm^2/s, making these measured free diffusion coefficients seem reasonable.[24]

6.3.3 Applications

We have shown that the signal decay for lightly restricted diffusion in a single compartment can mimic the signal for spins in multiple distinct compartments. However, the dependence of the signal on the diffusion time Δ can serve as a signature, potentially providing a way to distinguish between the single and multiple compartment systems.
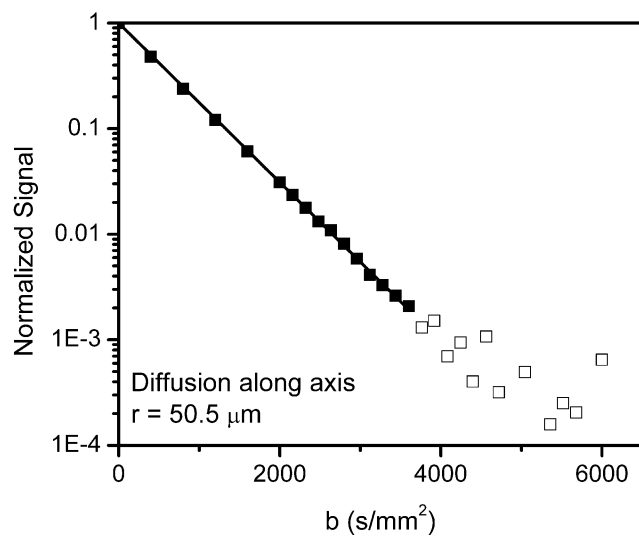
Figure 6.4. The results for diffusion along the long axis of the smaller cylinder. The free diffusion coefficient was obtained by fitting the closed squares to a mono-exponential decay. The open squares were disregarded during fitting for signal to noise reasons.

For lightly restricted diffusion, the amplitude ζ of the slowly diffusing signal component increases with diffusion time. Very approximately, the amplitude ζ is expected to be linear in α and to vary as $\Delta^{1/2}$. At large enough Δ, corresponding to $\alpha \geq 1$, the decay will be nearly mono-exponential, because all spins sample all the environments (close to walls and far from walls). By comparison, in a true multiple compartment system, the amplitudes of the components are fixed at the relative numbers of spins in each (often, this is the relative volumes of the compartments). Exchange between compartments may affect this clean dichotomy, as exchange eventually yields nearly mono-exponential decays at sufficiently long diffusion times.

6.4 Conclusions

It is clear that care must be taken when interpreting multiple exponential signal decay in a diffusion experiment. Here we have demonstrated that even a simple container can give rise to non-mono-exponential signal decay if the conditions are right, namely, that only a small portion of the spins are allowed to sample the barrier of the space during the time that diffusion is being measured. In this case, the signal is well modeled by a bi-exponential decay in agreement with calculations published earlier. One way to distinguish a true multi-compartment system from the present case of lightly restricted diffusion in a single compartment is by the diffusion-time dependence of the signal decay, particularly the relative amplitudes of the components.

[1] C. Boesch, MR and order in biological tissue, NMR Biomed. 14 (2001) 55-160.

[2] P.C. Van Zijl, D. Le Bihan, Diffusion tensor imaging and axonal mapping-state of the art, NMR Biomed. 15 (2002) 431-593.

[3] D.G. Cory, A.N. Garroway, Measurement of translational displacement probabilities by NMR: An indicator of compartmentation, Magn. Reson. Med. 14 (1990) 435-444.

[4] P.W. Kuchel, A. Coy, P. Stilbs, NMR "diffusion-diffraction" of water revealing alignment of erythrocytecs in a magnetic field and their dimensions and membrane transport characteristics, Magn. Reson. Med. 37(5) (1997) 637-643.

[5] L.L. Latour, P.P. Mitra, R.L. Kleinberg, C.H. Sotak, Time-dependent diffusion coefficient of fluids in porous media as a probe of surface-to-volume ratio, J. Magn. Reson. A 101 (1993) 342-346.

[6] M.D. Hurlimann, K.G. Helmer, L.L. Latour, C.H. Sotak, Restricted diffusion in sedimentary rocks: Determination of surface-area-to-volume ratio and surface relaxivity, J. Magn. Reson. A 111 (1994) 169-178.

[7] L.L. Latour, K. Svoboda, P.P. Mitra, C.H. Sotak, Time-dependent diffusion of water in a biological model system, Proc. Nat. Acad. Sci. USA 91 (1994) pp 1229-1233.

[8] R.W. Mair, G.P. Wong, D. Hoffmann, M.D. Hurlimann, S. Patz, L.M. Schwartz, R.L. Walsworth, Probing porous media with gas diffusion NMR, Phys. Rev. Lett. 83(16) (1999) 3324-3327.

[9] P.N. Sen, L.M. Schwartz, P.P. Mitra, Probing the structure of porous media using NMR spin echoes, Magn. Reson. Imaging. 12(2) (1994) 227-230

[10] P.T. Callahan, Principles of Nuclear Magnetic Resonance Microscopy, Clarendon Press, Oxford, 2006.

[11] J.V. Sehy, J.J. Ackerman, J.J. Neil, Evidence that both fast and slow water ADC components arise from intracellular space, Magn. Reson. Med. 48 (2002) 765–770.

[12] C. Beaulieu, P.S. Allen, Water diffusion in the giant axon of the squid: implications for diffusion-weighted MRI of the nervous system, Magn. Reson. Med. 32 (1994) 579–583.

[13] D.A. Yablonskiy, A.L. Sukstanskii, J.C. Leawoods, D.S. Gierada, G.L. Bretthorst, S.S. Lefrak, J.D. Cooper, M.S. Conradi, Quantitative in vivo assessment of lung microstructure at the alveolar level with hyperpolarized 3He diffusion MRI, Proc. Natl. Acad. Sci. USA 99 (2002) 3111–3116.

[14] A.L. Sukstanskii, J.J.H. Ackerman, D.A. Yablonskiy, Effects of barrier-induced nuclear spin magnetization inhomogeneities on diffusion-attenuated MR signal, Magn. Reson. Med. 50 (2003) 735-742.

[15] P.P. Mitra, P.N. Sen, L.M. Schwartz, P. Le Doussal. Diffusion propagator as a probe of the structure of porous media, Phys. Rev. Lett. 68 (1992) 3555-3558.

[16] B. Putz, D. Barsky, K. Schulten. Edge enhancement by diffusion in microscopic magnetic resonance imaging, J. Magn. Reson. 97 (1992) 27–53.

[17] P.T. Callaghan, A. Coy, L.C. Forde, C.J. Rofe, Diffusive relaxation and edge enhancement in NMR microscopy, J. Magn. Reson. A 101 (1993) 347–350.

[18] T.M. de Swiet, Diffusive edge enhancement in imaging, J. Magn. Reson. B 109 (1995) 12–18.

[19] B. Saam, N. Drukker, W. Happer, Edge enhancement observed with hyperpolarized ^{3}He, Chem. Phys. Lett. 264 (1996) 481-487.

[20] J.E. Tanner, Use of the stimulated echo in NMR diffusion studies, J. Chem. Phys. 52 (1970) 2523-2526.

[21] L.Z. Wang, A. Caprihan, E. Fukushima, The narrow-pulse criterion for pulse-gradient spin-echo diffusion measurements, J. Magn. Reson. A 117 (1995) 209-219.

[22] E.O. Stejskal, J.E. Tanner, Spin diffusion measurements: spin echoes in the presence of a time-dependent field gradient, J. Chem. Phys. 42 (1965) 288–292.

[23] G.L. Bretthorst, How accurately can parameters from exponential models be estimated? A Bayesian view, Concepts Magn. Reson. 27A (2005) 73-83.

[24] K. Krynicki, C.D. Green, D.W. Sawyer, Pressure and temperature dependence of self-diffusion in water, Discuss. Faraday Chem. Soc. 66 (1978) 199–208.

Appendix A - Bulk Gas Measurements

This work on bulk gas follows the work of Saam[1] (for helium) and Chang[2] (for octafluoropropane) closely. T_1 and diffusion were measured for bulk gas mixtures of oxygen and either helium or octafluoropropane (C_3F_8) gas. The results for bulk gases agreed with published results for helium and disagreed with earlier results from this lab for C_3F_8. It was determined that the earlier results for octafluoropropane gases were taken with samples not at the stated pressure.

As described in chapter 2, the bulk samples were prepared by filling a mixing chamber on a gas apparatus with the desired final partial pressure of the gas (helium or C_3F_8). Then the mixing chamber was closed off and the gas apparatus was evacuated up to the valve of the mixing chamber. The gas apparatus was then filled with oxygen at a higher pressure than the gas in the mixing chamber (so that the gas flow would into, rather than out of, the mixing chamber when the mixing chamber was reopened) and the mixing chamber was filled with oxygen until the desired total pressure was reached and the mixing chamber was closed again. The fundamental assumption is that none of the helium or C_3F_8 gas leaves the mixing chamber as oxygen is being admitted. To this end, the valve is closed immediately upon reaching the desired total pressure. Then the mixing chamber was removed from the gas apparatus and shaken for at least ten minutes (the chamber was filled with metal spheres to aid in quickly producing uniform gas concentration). Next the gas mixture was released into an evacuated glass sample chamber to a pressure of a little less than 1 atm. The sample chamber was then flame sealed at a point at least 10 inches away from the body of the chamber. The chamber was sealed far away from the body of the sample to avoid warming the gas in the chamber

body and changing the density and pressure inside the sample. The free diffusion was measured at several diffusion times as well as measuring T_1 in each sample, using the same sequences and techniques described earlier for the lung samples. Four C_3F_8 samples were made, all with a total pressure of 0.9907 atm: one pure C_3F_8 sample and three samples of carefully controlled mixes of C_3F_8 and oxygen. Four helium/oxygen mixture samples were made, all at a pressure slightly below an atmosphere (0.996 atm).

As noted in Saam's work, the T_1 of a helium/oxygen gas mix is determined by the partial pressure of the oxygen in the mix. Using the T_1 measurements presented in Table A.1 for helium/oxygen bulk gas mixes

[A.1]
$$T_1 = \frac{1}{0.415 \pm 0.003 \, (\text{$\frac{1}{s \cdot atm}$}) P_{O_2}}$$

where P_{O2} is the partial pressure of oxygen in the sample (Fig. A.1). This result is in good agreement with the results in Saam's paper, T_1^{-1}=0.418±0.010 s^{-1} per atm O_2 (please note the paper uses units of amagats O_2 rather than atmospheres. T_1 from Saam's paper was converted using 1 atm = 0.932 amg for gas at STP).

The free diffusion measurements for the helium/oxygen mix (presented in Tab. A.1) yields $1/D_0 = (0.72\pm0.06) \, P_O + (0.54\pm0.03)$. Using the relationship

[A.2]
$$\frac{1}{D} = \frac{P_{O_2}}{D_{O_2}} + \frac{P_{He}}{D_{He}}$$

and remembering that the total pressure of the sample is approximately 1 atm, one finds that

[A.3]
$$D_{O_2} = 0.79 \pm 0.04 \, \text{$\frac{cm^2}{s}$}$$
$$D_{He} = 1.9 \pm 0.1 \, \text{$\frac{cm^2}{s}$}$$

where D_{O2} is the free diffusion of infinitely dilute helium in oxygen and D_{He} is the free

diffusion of pure helium gas (Fig A.2), all at 1 atm total pressure.

For C_3F_8, the T_1 relationship is not quite as simple. However, for the partial

pressures of C_3F_8 in the bulk gas samples and well as in the lung, the T_1/pressure

relationship is approximately linear. Consequently, assuming the total pressure is 1 atm,

a good approximation of the T_1/partial pressure relationship from the measurements in

Table A.2 is

[A.4] $$T_1 = (0.0138 \pm 0.0002)(s/atm)P_{C_3F_8} + (0.0070 \pm 0.0001)s$$

Giving a T_1 of 0.0208s for pure octafluoropropane. The diffusion measurements yield

$1/D_0 = (35.5 \pm 0.4) P_{C3F8} + (12.6 \pm 0.3)$. Using the same diffusion/pressure relationship as

for helium one finds that

[A.5] $$D_{O_2} = (0.079 \pm 0.002)\,cm^2/s$$
$$D_{C_3F_8} = (0.0208 \pm 0.0002)\,cm^2/s$$

where D_{O2} is the free diffusion of infinitely dilute octafluoropropane in oxygen and D_{C3F8}

is the free diffusion of pure octafluoropropane gas (Figs. A.3 and A.4), at 1 atm total

pressure. These numbers are not in good agreement with the numbers in Chang's paper,

but it was determined that samples used in Chang's study were not at the specified

pressure. Instead they were at lower pressure, due to the fact that the samples were

flamed sealed very close to the body of the sample. This sealing process heated the gas

in the samples during the sealing process and lowered the density and pressure of the

sealed sample. Figures A.5 and A.6 compare the bulk gas samples used in Chang's study

and the bulk gas samples used in this study.

Helium/O2 mixture samples (total pressure 0.996 atm)			
He partial pressure (atm)	O_2 partial pressure (atm)	T_1 (s)	Diffusion (cm^2/s)
0.707	0.289	8.39 ± 0.09	1.343 ± 0.003
0.596	0.400	6.0 ± 0.1	1.20 ± 0.08
0.476	0.520	4.64 ± 0.07	1.11 ± 0.02
0.396	0.600	no measurement	1.02 ± 0.06

Table A.1. T_1 and diffusion measurements for the helium and oxygen mixture sample.

The total pressure for each sample was 0.996 atm.

C_3F_8/O_2 mixture samples (total pressure 0.9907 atm)		
C_3F_8 partial pressure (atm)	T_1 (s)	Diffusion (cm^2/s)
0.9907	0.0208 ± 0.0003	0.021 ± 0.001
0.753	0.0173 ± 0.0003	0.0254 ± 0.0007
0.507	0.0138 ± 0.0004	0.0327 ± 0.0007
0.245	0.0105 ± 0.0003	0.047 ± 0.002

Table A.2. T_1 and diffusion measurements for samples of a mixture of C_3F_8 and O_2. The

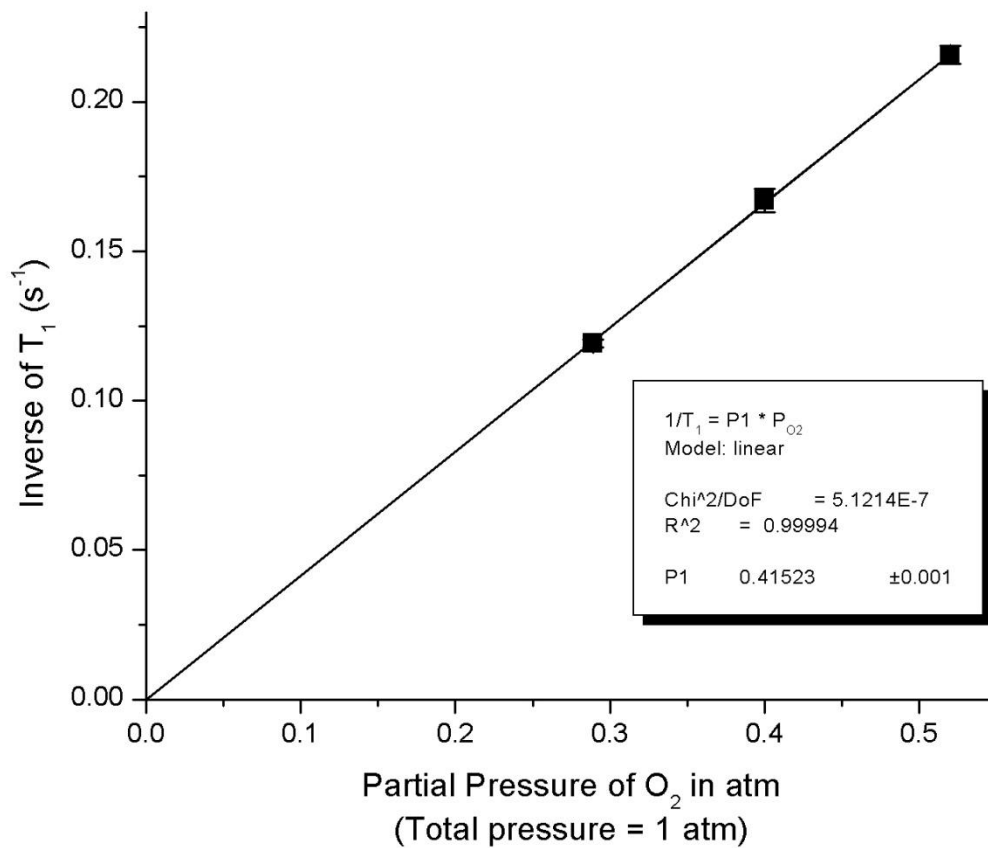total pressure for all samples was 0.9907 atm.

Figure A.1. Dependence of T_1 on the partial pressure of oxygen in a helium/oxygen bulk
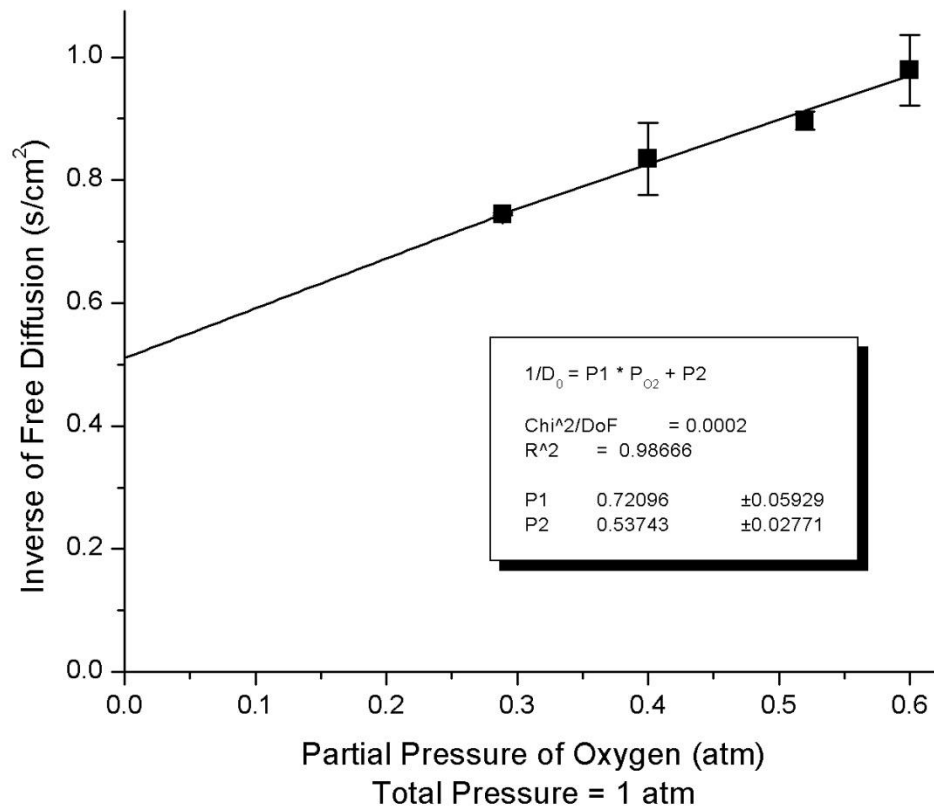
gas mixture.

Figure A.2. Dependence of the free diffusion coefficient in a helium/oxygen mixture on
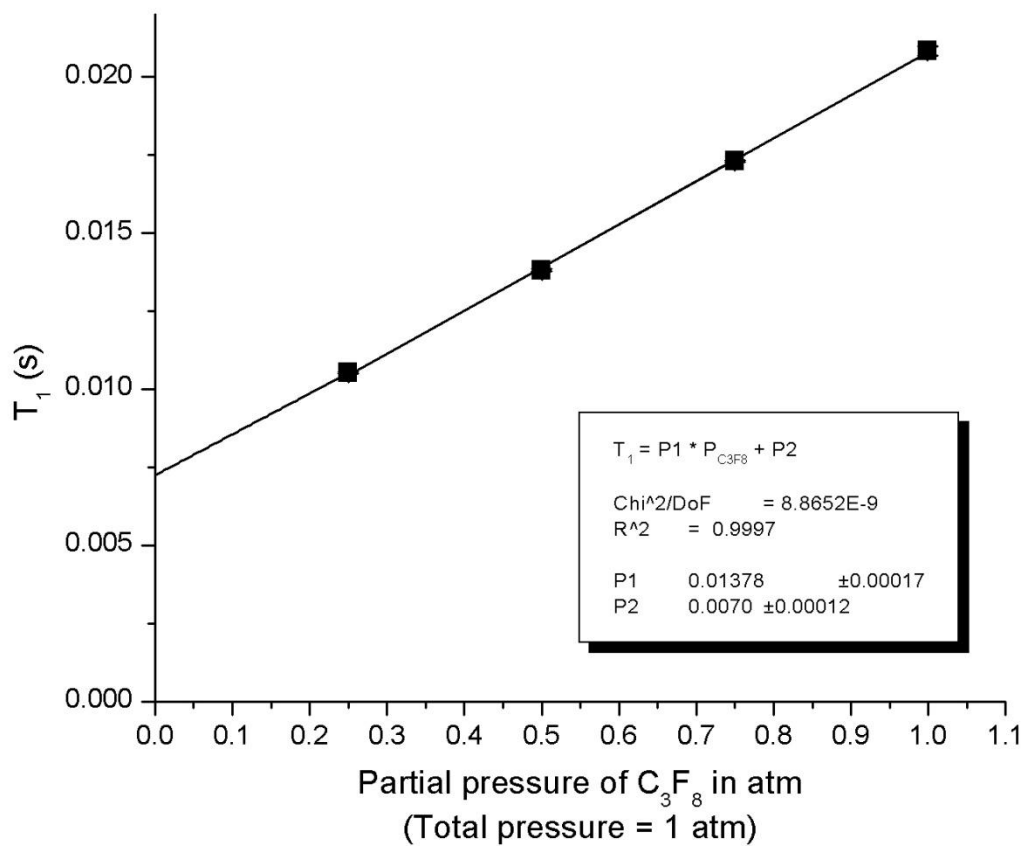
the partial pressure of oxygen.

Figure A.3. Dependence of T_1 on the partial pressure of octafluoropropane in a C$_3$F$_8$/oxygen mixture.
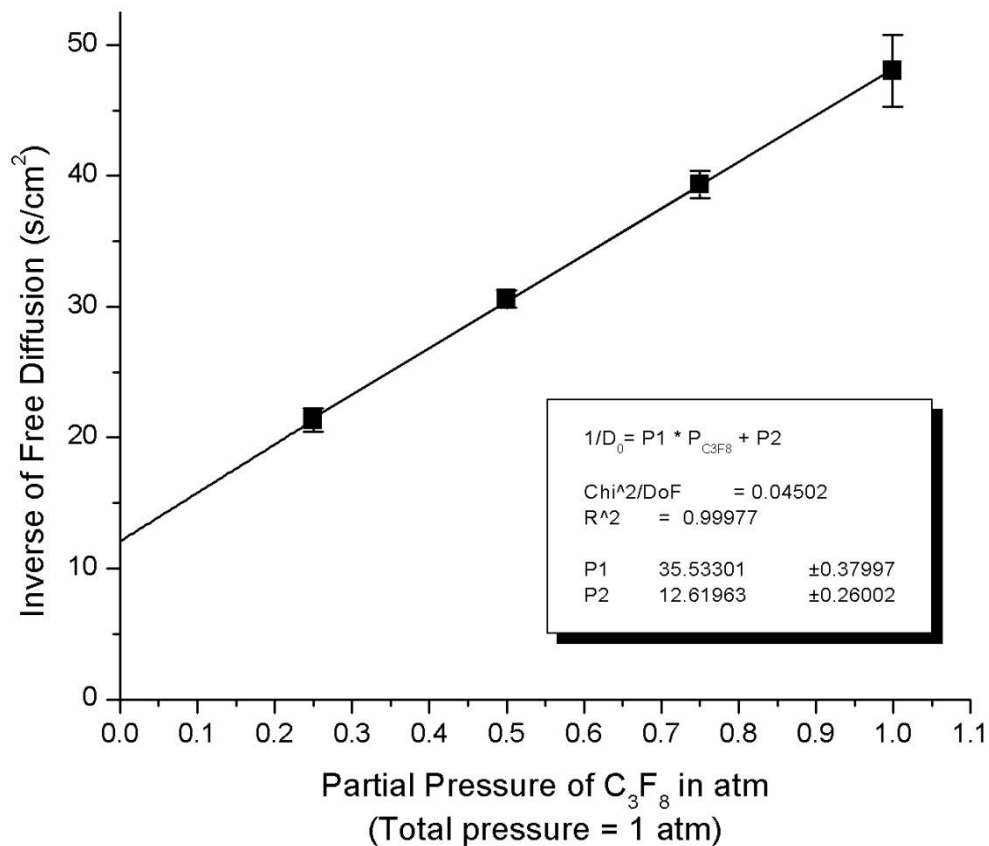
Figure A.4. Dependence of the free diffusion coefficient on the partial pressure of

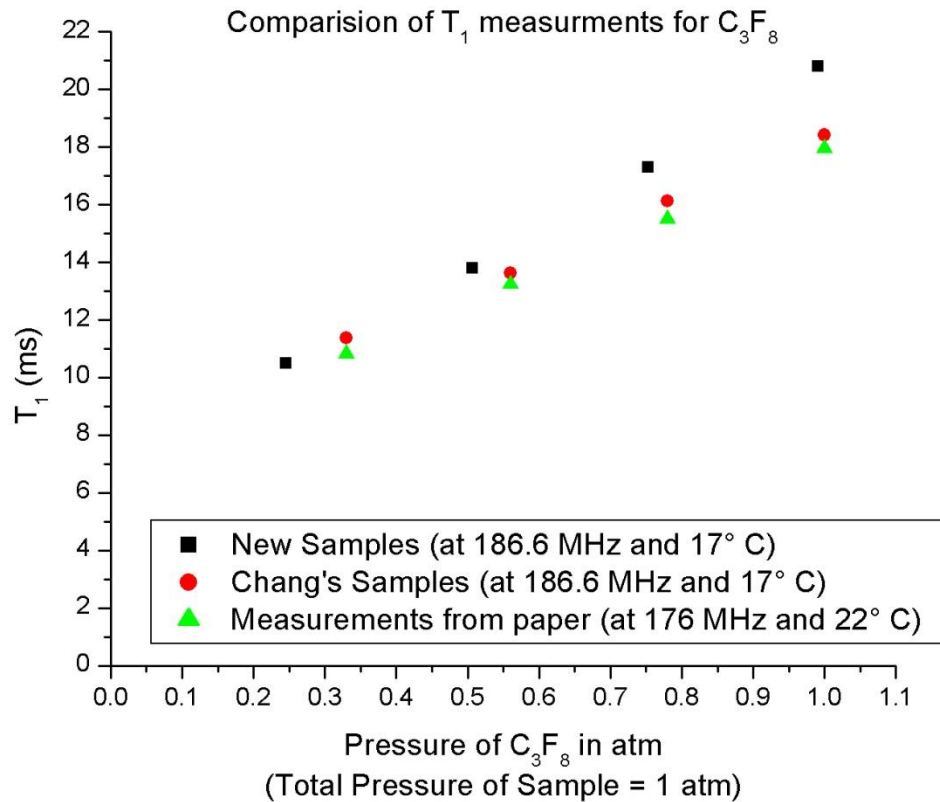octafluoropropane in a C_3F_8/oxygen mixture.

Figure A.5. Comparison of T_1 for C_3F_8 as measured in this study and in ref. 2. Because the samples in the paper with measured in a different magnet with a different field and at a different temperature (green triangles), the samples were measured again in the magnet used in this study (red circles) as T_1 is expected to vary with temperature[2]. The measurements at 186.6 MHz should be compared (black squares and red circles). The pressures reported in the paper are used to graph the paper's samples, although method used to seal them probably means the actual pressures, both partial and total, are lower.
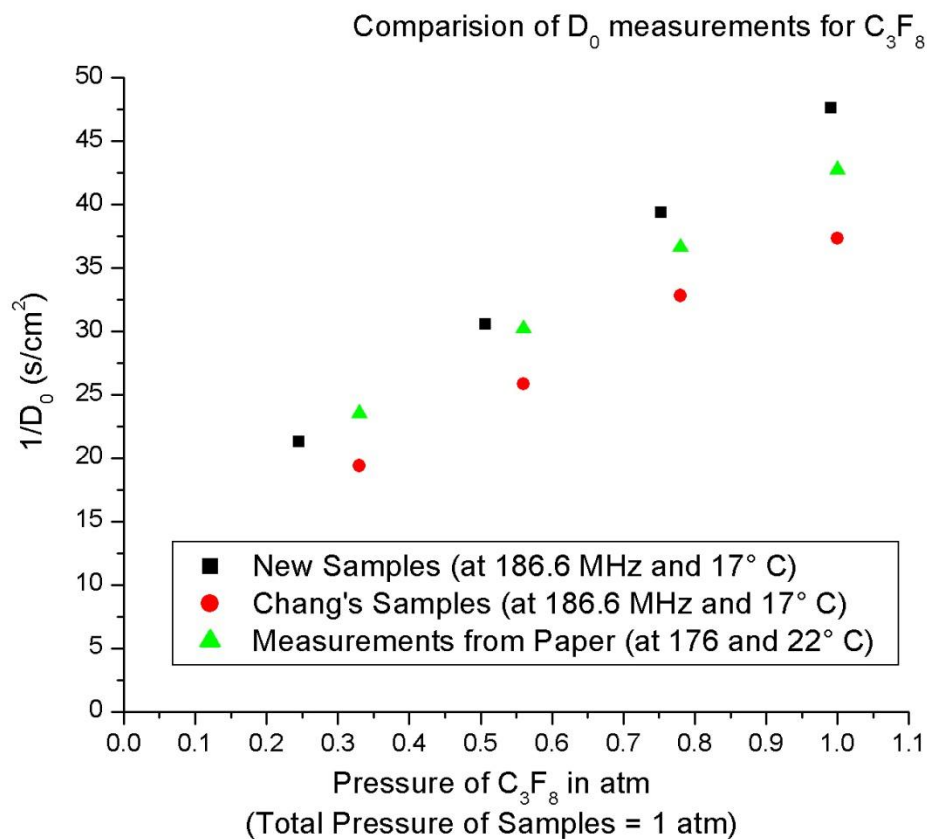
Figure A.6. Comparison of D_0 for C_3F_8 as measured in this study (black squares) and in reference 2 (green triangles). Since D_0 is expected to vary with temperature and Larmor frequency[2] the paper's samples were measured again in the new magnet (red circles). The measurements at 186.6 MHz should be compared (black squares and red circles). The reported pressures for the paper's samples are probably higher than the actual pressures, due to the method used to seal them.

[1] B. Saam, W. Happer, H. Middleton, Nuclear relaxation of ^{3}He in the presence of O2, Phys Rev A 52 (1995) 862-865.

[2] Y.V. Chang, M.S. Conradi, Relaxation and diffusion of perfluorocarbon gas mixtures with oxygen for lung MRI, JMR 181 (2006) 191-198.

Appendix B – Equipment

B.1 rf Coils

Two rf coils were used in this study. Both are homemade single-turn solenoids inductively coupled to the MR electronics. They are 1.75" in diameter, close fitting to the outside surface of the lung sample cylinder.

The rf coil for helium frequencies is 2.5 cm in length and tuned to 151.1 MHz. It is a copper strap with an equivalent 11pf capacitor (two 22 pf capacitors in series) connected in parallel with a 2-15 pf variable capacitor. The helium coil has a quality factor of 275.

The rf coil for fluorine is 3.2 cm in length and tuned to 186.65 MHz. It is also a copper strap with a 10 pf capacitor in parallel with a 2-10 pf variable capacitor. The fluorine coil has a quality factor of 115.

Figure B.1. Lung sample in cylinder with rf coil. This is the coil for helium. The two 22

pf capacitors in series and the variable capacitor can been seen on the top of the rf coil

B.2 Howard Gradients

Diffusion for all samples was measured with the x-gradient (along the long axis of the *sample*), but all three gradient directions were measured during study preparation. The gradient pulses were monitored inside the bore with an inductive pick-up coil set with an integrating amplifier made by Yulin Chang simultaneously with the generating current from the gradient amplifiers. Both the rise time of the gradients and the gradient pulse amplitude were measured. The results are shown in Figs. B2-B6. The slope of the gradient rise was constant, so the rise time of the gradients depended on the final gradient strength. The rise time results from the inductive coil agreed with the output from the current monitor, although in general the rise time as measured in the magnet bore with the inductive coil was a few microseconds longer than the rise time measured from gradient amplifiers as output by the current monitor.
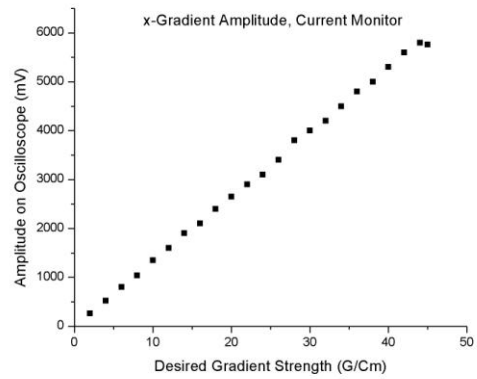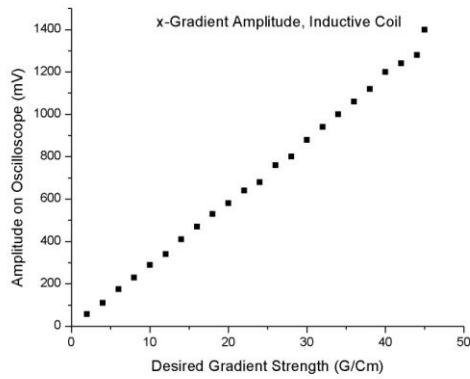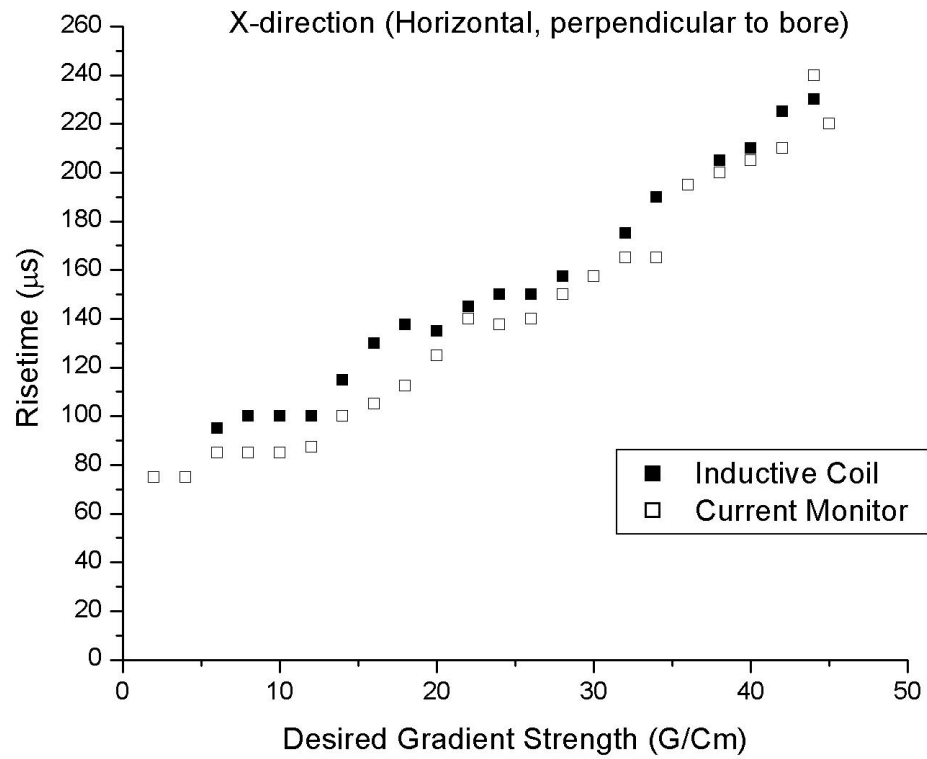
Figure B.2. Graphs for x-gradients. The fit for the amplitude as measured by the inductive coil is $y = (29.5\pm0.1)$ mV/(G/cm) x. For the current monitor it's $y = (131.9\pm0.4)$ mV/(G/cm) x.
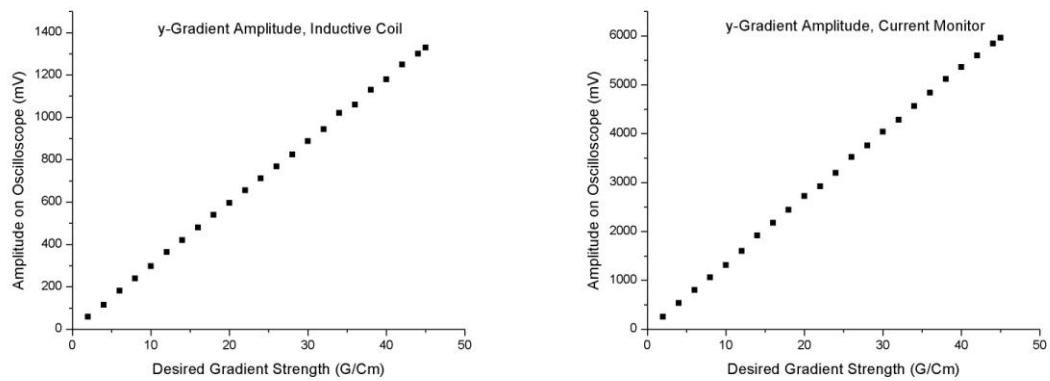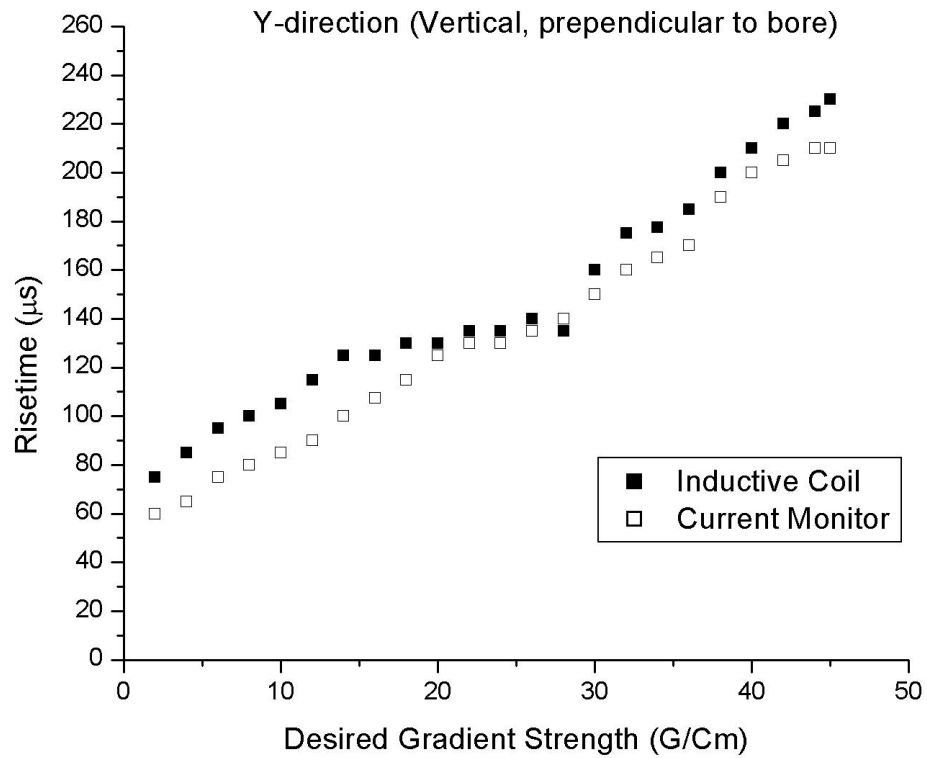
Figure B.3. Graphs for y-gradients. The fit for the amplitude as measured by the inductive coil is $y = (29.65 \pm 0.04)$ mV/(G/cm) x. For the current monitor it's $y = (133.9 \pm 0.2)$ mV/(G/cm) x.
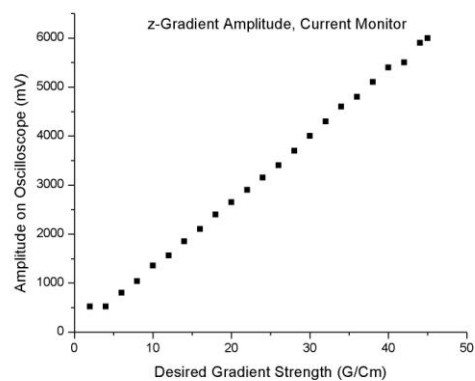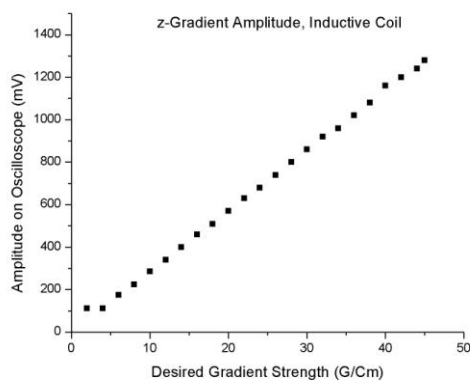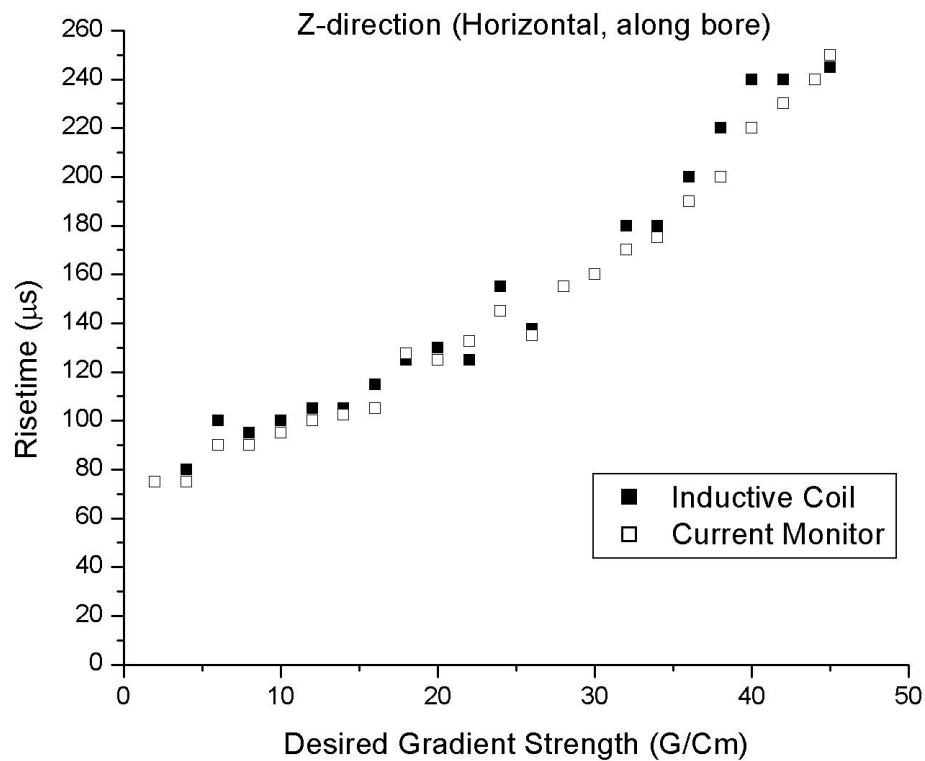
Figure B.4. Graphs for z-gradients. The fit for the amplitude as measured by the inductive coil is $y = (28.5 \pm 0.1)$ mV/(G/cm) x. For the current monitor it's $y = (133.3 \pm 0.5)$ mV/(G/cm) x.

B.3 Tissue Cutter

The lung samples were cut using a 1 3/8" diameter cylindrical tissue cutter made of hardened steel. Hardened steel was used because stainless steel was found to lose its cutting edge much too quickly to cut completely through a 2 inch thick slab. The tissue cutter was stored with the lungs at 4 °C overnight before cutting to avoid the simultaneous stress of pressure from cutting a lung which was frozen solid and a temperature drop to 4° C from room temperature. Pre-cooling the tissue cutter also help retard thawing of the lung tissue during cutting. After cutting, the tissue cutter was cleaned and rubbed down with cooking oil to prevent rusting.

Figure B.5. The cutting apparatus. The stainless steel meat cutter of 1 3/8 inch diameter

(sharp edge facing down in the picture), a plastic cutting board, and plastic cylinder to

assist in removing the cut core from the meat cutter. A six inch ruler is placed in the

photograph for scale.

B.4 Sample Cylinder

The lung samples were placed in a sample cylinder designed with two objectives in mind; to allow gas to flow through the sample during filling, and to prevent, as much as possible, helium gas from escaping by leaks or permeation. The sample cylinder was designed to have a body with an outer diameter of 1.75 inches and an inner cavity for the lung sample with a diameter of 1.35 inches and a cap with matching dimensions. Once the lung sample was cut and placed in the body of the sample cylinder, the cap was glued on with 5-minute epoxy. There were holes threaded for pipe thread fittings on each end of the cylinder so fittings could be installed to allow gas filling. In addition to the cylinder diagram in Fig. B.6 a photograph of the sample cylinder can be found in Fig 3.3 in chapter 3.

Tests showed that while helium passes slowly through the acrylic used for the body of the cylinder, it escaped very rapidly through rubber tubing. Consequently metal fittings and tubing was used. Brass NPT to swage fittings (Swagelok, 1/4 inch NPT to 1/8 inch Swagelok tube fitting) attached to 1/8" copper tubing, leading out to brass ball valves (Swagelok; The commercial steel screws in the valves were replaced with brass screws so they would not distort the uniform field of the MR magnet).

Side view

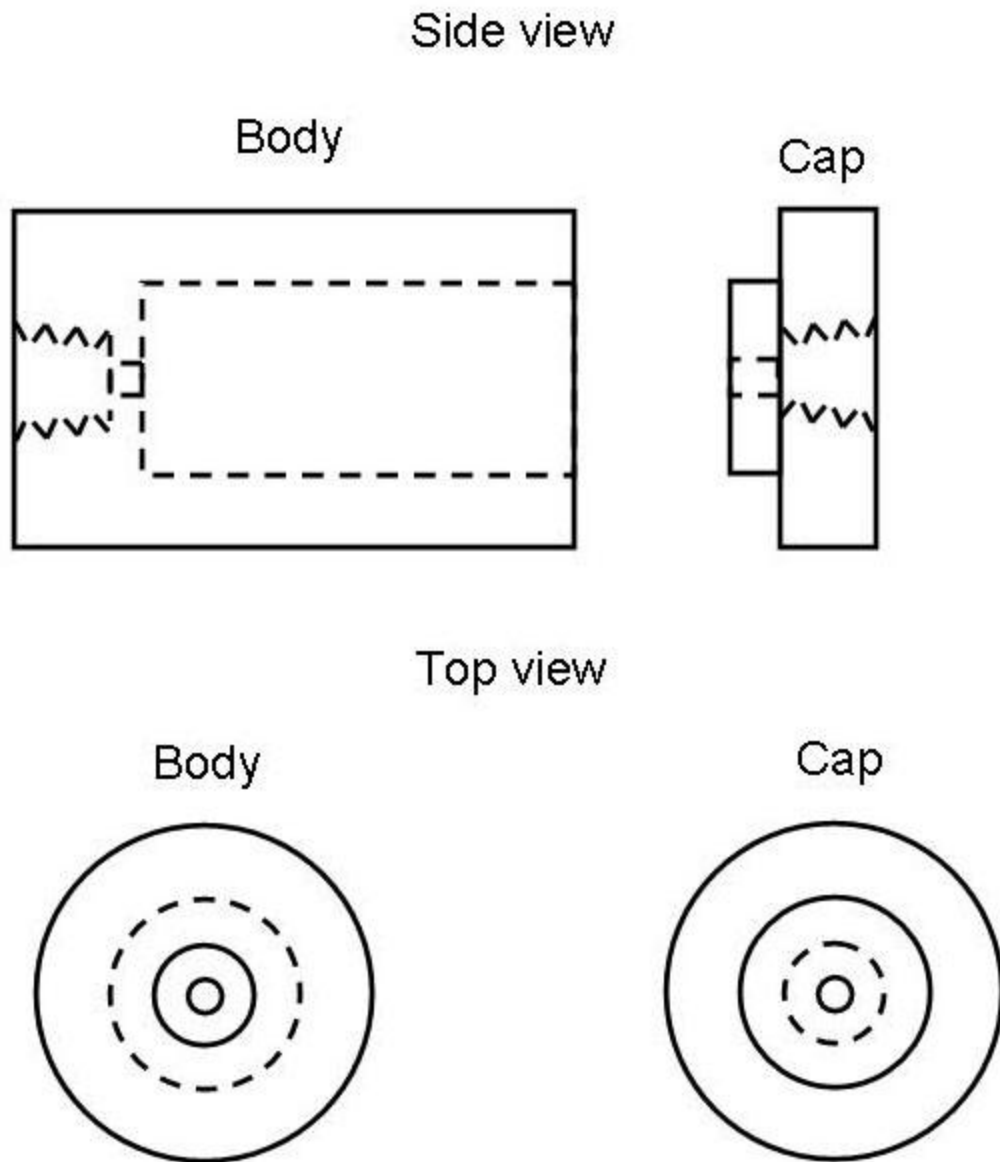### Body

Cap

Top view

Body

Cap

Figure B.6. Diagram for the body and cap of the lung sample container. Both body and cap were made from acrylic with an inner diameter of 1.35 inches and an outer diameter of 1.75 inches. Each had a threaded hole for a 1/4 inch pipe-thread fitting. Once the lung sample was placed inside the inner cavity of the body the cap was glued on.

B.5 Fixation Box

The lungs used in this study were fixed with formalin vapor in a large, plastic box while attached to apparatus that imitated the breathing cycle while the lung was undergoing fixation. Descriptions of similar fixation boxes can be found in papers by Mittermayer[1] and Wright[2]. Our fixation box was designed by Richard Jacob and Jason Woods.

The main structure is a clear plastic box about 3' x 2' x 2', with a barbed fitting attachment on the ceiling of the box for the lung bronchus/tubing arrangement, a shelf to rest the weight of the lung, and reservoir for formalin with a submerged heating coil (Fig. B.6). The breathing apparatus is attached to the lung and surrounding space via holes in the side and top of the box. A diaphragm pump continuously moved air in and out of the lung, while timing switches change the direction of flow (Fig. B.7). A water column and a bypass valve across the pump regulate the differential pressure across the lung tissue. The exhaust air is filtered through activated charcoal to remove the formalin vapor.

---

[1] C. Mittermayer, K. Wybitul, W.S. Rau, P. Ostendorf, U.N. Riede. Standardized fixation of human lung for radiology and morphometry: description of a "two chamber"-system with formaldehyde vapor inflation. Pathol Res Pract 162 (1978) 115-130.

[2] B.M. Wright, G. Slavin, L. Kreel, K. Callan B. Sandin, Postmortem inflation and fixation of human lungs: A technique for pathological and radiological correlations, Thorax 29 (1974) 189-194.
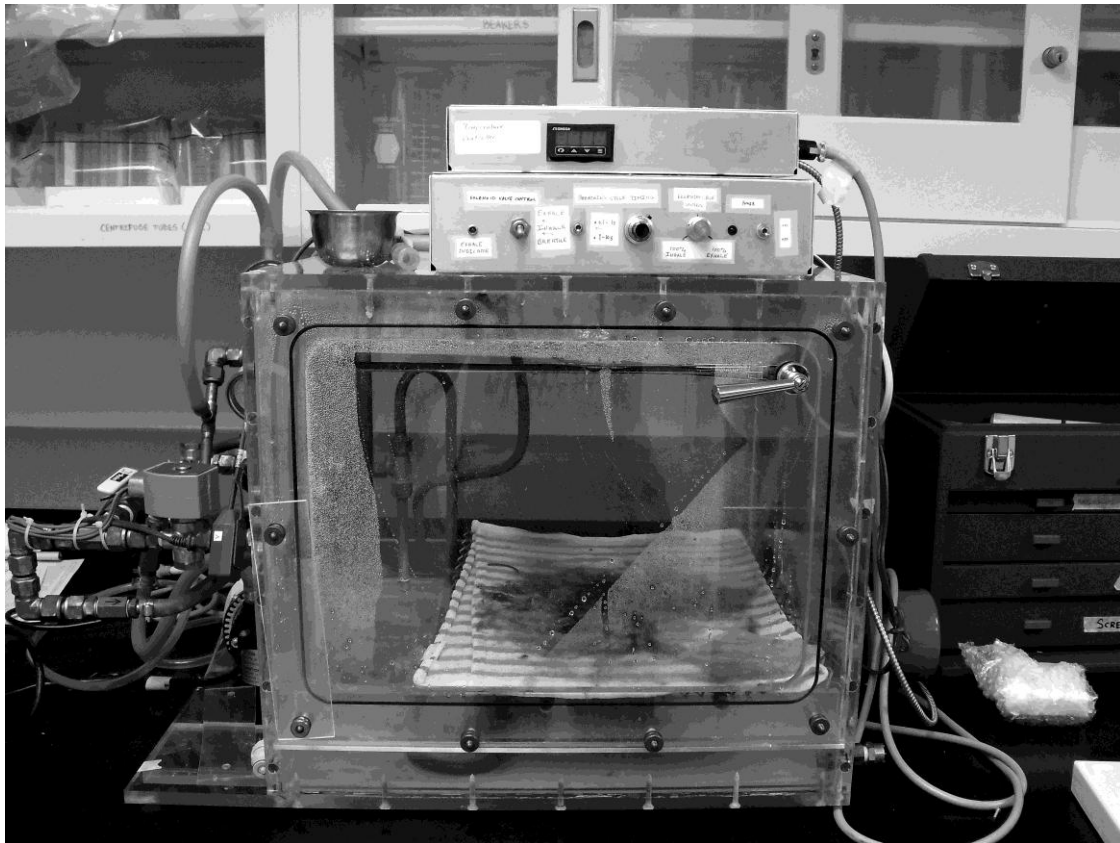
Figure B.7. Photograph of the formalin fixation box. The electronics on top control the switches which change airflow directions (low box) and regulate the power to the reflux heater (upper box).
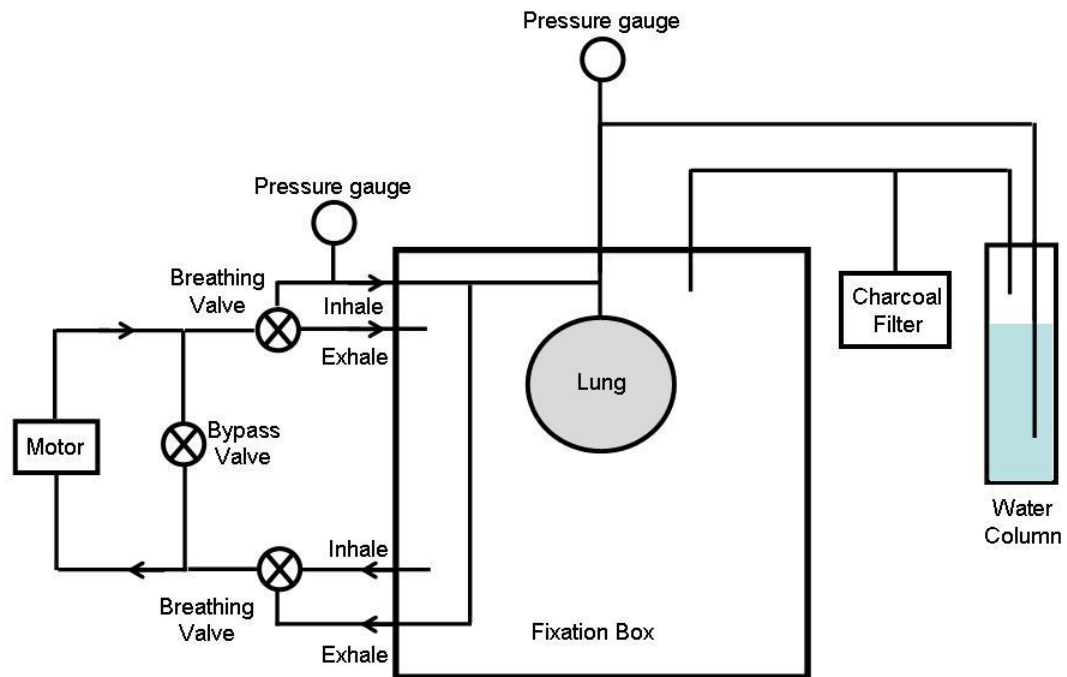
Figure B.8. Schematic of the breathing apparatus for lung fixation. The breathing valves are electrically operated valves driven together by a timer circuit (the lower of the electronics boxes in the previous figure). The "Inhale" and "Exhale" marking denote which of the lines are active during that respective portion of the breathing cycle. The water column prevents the pressure differential across the lung from ever becoming too great. If the pressure in the lung is ever greater than the water lever (generally 10 inches water), air will bubble through the water column and relieve pressure in the lung.

Appendix C - Stimulated Echo Sequence

C.1 Phase Cycling Discussion

Phase cycling is a technique generally used to eliminate unwanted signals in MR. It refers to changing the direction, or phase, along which one applies rf pulses. To use phase cycling the sequence in question must be repeated multiple times in order to go through the entire sequence, or cycle, of rf pulse directions. For example, in a spin echo (90°-180°-echo, see Fig. C.1), the 90° rf pulse could be always applied along the x-axis while the 180° rf pulse is applied along the x-axis for the first iteration of the sequence and then along the negative x-axis for the second iteration. Then the free induction decay (FID) from the 180° rf pulse would be along the positive y-axis one time and along the negative y-axis the second time, and thus would cancel when the two signals were added together. However, the echo from the 90°-180° rf pulse combination would be along the negative y-axis both times, and thus would add when the signals were combined (obviously there would not be a FID from a perfect 180° rf pulse, but physical rf pulses are rarely perfect).

In the more complicated case of a stimulated echo sequence, there are three FIDs and three extra echoes in addition to the desired stimulated echo. To simply cancel these extra signals, a four-step phase cycle is needed. However, because the second 90° rf pulse of the stimulated echo can store either the spins along the x-axis or the spins along the y-axis but not both, for completeness the phase cycle should also include steps that cause the second 90° rf pulse to store spins from both the x- and y-directions. Thus the phase cycle needs eight steps. In Table C.1, note that the first four steps of the phase cycle have the first and second rf pulses either in phase or 180° out of phase, while the

second four steps have a phase shift of 90°. This switching of the second rf pulse's

phase insured that spins from both transverse directions were stored.

In most cases, storing spins from both directions is of little practical importance,

because the spins are so highly dephased by the second 90° rf pulse that they cover the

directions in the transverse plane uniformly. However, in this particular experiment, due

to the low b-values used, the dephasing was minimal and it consequently it made quite a

difference if the storage axis is the one about which the spins are clustered or the one

orthogonal to that.

This sequence was tested using a water phantom, as mentioned in chapter 3. Part

of that testing included starting acquisition immediately after the final rf pulse and the

spacing between the rf pulses such that the four echoes and one FID that occur after the

final rf pulse were distinct and easy to distinguish in the time domain.   Then each phase

cycle step was run individually and the phases of the FID and each echo relative to the

receiver phase was checked against its expected phase, to ensure that the phase cycle was

working properly.

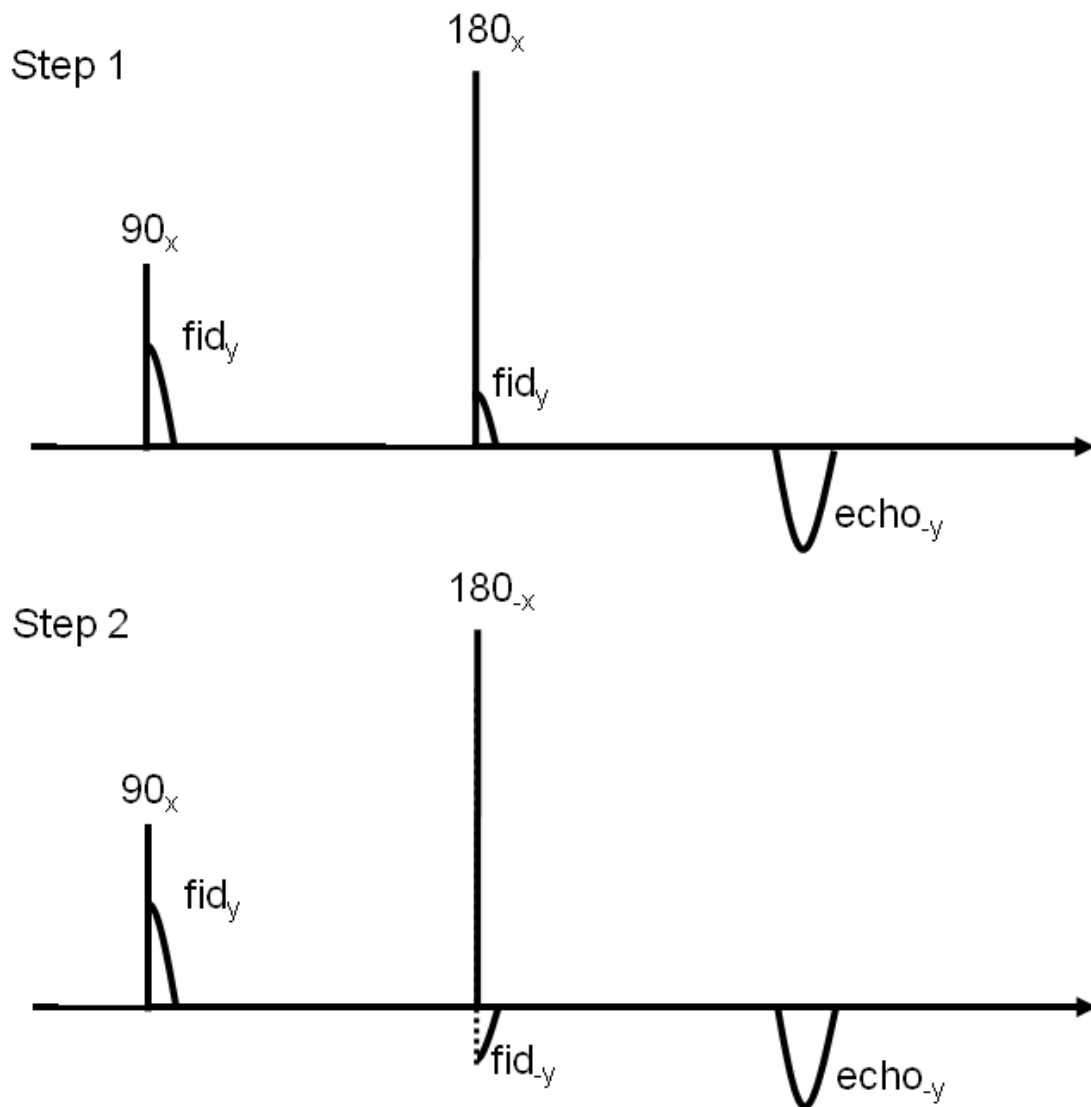| Cycle Step	1st 90° rf pulse	2nd 90° rf pulse	3rd 90° rf pulse	receiver
1	X	X	X	X
2	-X	X	X	-X
3	X	-X	X	-X
4	-X	-X	X	X
5	X	Y	X	Y
6	-X	Y	X	-Y
7	X	-Y	X	-Y
8	-X	-Y	X	Y

Table C.1 Phase cycling steps

Figure C.1 Simple 2-step phase cycle illustration on a spin echo sequence. The signals

from the two steps are added together, with the result that the FIDs from the 180° rf pulse

will cancel each other while the echoes will add.

C.2 Core for Modified Stepuls.c

```
#ifndef LINT
static char SCCSid[] = "@(#)vnmrs_stepuls.c 21.1 03/21/08 Copyright (c)
2003-2005 Varian,Inc. All Rights Reserved";
#endif
/*
 * Varian,Inc. All Rights Reserved.
 * This software contains proprietary and confidential
 * information of Varian, Inc. and its contributors.
 * Use, disclosure and reproduction is prohibited without
 * prior consent.
 */
/*  stepuls - ADC pulse sequence

             P1-tdelta-trise-P1-tm-P1-tdelta-trise-Acquire

             ticks=1 enables external trigger
             p1   - 90 deg pulse
             flip1 - 90deg
             p1pat - pulse shape (e.g. hard, gauss)
             tpwr1  - pulse power (dB)
             tpwr1f - fine power (0-4k)

           gdiff - gradient amplitude G/cm
           gf - gradient on/off flag
             gradient is applied along slice direction and selected via
orient
*/

#include <standard.h>
#include <string.h>
#include "sgl.c"

/* Phases for phase cycling */
/*  MM – Old phase cycling
static int ph1[8]   = {0, 2, 0, 2,  0, 2, 0, 2};
static int ph2[8]   = {0, 0, 2, 2,  0, 0, 2, 2};
static int ph3[8]   = {0, 0, 0, 0,  2, 2, 2, 2};
static int phobs[8] = {0, 2, 2, 0,  2, 0, 0, 2};
*/
/* MM – new phase cycling */
static int ph1[8]   = {0, 2, 0, 2,  0, 2, 0, 2};
static int ph2[8]   = {0, 0, 2, 2,  1, 1, 3, 3};
static int ph3[8]   = {0, 0, 0, 0,  0, 0, 0, 0};
static int phobs[8] = {0, 2, 2, 0,  1, 3, 3, 1};




pulsesequence()
{
   double pd, seqtime;
   double ted1,ted2,gf,tm,mintDELTA;

  /* Real-time variables used in this sequence **************/
```

138

```
int    vph1 = v1;    // Phase of first RF pulse
int    vph2 = v2;    // Phase of second RF pulse
int    vph3 = v3;    // Phase of third RF pulse

init_mri();                   /****needed ****/

init_rf(&p1_rf,p1pat,p1,flip1,rof1,rof2);    /* hard pulse */
calc_rf(&p1_rf,"tpwr1","tpwr1f");

gf=1.0;
if(diff[0] == 'n') gf=0;

temin =  2*(p1 + rof1 + rof2 + tdelta + trise + alfa);
temin = temin + 4e-6;  /* ensure that te_delay is at least 4us */
if (minte[0] == 'y') {
  te = temin;
  putvalue("te",te);
}
if (te < temin) {
 abort_message("TE too short.  Minimum TE=
%.2fms\n",temin*1000+0.005);
}

ted1 = te/2 - p1 - rof1 - rof2 - tdelta - trise;
ted2 = te/2 - p1 - rof1 - rof2 - tdelta - trise - alfa;

if(ted2 <= 0) {
    abort_message("%s: TE too short. Min TE = %f
ms",seqfil,temin*1e3);
}

mintDELTA = ted1 + 2*(p1+rof1+rof2) + tdelta + trise;
if(tDELTA <= mintDELTA) {
    abort_message("%s: tDELTA too short. Min tDELTA = %f
ms",seqfil,mintDELTA*1e3);
}
tm = tDELTA - ted1 - 2*(p1+rof1+rof2) - trise - tdelta;

seqtime = at + 3*(p1+rof1+rof2) + 2*(tdelta+trise) + tm + ted1 +
ted2 + alfa;
pd = tr - seqtime;  /* predelay based on tr */
if (pd <= 0.0) {
    abort_message("%s: Requested TR too short.  Min TR = %f
ms",seqfil,seqtime*1e3);
}
/* Create phase cycling */
settable(t1,8,ph1);   getelem(t1,ct,vph1);
settable(t2,8,ph2);   getelem(t2,ct,vph2);
settable(t3,8,ph3);   getelem(t3,ct,vph3);
settable(t4,8,phobs); getelem(t4,ct,oph);

rotate();
delay(pd);
if (ticks) {
  xgate(ticks);
  grad_advance(gpropdelay);
}
```

```
   /* --- observe period --- */
   obsoffset(tof);       /* spectroscopy sequence use tof */
   obspower(p1_rf.powerCoarse);
   obspwrf(p1_rf.powerFine);
   shapedpulse(p1pat,p1,vph1,rof1,rof2);

   obl_gradient(0,0,gdiff*gf);   /* x,y,z gradients selected via orient
*/
   delay(tdelta);
   zero_all_gradients();
   delay(trise);
   delay(ted1);

   shapedpulse(p1pat,p1,vph2,rof1,rof2);
   delay(tm);
   shapedpulse(p1pat,p1,vph3,rof1,rof2);

   obl_gradient(0,0,gdiff);   /* x,y,z gradients selected via orient */
   delay(tdelta);
   zero_all_gradients();
   delay(trise);
   delay(ted2);

}
/***********************************************************************
*********
      Modification History

20080104 minte; phase cycling included

Michelle Milne: phase cycling modified to include both x and y
transverse magnetization in storage

***********************************************************************
********/
```